Chemistry of gold nanoparticles radiosensitizing effect

Viacheslav Shcherbakov

université PARIS-SACLAY

Chemistry of gold nanoparticles radiosensitizing effect

Chimie de l'effet radiosensibilisant des nanoparticules d'or

Thèse de doctorat de l'université Paris-Saclay

École doctorale n°571, Sciences chimiques : molécules, matériaux, instrumentation et biosystèmes (2MIB)
Spécialité de doctorat : Chimie
Graduate School : Chimie. Référent : Faculté des sciences d'Orsay

Thèse préparée dans l'unité de recherche **Institut de Chimie Physique (Université Paris-Saclay, CNRS)**, sous la direction de **Mehran MOSTAFAVI**, Professeur

Thèse soutenue à Paris-Saclay, le 22 avril 2022, par

Viacheslav SHCHERBAKOV

Composition du Jury

Fabienne TESTARD Directrice de recherche, CEA, Gif-sur-Yvette, France	Présidente
Lucie SANCEY Directrice de recherche, CNRS, Grenoble, France	Rapportrice & Examinatrice
Tomer ZIDKI Maître de conférences, HDR, Ariel University, Ariel, Israël	Rapporteur & Examinateur
Marie DAVÍDKOVÁ Chercheuse, Nuclear Physics Institute CAS, Prague, Czech Republic	Examinatrice
Mehran MOSTAFAVI Professeur, Université Paris-Saclay	Directeur de thèse

THESE DE DOCTORAT

NNT : 2022UPASF032

université PARIS-SACLAY

ÉCOLE DOCTORALE
Sciences Chimiques : Molécules, Matériaux, Instrumentation et Biosystèmes (2MIB)

Titre : Chimie de l'effet radiosensibilisant des nanoparticules d'or

Mots clés : radiosensibilisation, nanoparticule d'or, radical, catalyse

Résumé : Les nanoparticules d'or (AuNPs) constituent une classe prometteuse de radiosensibilisateurs, des agents qui augmentent l'efficacité de la radiothérapie. En 2004, il a été démontré que les AuNPs accélèrent la réduction de la taille des tumeurs chez les souris après un traitement par radiation. L'utilisation de l'or a été motivée par l'effet dit d'augmentation de la dose. L'or ayant un numéro atomique élevé (Z=79), il absorbe plus d'énergie dans la gamme des keV que l'eau ou les tissus mous, ce qui augmente l'ionisation globale du volume irradié en raison de l'émission d'électrons secondaires et de photons. Plus tard, des expériences in vivo et in vitro ont montré que l'effet d'augmentation de la dose ne pouvait pas expliquer la radiosensibilisation observée.

Aujourd'hui, le mécanisme proposé pour la radiosensibilisation induite par les nanoparticules comprend différents effets physiques, chimiques et biologiques. Cependant, il n'y a pas de consensus sur le mécanisme exact. Les effets chimiques sont généralement associés à une formation accrue d'espèces réactives de l'oxygène (ROS), telles que les radicaux hydroxyles ($^{\bullet}OH$), les radicaux superoxydes ($O_2^{\bullet-}$) et le peroxyde d'hydrogène (H_2O_2), en présence de nanoparticules. La principale méthode de détection des ROS dans les études biologiques est l'utilisation de colorants fluorescents. Elle est basée sur l'oxydation d'une molécule non fluorescente en une molécule fluorescente lors de la réaction avec les ROS, en supposant que l'augmentation de l'intensité de la fluorescence est proportionnelle à l'augmentation de la concentration des ROS. Cependant, le processus d'oxydation d'un colorant est un processus à plusieurs étapes qui comprend la formation d'une variété de produits (pas seulement le produit fluorescent). Les AuNPs possèdent une activité catalytique, qui peut modifier les voies de réaction.

Dans le présent travail, nous avons examiné l'idée d'une production accrue de ROS en présence d'AuNPs avec et sans l'utilisation de rayonnements ionisants.

Tout d'abord, nous avons étudié l'effet des AuNPs sur la radiolyse de l'eau en mesurant directement l'évolution des rendements en électrons solvatés dans le temps en utilisant la technique de radiolyse par impulsions picosecondes. Il n'y a pas eu d'augmentation de la production de radicaux primaires de l'eau en présence de AuNPs de différentes tailles et à une concentration allant jusqu'à 3 mM d'or (600 µM/m ou 0,06 % en poids) sous un faisceau d'électrons de 8 MeV.

Ensuite, nous avons étudié l'effet des AuNPs sur la chimie des radicaux organiques par des expériences en régime permanent utilisant la radiolyse gamma. Pour deux types de radicaux produits dans des réactions avec des radicaux $^{\bullet}OH$: le radical α-hydroxyisopropyle formé par l'abstraction de l'atome $^{\bullet}H$ du carbone α du 2-propanol, et les produits formes á partir de l'adduit OH sur de le cycle benzénique de l'acetanilide, nous avons constaté que les AuNPs catalysaient l'oxydation des radicaux organiques transitoires. Ces résultats démontrent que la détection des ROS par des colorants fluorescents ne peut pas être utilisée en présence de nanoparticules catalytiquement actives comme l'or car, dans cette méthode, les radicaux organiques transitoires sont toujours formés comme intermédiaires et les produits des réactions peuvent être modifiés.

En outre, les résultats préliminaires sur l'oxydation de la vitamine C par l'oxygène moléculaire catalysée par les AuNPs sans rayonnement ionisant sont présentés, démontrant la capacité des AuNPs à catalyser les réactions RedOx, ce qui doit être pris en compte lorsque l'on travaille avec des cellules vivantes.

Tous nos résultats indiquent que la propriété cruciale des nanoparticules causant l'effet radiosensibilisant est leur activité catalytique. Dans cette optique, nous proposons un nouveau mécanisme de radiosensibilisation induit par les AuNPs basé sur nos résultats et prenant en compte les données de la littérature.

université PARIS-SACLAY

ÉCOLE DOCTORALE
Sciences Chimiques: Molécules, Matériaux, Instrumentation et Biosystèmes (2MIB)

Title : Chemistry of gold nanoparticles radiosensitizing effect

Keywords : radiosensitization, gold nanoparticle, radical, catalysis

Abstract : Gold nanoparticles (AuNPs) are a promising class of radiosensitizers, agents that increase radiotherapy efficacy. In 2004, it was demonstrated that (AuNPs) accelerated tumour size reduction in mice after radio treatment. The use of gold was motivated by the so-called dose enhancement effect. Since gold has a high atomic number (Z=79), it absorbs more energy at the keV range than water or soft-tissue, increasing the overall ionization of irradiated volume due to the emission of secondary electrons and photons. Later, *in vivo* and *in vitro* experiments showed that the dose enhancement effect could not explain the observed radiosensitization.

Nowadays, the proposed mechanism of nanoparticle-induced radiosensitization includes different physical, chemical and biological effects. However, there is no consensus on the exact mechanism. The chemical effects are usually associated with increased formation of reactive oxygen species (ROS), such as hydroxyl radicals ($^{\bullet}OH$), superoxide radicals ($O_2^{\bullet-}$) and hydrogen peroxide (H_2O_2), in the presence of nanoparticles. The primary method to detect ROS in biological studies is the use of fluorescent dyes. It is based on the oxidation of a non-fluorescent molecule to a fluorescent one in the reaction with ROS, assuming that increase in fluorescent intensity is proportional to the increase in ROS concentration. However, a dye oxidation process is a multistep process that includes the formation of a variety of products (not only the fluorescent one). AuNPs possess catalytic activity, which can change reaction pathways.

In the current work, we examined the idea of increased ROS production in the presence of AuNPs with and without the use of ionizing radiation.

First, we studied the effect of AuNPs on water radiolysis by directly measuring solvated electron yields evolution in time using the picosecond pulse radiolysis technique. There was no increase in primary water radicals production in the presence of AuNPs of different sizes and at a concentration up to 3 mM of gold (600 µM/m or 0.06 wt.%) under an 8 MeV electron beam irradiation.

Then, we studied AuNPs' effect on the chemistry of organic radicals by steady-state experiments using gamma radiolysis. For two types of radicals produced in reactions with $^{\bullet}OH$ radicals: α-hydroxyisopropyl radical formed by $^{\bullet}H$ atom abstraction from α-carbon of 2-propanol, and OH-adducts of acetanilide formed by $^{\bullet}OH$ radical attachment to a benzene ring, we found that AuNPs catalyzed oxidation of transient organic radicals. These results demonstrate that ROS detection by fluorescent dyes cannot be used in the presence of catalytically active nanoparticles such as gold because, in this method, transient organic radicals are always formed as intermediates and the products of the reactions can be modified.

In addition, the preliminary results on Vitamin C oxidation by molecular oxygen catalyzed by AuNPs without ionizing radiation are presented, demonstrating the ability of AuNPs to catalyze RedOx reactions, which has to be considered when working with living cells.

All our results indicate that the crucial properties of nanoparticles causing the radiosensitizing effect is their catalytic activity. In this view, we propose a new mechanism of radiosensitization induced by AuNPs based on our results and taking into account literature data.

Acknowledgements

Becoming a PhD has been my dream since high school. More than ten years have passed since then, and now my thesis is written. I would like to thank all the people who helped me make my dream come true.

I would like to start with my family. I am extremely grateful to my grandparents, who were engineers. Perhaps they were the first to inspire me to study the natural sciences. I would like to express my deepest thanks to my mother and brother for supporting me in all my endeavours, especially my passion for chemistry and, of course, for supporting my decision to move first to Moscow and then to France. I cannot begin to express my thanks to my beloved wife for her love and care. I cannot imagine that I would have done all this without her support. I should also appreciate my friend Alexey for his mental support during a difficult time at the end of my PhD journey.

I am grateful to my chemistry teachers, Lidia I. Kuznetsova and Julia Chernova. I would also like to express my gratitude to Prof. Marina Y. Koroleva, my first supervisor at Mendeleev University. I would also like to thank Dr. Victor Popov for his advice during my university time in Russia and for introducing me to Dr. Sergey A. Denisov.

I would like to extend my deepest gratitude to my supervisors, Prof. Mehran Mostafavi and Dr. Sergey A. Denisov. I was extremely lucky to work under the guidance of such knowledgeable scientists. I really enjoyed the spirit of science, freedom and critical thinking in our group. I could not imagine a better research team for my thesis. I would like to thank Professor Mostafavi for his wisdom, optimism, and guidance. I thank Dr. Denisov for numerous scientific discussions and an equal number of philosophical conversations about science and life. Moreover, it is impossible to overestimate his help in various issues that I encountered during my stay in France.

I appreciate the PhD evaluation committee members, Dr. Sophie Le Caer, Dr. Laura Baciou and Dr. Pascal Pernot, for their valuable comments and advice regarding experimental results. I would also like to thank Dr. Lucie Sancey and Dr. Tomer Zidki for agreeing to be reviewers of my work, and Dr. Fabienne Testard and Dr. Marie Davidkova for agreeing to be jury members for the defense of my dissertation.

I am particularly grateful for the assistance given by Mireille Benoit, Alexandre Demarque, Jean-Philippe Larbre, Pierre Jeunesse Audrey Gayral in experimental work. I also thank Ning Chen and Coline Tavet for contributing to some experiments included in this work

during their internships in our research group. It was very pleasant to work with all of these people.

My warmest thanks go to my friend Dr. Teseer Bahry, who helped me so much from the first day of my work in ICP. I would like to thank all students and researchers I met in ICP, Dr. Hana Valenta, Marija Knezevic, Aisara Amanova, Dr. Sarah Al Gharib, Cong Wang, Dr. Chiraz El Saddik, and many others, for the warm work environment in the lab, numerous discussions about the life of PhD students, funny moments, and rare but lovely after-work parties.

Finally, I would like to thank the administration of ICP, University Paris-Saclay, and doctoral school 2MIB for administrative and financial support of my PhD project.

CONTENTS

GENERAL INTRODUCTION

Radiotherapy (or radiation therapy) is one of the main cancer-fighting methods along with surgery and systemic therapies (e.g., chemo-, target-, immunotherapies). About 50% of patients receive radiation treatment alone or in combination with other methods.[1] At the same time, it is the cheapest way for cancer care, accounting for only 5% of the total costs.[2] Despite radiotherapy effectiveness, it is often accompanied by undesirable side effects. In most cases, patients experience nausea, vomiting and fatigue after radiation, which significantly reduces their quality of life. Radiotherapy also causes visible damage to the skin and can provoke secondary cancers. Moreover, the use of ionizing radiation is limited by the dose allowed for healthy tissues and vital organs close to the tumour. In some cases, the delivered dose is simply not enough to kill cancer cells.

One of the ways to increase radiotherapy efficacy and decrease side effects is to utilize radiosensitizers, agents that increase cell death caused by radiation. Nanoparticles are promising radiosensitizers, which demonstrated their ability to increase cell death and tumour destruction caused by radiation in many research works done last 17 years. For the first time, the radiosensitizing effect of nanoparticles was demonstrated by gold nanoparticles (AuNPs). To date, AuNPs are the most frequently studied. However, they are not yet applied in clinics. The use of gold was suggested because of its physical properties, namely its high atomic number (Z), which causes higher energy absorption than water or soft tissue, leading to higher dose deposition. Later on, the discrepancy between the observed radiosensitizing effect and the predicted results by the initial “physical” hypothesis prompted scientists to look for other mechanisms in biology and chemistry. Nowadays, it is believed that AuNPs' radiosensitizing effect includes different physical, chemical, and biological processes. The chemistry of radiosensitization remains the most little-studied area. The main reason is that AuNPs have long been considered chemically inert. In biomedical research, nanoparticles are still often assumed as inert materials. Another reason is that chemists, especially radiation chemists, are less involved in studying AuNPs' radiosensitizing effect than physicists and biologists. We believe that the mechanism of the AuNps radiosensitizing effect is still not understood due to insufficient study of the role of AuNPs' chemical properties.

The work you are reading is devoted to chemical aspects of radiosensitization induced by AuNPs. In my thesis, I use the knowledge of radiation chemistry to approach the key questions on the mechanism of AuNPs induced radiosensitization. With an experimental approach and quantitative measurements, I show that gold nanoparticles' catalytic effect,

which can play a key role in chemical transformation in biological systems, is usually omitted.

The manuscript consists of 6 chapters. In Chapter 1, the essential notions and basic knowledge of radiation chemistry are introduced to understand the work results. The chapter also contains the state of thoughts on radiotherapy and radiosensitization. Current understanding of nanoparticle-induced radiosensitization mechanism is given at the end of the chapter, along with a discussion of the research objectives of the thesis.

Chapter 2 contains information about AuNPs used in experiments. In the following two chapters, the effects of aqueous solutions containing AuNPs under ionizing radiation (electron beam and gamma radiation) are investigated, first the effect on water radiolysis and formation of primary water radicals by means of pulsed radiolysis (Chapter 3), then gold nanoparticles interaction with secondary organic radicals (Chapter 4). The results presented in these two chapters allow us to reject some of the proposed hypotheses about the mechanism of nanoparticles' radiosensitizing effect and show that the catalytic properties of nanoparticles play an important role. Subsequently, Chapter 5 presents preliminary results of the gold nanoparticles' catalytic activity in the oxidation of mild electron donors without radiation. The results explain why oxidative stress is often observed in the living cells loaded with different nanoparticles. In the concluding Chapter 6, summarizing all of the experimental results as well as the literature data, a new vision of the radiosensitization mechanism is presented.

CHAPTER 1. STATE OF THE ART

Contents

1.1. IONIZING RADIATION AND CONDENSED MATTER

Ionizing radiation is a form of energy that can eject electrons from atoms and molecules of materials. In our experiments, we used two radiation sources: an 8 MeV electron beam (ELYSE electron accelerator) and a source of gamma radiation (^{60}Co) emitting two photons with an average energy of 1.25 MeV. These two sources are different in nature, ionizing photons and accelerated charged particles. Nevertheless, in both cases, the energy transfer occurs mainly through inelastic collisions of secondary electrons arising from the first interaction of primary radiation with matter. For 8 MeV electrons, the interaction occurs mainly by Inelastic Collisions, while for the gamma radiation it occurs mainly by the Compton effect. Several ionization in small isolated vicinity form spurs (Figure 1.1).

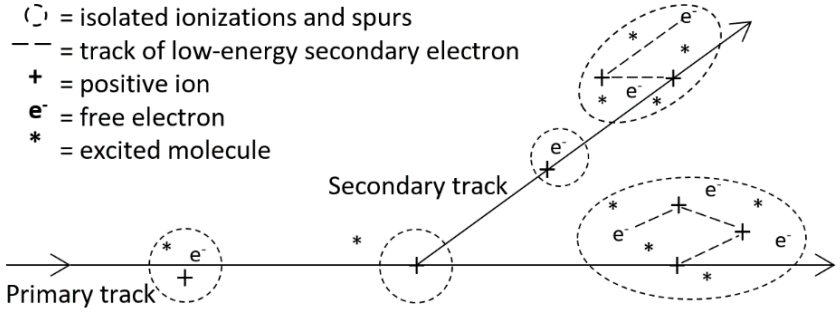

Figure 1.1. Distribution of ions and excited molecules in the track of a fast electron.[3]

Ionizing radiation is also classified by linear energy transfer (LET), a physical parameter, which characterizes the amount of energy transferred to the matter per unit of distance. High- and low-LET radiation produce tracks with different structures (Figure 1.2). In the case of high-LET, the track is much denser, ionization and excitation events occur close to each other.

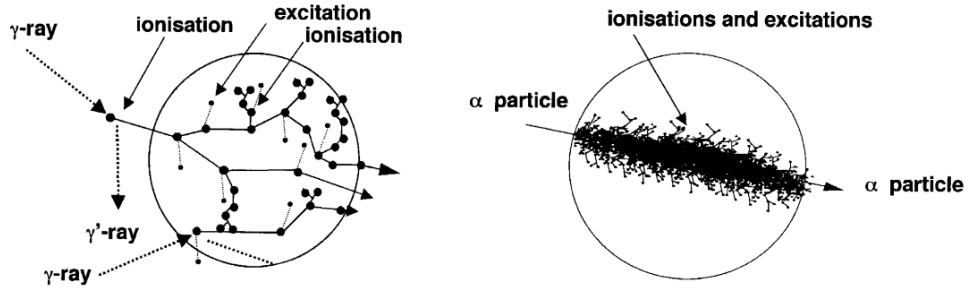

Figure 1.2. Schematic representation of the track structure of low-LET (left) and high-LET (right) radiation.[4]

LET is applied for directly ionizing radiation such as electrons. In the case of gamma photons, LET corresponds to secondary electrons. Both types of radiation used in our experiments produce a track structure of low-LET radiation.

Ionization processes depend not only on radiation but also on the matter it interacts with. There is a difference in the interaction of ionizing radiation with the gas phase and condensed matter. Condensed matter, such as liquids, has a short distance between species and low mobility, which leads to solvation and cage effects in solutions. One of the most critical characteristics of condensed matter affecting energy absorption is the Z number.

Heterogeneous systems consisting of solid-phase (metals with high Z) and liquid-phase (water, low Z) were used in all experiments presented in the current manuscript. Therefore, we will first discuss ionization processes occurring in water and then some effects associated with the presence of a solid phase with a high Z number in aqueous solutions.

1.1.1. Water radiolysis

Radiolysis is a dissociation of molecules by ionizing radiation. It starts from energy absorption by water molecules, which leads to ionization and excitation processes (Figure 1.3). The following pre-thermal step includes hydroxyl radicals ($^{\bullet}OH$) formation by proton transfer from water radical cation ($H_2O^{\bullet+}$) to a neutral water molecule as well as by dissociation of excited water molecules into ($^{\bullet}OH$) and hydrogen atoms ($H^{\bullet}$).

Stage			Time scale
Energy absorption	$H_2O \xrightarrow{\text{excitation}} H_2O^*$		10^{-16} s
	$H_2O \xrightarrow{\text{ionization}} H_2O^{\bullet+} + e^-$		
Pre-thermal step	$H_2O^{\bullet+} + H_2O \rightarrow H_3O^+ + {}^{\bullet}OH$		10^{-14} s
	$H_2O^* \rightarrow H^{\bullet} + {}^{\bullet}OH$		10^{-13} s
	$e^- \xrightarrow{\text{solvation}} e_s^-$		10^{-12} s
Reactions in spurs	$e_s^- + e_s^- \xrightarrow{H_2O} H_2 + 2OH^-$	0.55	Rate constant ($\times 10^{10}$, $M^{-1}s^{-1}$)
	$e_s^- + H^{\bullet} \rightarrow H_2 + 2OH^-$	2.50	
	$e_s^- + H_3O^+ \rightarrow H^{\bullet} + H_2O$	2.30	
	$e_s^- + {}^{\bullet}OH \rightarrow OH^-$	3.00	
	${}^{\bullet}OH + {}^{\bullet}OH \rightarrow H_2O_2$	0.55	
	${}^{\bullet}OH + H^{\bullet} \rightarrow H_2O$	2.00	
Homogenous step of water radiolysis	$e_s^-, {}^{\bullet}H, {}^{\bullet}OH, H_2, H_2O_2$		10^{-7} s

Figure 1.3. Stages of water radiolysis.[5]

The electron released after water ionization has kinetic energy and can ionize and excite other water molecules, provoking a cascade of secondary electrons. After all, these secondary electrons losing all kinetic energy become partially solvated (e^-_{pre}) having potential energy only (Figure 1.4). Then the solvation process occurs, which is a reorganization of solvent molecules around the electron. Such electron in a cavity of solvent molecules is called solvated (e^-_s). In the particular case of water, it is called hydrated electron (e^-_{aq}). The hydrated electron has an energy of -1.6 eV. The complete solvation in water occurs within one picosecond.[6] The hydrated electron is a strong reductant with a redox potential of -2.8 V NHE.[5]

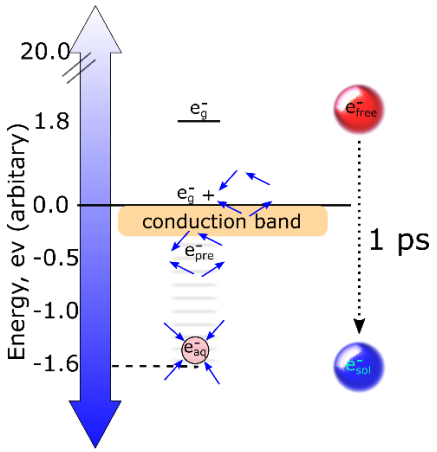

Figure 1.4. The schema of electron solvation.

Hydroxyl radical is considered to be the most harmful radical for living organisms. Due to its high redox potential of 1.9 V NHE,[5] it is able to oxidize any biomolecules like proteins, fatty acids, DNA and RNA bases, etc. Produced radicals are highly reactive and react with each other in spurs (Figure 1.3), leading to the formation of molecular products of water radiolysis such as hydrogen peroxide (H_2O_2) and molecular hydrogen (H_2).

The first acts of ionization produce spurs, where primary water radicals are formed during the pre-thermal step of water radiolysis. Due to thermal diffusion, their size is increased with time, decreasing the probability of radical-radical interaction. After 100 ns, water radiolysis products have a homogeneous distribution in the solution. Therefore, in radiolysis, non-homogeneous (reactions in spurs) and homogeneous steps are distinguished (Figure 1.3).

Living systems mainly consist of water; therefore, water radiolysis is important for biological studies. Due to the biological consequences of water radiolysis, two more stages are distinguished: the biochemical steps (~10^{-3} to 10^4 s) and the biological stage

(~10^2 to ~10^8 s). Secondary radicals form, evolve, and react within the biochemical step, whereas the biological stage covers a wide range of time from mitosis to late biological effects.[7]

1.1.2. Radiolytic yield

The number of species produced per unit of absorbed energy is called radiolytic yield. Previously, the radiolytic yield was expressed as the number of species produced per 100 eV of absorbed energy. Nowadays, it is expressed in moles of species produced per 1 joule of absorbed energy (mol J^{-1}). The relation between old and SI units is 1/100 eV= 1.0375 mol J^{-1}. Despite that SI units are more convenient in chemistry, the units in a number of species produced per 100 eV give more physical meaning. For example, considering the ionization energy of most of the molecules as 10 eV, we cannot expect the radiolytic yield more significant than 10 per 100 eV. The initial radiolytic yield of solvated electrons in most solvents is around 4.2 per 100 eV because not all absorbed energy leads to ionization. For example, initial radiolytic yields (at 10 ps) of solvated electrons and hydroxyl radicals in water are 4.4 and 5.2 × 10^{-7} mol J^{-1}, respectively.[8] The fast decay of solvated electrons and •OH radicals within the first nanosecond (Figure 1.5) is due to the short distance between the radicals in spurs.

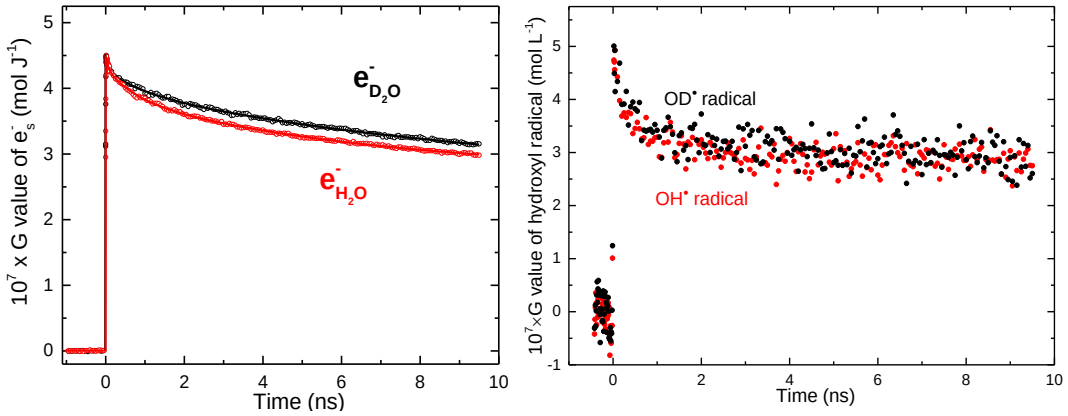

Figure 1.5. Radiolytic yields of solvated electrons and hydroxyl radicals in H_2O and D_2O versus time, measured by pulse-radiolysis technique.[8]

Spurs increase in size due to thermal diffusion, reducing the probability of radical reactions, which leads to a uniform distribution of radiolysis products in water approximately 100 ns after energy absorption. Radiolytic yields of the products at the homogenous step of water radiolysis are well-studied for ionizing radiation with different LET and various conditions, e.g., pH (Table 1.1). Gamma radiation and accelerated

electrons have a LET value of 0.2–0.3 keV μm^{-1}, whereas, in the case of 5.3 MeV alpha particles (^{210}Po), the LET value is 140 keV μm^{-1}.[5]

Table 1.1. Radiolytic yields (G) of water radiolysis products at 100 ns.[5]

Radiation source	pH	G, [μmol J^{-1}]				
		e_s^-	$^{\bullet}OH$	$^{\bullet}H$	H_2	H_2O_2
Electrons (0.1-10 MeV)	3 - 11	0.28	0.28	0.06	0.047	0.073
Electrons (0.1-10 MeV)	0.5	0	0.301	0.378	0.041	0.081
5.3 MeV α particles (^{210}Po)	0.5	0	0.052	0.062	0.163	0.150

At low pH, solvated electrons are scavenged by H^+ forming $H^{\bullet}$. It also affects the yield of $^{\bullet}OH$, which is slightly higher than at neutral pH. The reason is that $^{\bullet}OH$ radicals react slower with $^{\bullet}H$ atoms than with solvated electrons. Therefore, more $^{\bullet}OH$ radicals avoid recombination at low pH. The spurs are closer together for high LET radiations, such as alpha particles. This leads to their faster overlap, which increases the probability of reactions between radicals leading to higher yields of H_2 and H_2O_2.

1.1.3. Dosimetry

Dosimetry is an important part of radiation research, devoted to determining absorbed doses by materials. Nowadays, there are a lot of well-established methods of dosimetry. In principle, all of them are based on the measurements of changes in matter caused by radiation, such as heating, ionization, formation of radicals, etc.

Some methods are more fundamental and used for absolute dosimetry and characterization of radiation machines, for example, ionization chambers.

Chemical methods, such as Fricke dosimetry, are usually used in radiation chemistry. Fricke dosimetry is based on Fe^{2+} oxidation to Fe^{3+} during water radiolysis in a very acidic aqueous solution. Then, the concentration of formed Fe^{3+} is measured by its absorption, and the dose can be calculated by Equation 1.1, representing the relation between the concentration (C, mol L^{-1}), applied dose (D, Gy or J kg^{-1}), radiolytic yield (G, mol J^{-1}), ρ - solution density in kg L^{-1}.

$$C = D \times G \times \rho \quad \text{(eq. 1.1)}$$

In principle, any radiation-induced reactions can be used for dosimetry if the radiolytic yield of produced or consumed species is known. However, one should never forget that radiolytic yield is a function of time. Therefore, it is crucial to know the kinetics of the reaction between water radicals and the solute. Moreover, it must be confirmed that the

reaction mechanism stays unchanged under different experimental conditions for the broad application of a new method.

1.1.4. Cross-section and dose enhancement effect

With regard to the interaction of ionizing radiation with condensed matter, cross-section means a probability of ionization acts when radiation passes through the media. For the particular energy of radiation, the cross-section depends on the electron density of the media. If the irradiated system consists of two substances, the energy will be absorbed by both proportionally to the electron density. Therefore, even a relatively small fraction of a material with high-Z increases energy absorption by the system. The energy absorbed by high-Z materials like gold leads to the emission of secondary photons and electrons by photoelectric and Compton effects, which causes additional ionization of surrounding media.

A rough estimation of the dose enhancement effect based on the difference in mass-energy absorption coefficient for a given energy and gold concentration is given in Table 1.2. Figure 1.6 represents the mass-energy absorption coefficient of gold compared to soft tissue.

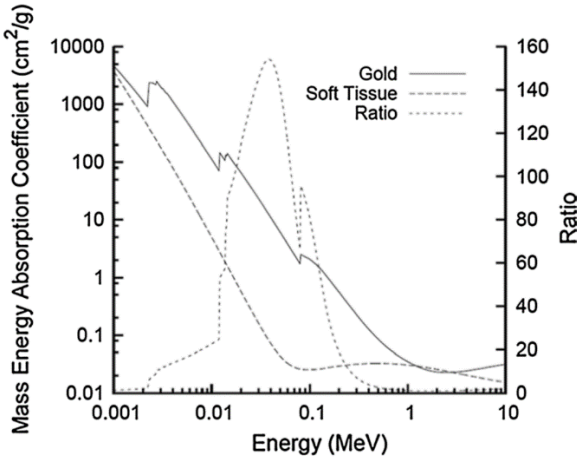

Figure 1.6. The mass-energy absorption coefficient of gold and soft tissue.[9]

Table 1.2. Estimated dose enhancement effect for gold at different concentrations and three different energies of ionizing radiation.

Gold concentration			**Dose enhancement**		
wt.%	***µg/ml***	***mM***	***10 keV***	***40 keV***	***1 MeV***
0.65	6580	33	13 %	100 %	0 %
0.06	600	3	1.2 %	9 %	0 %
0.01	100	0.5	0.2 %	2 %	0 %

The probability of absorbing 40 keV photon is 150 times higher for gold than soft-tissue or water. But we have to take into account the mass proportions. For example, if the metal concentration is low even at 40 keV the interaction occurs with more abundant water molecules. Also, if the energy is close to 1 MeV, it will not cause the dose enhancement even at a relatively high gold concentration.

1.2. RADIOTHERAPY

Already a year after the discovery of X-rays in 1895 by Wilhelm Roentgen, they began to be used to treat cancer. In 2020, about 10 million patients have been treated by radiotherapy as one of the main cancer-fighting methods along with surgery and systemic therapies (e.g., chemo-, target-, immunotherapies). In general, about 50% of patients receive radiation treatment alone or in combination with other methods.[10] At the same time, it is the cheapest way for cancer care, accounting for only 5% of the total costs.[2] Despite radio-treatment effectiveness, it is often accompanied by different side effects. In the worst-case, radiotherapy might lead to the formation of secondary cancer. The second most problematic side effect is visible skin lesions at the radiation site. Treatment of each type of cancer with radiation therapy has different side effects, such as fatigue, hair loss, nausea, vomiting, headache, blurred vision – the classic symptoms of radiation sickness. The use of radiation is limited by the dose allowed for healthy tissues and vital organs close to the tumour. In some cases, the allowed dose is not enough to kill cancer cells. Therefore, there is always a need to improve radiotherapy's effectiveness and decrease side effects.

There are two ways to deliver radiation to a tumour: using external radiation sources or injecting radioactive materials directly into or near the tumour (brachytherapy). Radiation causes cell damage via direct ionization of biomolecules and by indirect effect producing radicals and molecules such as H_2O_2 in water radiolysis (Figure 1.7). Since cells contain up to 70-80% water, the indirect effect is considered the main way of damage.

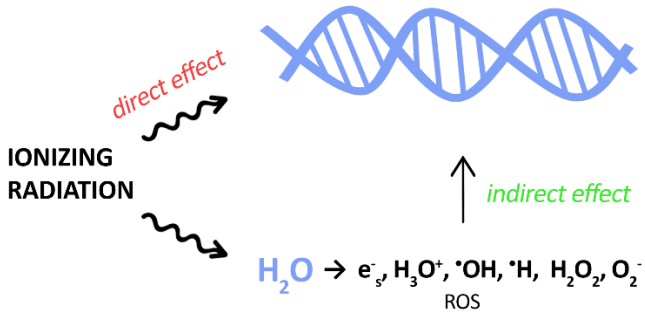

Figure 1.7. Direct and indirect damage caused by ionizing radiation.

Over the past decades, dose deposition has significantly been improved by developing software and radiation sources. The transition from conventional radiotherapy to 3D conformal radiotherapy and intensity-modulated radiotherapy (IMRT) significantly decreased irradiation of healthy tissues. Also, utilization of protons and other heavy ions instead of X-rays and electrons helped to achieve better dose distribution due to the Bragg peak, which allows depositing most of the energy of the radiation beam at a certain distance from the source.

The application of fractionated radiotherapy is another way that greatly improves radiotherapy outcomes. It was found that the delivery of the same dose in several steps is less dangerous for normal cells compared to one step. Fractionated radiotherapy was based on four factors: repair, redistribution, repopulation, and reoxygenation.[11] The fifth factor - radiosensitivity complements the so-called "5 R's of radiotherapy".[1,12] The four factors are briefly described below and cell radiosensitivity will be discussed in the next section.

- Repair: DNA molecules are essential for cell survival and normal functioning. Therefore, there are systems to repair DNA damage in cells and keep its level as low as possible. Ionizing radiation causes DNA single and double-strand breaks (SSB and DSB). Radiation of 1 Gy can create ca. 40 DSBs per cell. Even one remaining DSB is important and can induce apoptosis, necrosis, mitotic catastrophe, or permanent growth arrest of the cell. Thus, unrepaired DSBs may determine the anti-tumour effects of ionizing radiation. The capacity of cells for DSB repair is an essential parameter affecting radiotherapy effectiveness. When the dose of radiation is divided into several smaller fractions delivered at intervals of hours, cells have a better chance of repairing damage, which increases their survival. It is generally accepted that normal cells can recover more successfully than tumour cells. Thus, fractionated radiotherapy can protect normal tissues without decreasing the antitumor effect.[1,12]
- Redistribution: During replication, cells pass through 4 phases of the cell cycle (G1, S, G2, and M). In each phase, cells have different radiosensitivity. Cells in M phases are the most sensitive to radiation, while they are the most radio-resistant in the S phase. Therefore, when the same dose is delivered in multiple fractions, more cells will be irradiated in more radiosensitive phases of the cell cycle.
- Repopulation: active growth and proliferation of cancer cells reduce the effectiveness of radiation therapy. However, radiation leads to the arrest of the cell cycle, which

slowdowns cell proliferation and growth. This process is more efficient when cells are in the more radiosensitive phase of the cell cycle.

- Reoxygenation: cells with low oxygen levels (hypoxia) are more radio-resistant than cells with normal oxygen levels (normoxia), emphasizing the critical role of oxygen in cell killing by radiation. In general, cells irradiated by low-LET radiation under normal oxygenated conditions are two- to three-fold more radiosensitive than cells irradiated under hypoxic or anoxic conditions.[1,13] Cancer cells often have low oxygen levels, which increases their radioresistance. Reoxygenation may result from increased or redistributed blood flow, reduced oxygen utilization by radiation-damaged cells, or rapid removal of radiation-damaged cells so that the hypoxic cells become closer to functional blood vessels.[10]

1.3. RADIOSENSITIZERS

According to the National Cancer Institute dictionary of cancer terms, radiosensitization is the use of drugs (radiosensitizers) that make tumour cells more sensitive to radiation therapy. The sensitivity of cells to radiation depends on many parameters, such as cell type, cell cycle stage, oxygen concentration, etc., which are discussed above.[1,12] The use of radiosensitizers aims to enhance the difference in response to irradiation by tumours and healthy tissues. This is shown schematically in Figure 1.8. The use of radiosensitizers increases the probability of cancer cure without complication at lower doses.

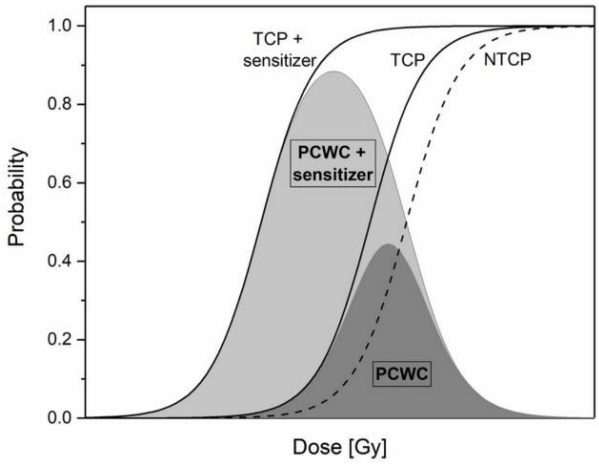

Figure 1.8. Tumour-targeted radiosensitizer's action on the probability of cure without complication (PCWC). The tumour control probability (TCP, solid line) and normal tissue complication probability (NTCP, dashed line) are shown as a function of the dose delivered to the patient. Two scenarios are illustrated with or without the use of a radiosensitizer, and the associated PCWC is shown by the surface in each case.[12]

At first, radiosensitizers were classified into five categories: suppressors of radio-protective substances, radiation-induced cytotoxic substances, inhibitors of post-radiation cellular repair processes, sensitizers by structural incorporation of thymine analogues into intracellular DNA and oxygen-mimetic sensitizers.[14,15] Later on, other types of radiosensitizers were developed, such as radiosensitizers targeting proteins involved in cell signalling and growth factors, which were discussed elsewhere.[16] In a more recent review, cancer radiosensitizers were classified into three large categories: small-molecule chemicals, nanostructure and macromolecules including microRNA, proteins and peptides as well as oligonucleotides and siRNAs.[17]

Different radiosensitizers affect outcomes of radiotherapy in different ways. For many radiosensitizers, the exact mechanism is not understood. For further discussion of experimental results, we need to consider a few types of radiosensitizers and mechanisms of their action.

1.3.1. Oxygen and its mimics

One of the first discovered radiosensitizers is oxygen, which acts by damage fixation (Figure 1.9). Radicals produced in water radiolysis, such as •OH radicals, quickly react with organic molecules in the cell, forming secondary organic radicals.[18,19] These radicals can be repaired by electron donors like glutathione (GSH).[17] However, oxygen can attach to such radicals preventing their reaction with protective molecules. There is a group of radiosensitizing molecules mimicking the oxygen effect. They are mainly compounds containing a nitro group e.g. nitroimidazole, misonidazole (2-nitro imidazole), Pimonidazole, Nimorazole (5-nitroimidazole).[17]

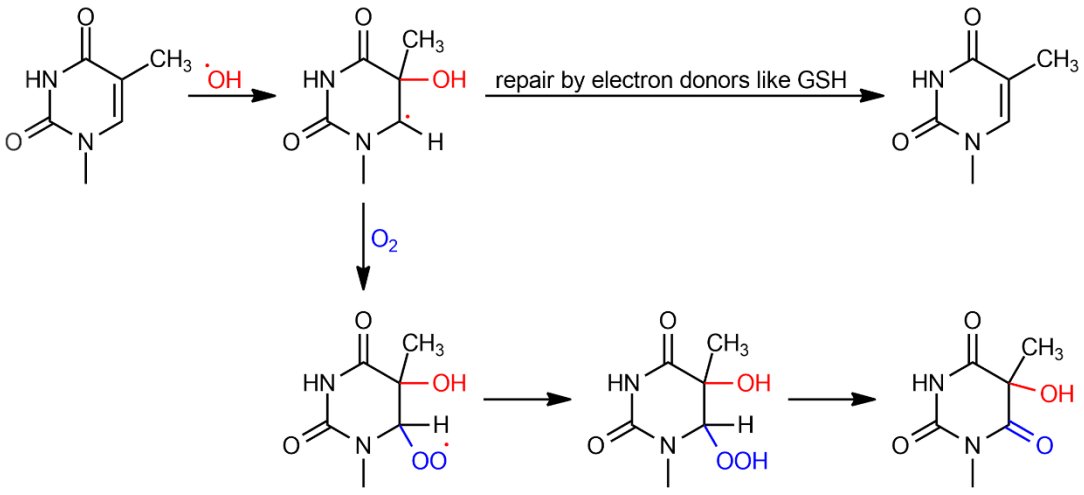

Figure 1.9. Mechanism of radical-mediated DNA damage and the effect of oxygen.[17]

1.3.2. Suppression of radio-protective substances

Reactive oxygen species produced during water radiolysis cause oxidative effects on cellular compounds. Electron donor molecules in cells play an essential role in radioprotection. Therefore, suppression of such radio-protective substances improves radiotherapy efficiency. In this respect, radiosensitizers can work in two ways: directly oxidize electron donors (e.g. glutathione, vitamin C, etc.) or suppress the functioning of enzymes (e.g. glutathione reductase, oxidoreductases, superoxide dismutase etc.), which produce radio-protective substances or scavenge ROS.[17]

1.3.3. Nanoparticles

In 2004, James F. Hainfeld et al. demonstrated that 1.9 nm gold nanoparticles (AuNPs) injected into cancer tumours in mice significantly slow down tumour growth after irradiation with X-rays of 250 kVp (Figure 1.10).[20] The mechanism of AuNPs action was explained by the dose enhancement effect discussed in section 1.1.3.

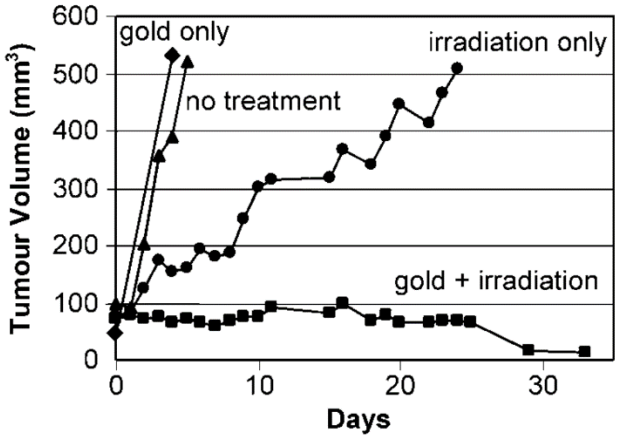

Figure 1.10. Average tumour volume after: (a) no treatment (triangles, n = 12); (b) gold only (diamonds, n = 4); (c) irradiation only (30 Gy, 250 kVp, circles, n = 11); (d) intravenous gold injection (1.35 g Au/kg) followed by irradiation (squares, n = 10).[20]

At first, AuNPs radiosensitizing effect was attributed to the dose enhancement only. Therefore, they were called "dose enhancers" in some works instead of radiosensitizers. In more recent works, the term "radiosensitization" is used for all cases when the use of any substances enhance the effect of radiation therapy (cell death or tumor shrinkage), regardless of their mechanism of action.

Since 2004, tremendous attention has been attracted to the use of nanoparticles as radiosensitizers. Most attention in research has been paid to AuNPs, not only because of the pioneering work but also because they are desirable material for bio-applications due

to their facile synthesis, small size, versatile surface chemistry, easy cell membrane penetration properties, and expected low toxicity.[21] However, to date, AuNPs have not been clinically tested for use in cancer radiation therapy.

There are two other types of nanoparticles made from high-Z materials that are being clinically tested as radiosensitizers for various types of tumours. Company Nanobiotix has recently received marketing authorization in Europe for the treatment of soft tissue sarcoma for a drug named Hensify® (the previous name used in the literature is NBTXR3), which is 50 nm hafnium oxide nanoparticles. AGuIX is a product owned by another company NH TherAguix. This drug is 5 nm nanoparticles made of a polysiloxane matrix loaded with gadolinium chelates. AGuIX is undergoing phase II clinical trials for brain metastases. Both products (Hensify® and AGuIX) were developed more than ten years ago. At that time, the dominant explanation of nanoparticles' radiosensitizing effect was physical dose enhancement. Therefore, both products contain high Z material Hf (Z = 72) and Gd (Z = 64). However, following Hainfeld's pioneering work, a rapidly growing number of works with *in vitro* and *in vivo* experiments clearly showed that the radiosensitizing effect caused by different nanoparticles could not be explained only by the dose enhancement effect.[22] It became evident that the mechanism of radiosensitization is more complex. It is currently assumed that nanoparticles such as gold can influence various physical, chemical, and biological processes, which ultimately leads to enhanced effects caused by ionizing radiation such as ionization of the media, cell death, formation, or destruction of molecules.

1.4. Mechanism of nanoparticles radiosensitizing effect

There is a sufficient number of reviews analyzing all available data,[23] and discussing individually chemical[24] or physical and biological[9,22] effects potentially responsible for the radiosensitizing effect. But, up to date, there is no clear and consistent explanation of the radiosensitization mechanism induced by AuNPs. Most review articles summarize interpretations rather than observations. This leads to the existence of many hypotheses that cannot be summarized. Even such assumptions have been put forward quote: "*the large degree of variability from one nanoparticle to another emphasizes that it is a mistake to generalize nanoparticle radiosensitizer mechanisms.*"[25] Perhaps one of the best attempts to summarize all proposed mechanisms of nanoparticles radiosensitizing effect has been made T. Guo.[26] Briefly, all effects of nanoparticles are also divided into physical, chemical, and biological, but the potential impact of each effect depending on conditions, such as

nanoparticles concentration, their surface, the energy of ionizing radiation, etc., was discussed.

The most commonly reported effects of nanoparticles will be discussed below, dividing them into physical, chemical and biological, as suggested in the literature.

1.4.1. Physical

The seminal work of J. Hainfeld[20] was inspired by a few previous studies utilizing gold as a dose enhancer. In the first experiments using foils, interface effects were studied between high-Z material and cell monolayer under X-ray radiation.[27] Then gold microspheres of 1.5–3 μm with concentration up to 3 wt.% were used to treat tumours in mice.[28] Such a high concentration of gold led to the radiosensitizing effect. Tumour treatment was more efficient with gold microspheres compared to radiation alone. An important point of this work is that the dose enhancement effect was verified by Fricke dosimetry (a chemical method to measure the dose). The dose enhancement effect was present only for X-ray ionizing radiation but not for γ-rays (^{137}Cs). Thus, the results were in agreement with the theoretical prediction because higher energy absorption by gold is expected only for the energy ranging from 10 to 100 keV, which is not the case for the ^{137}Cs gamma source. It is important to mention that J. Hainfeld used a high concentration of gold, up to 2.7 g of gold per 1 kg of mice weight, which corresponded to 7 mg Au/ g of the tumour, in combination with X-ray radiation. Therefore, it was logical to explain the observed radiosensitizing effect of AuNPs by dose enhancement as in previous works.

The dose enhancement was experimentally measured for silica-covered gold nanoparticles with different concentrations using thin filtered X-ray radiation.[29] The results showed ca. 1 wt.% of gold is required to enhance the dose two times for energies below 100 keV. However, the dose enhancement is absent for the ionizing radiation energy above 100 keV since there is no difference in energy absorption by gold (or another high-Z material) and water. Moreover, it is almost impossible to deliver such a high amount of metal to the tumour avoiding toxic effects. Figure 1.11 compares *in vivo* observed radiosensitizing effect plotted versus gold concentration with that predicted by the dose enhancement concept.[12,30] There are no works utilizing gold concentration higher than 0.4 wt.%. This summary shows that predicted dose enhancement does not correlate with gold concentration. For example, for ca. 0.02 wt.% and ca. 0.3 wt.% of gold, there is almost no difference in reported dose enhancement. It is valid for photons of keV and MeV energies and protons. Moreover, the observed effects are usually more significant than

the predicted ones. Such inconsistency opened a road to search for other mechanisms of nanoparticles action.[23]

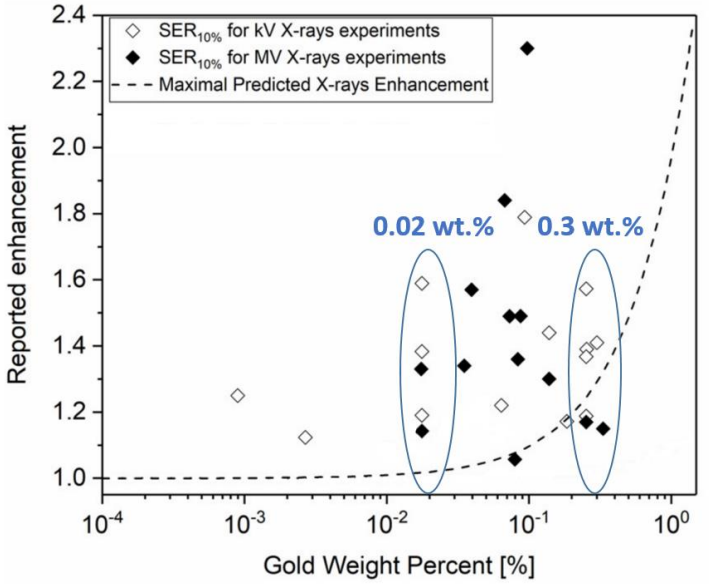

Figure 1.11. Comparison of observed *in vitro* experimental sensitization enhancement ratio (SER) with predicted dose enhancement values.[12,30]

As it was discussed in section 1.1.3, the dose enhancement effect occurs by photoelectric and Compton effects. Both effects lead to the emission of secondary electrons with sufficient energy, which can cross a significant distance ionizing the media. Therefore, these two effects enhance ionization homogeneously. In the Compton effect, an incident photon is scattered by an electron of the outer shell of an atom leading to its ejection. In contrast, in the photoelectric effect, an incident photon is fully absorbed, leading to the ejection of an electron from the inner shell. Further filling of inner-shell vacancies by outer-shell electrons leads to the emission of photons (fluorescence) and Auger electrons with low energy. Low-energy Auger electrons can travel only a few hundred nanometers.[9] Therefore, they cause ionization of the environment in a small neighbourhood next to the nanoparticle. For bulk gold, this effect is assumed to be negligible since Auger-electrons are quickly stopped by other gold atoms, but for gold nanoparticles, this effect is believed to play an important role in the radiosensitization. The main doubt regarding this nanoscale dose enhancement effect caused by low-energy electrons is that nanoparticles should be localized near the target, such as DNA or other bio-molecules. Otherwise, this effect will be negligible. Using conventional radiation sources, the amount of energy deposited in the NPs is extremely low, and such effect is minor.

1.4.2. Chemical

As noted in some review articles, the chemical effects are the least studied.[12,23] There are several reasons for this. First of all, gold nanoparticles have long been considered chemically inert, like bulk gold. To this day, in research works not dealing with catalysis, one can find the opinion that nanoparticles are chemically inert. Another reason is that chemists are much less involved in the study of radiosensitization than physicists or biologists.

Chemical effects proposed in the literature are associated with the effect of AuNPs on the concentration of reactive oxygen species (ROS), such as hydroxyl radicals ($^{\bullet}OH$), superoxide radicals ($O_2^{\bullet-}$) and hydrogen peroxide (H_2O_2). In most of the works, it is stated that ROS production is increased in the presence of AuNPs as with the use of ionizing radiation and without it.[12,23,24,26] A small number of cases when ROS concentration was decreased in the presence of nanoparticles was discussed elsewhere.[26] As it has been highlighted in the same article, it is important to distinguish between physical effects such as overall and local dose enhancement discussed in the previous section and increased ROS production due to the chemical impacts. The problem is that dose enhancement causes higher ionization of the media leading to a higher concentration of primary water radicals and ROS.

In the absence of ionizing radiation, the formation of superoxide radicals in the presence of AuNPs was reported. It has been proposed that oxygen can be reduced catalytically on the AuNPs surface by electron donors present in a cell.[31] Additional ROS formation during radiation exposure has also been reported. In this case, it has been suggested that secondary low-energy electrons emitted from AuNP interact and ionize oxygen-containing molecules in the vicinity of the nanoparticle, generating ROS.[24,32] This explanation is similar to the nanoscale dose enhancement discussed in the previous section. Therefore, the same doubt related to the extremely low amount of energy deposited directly in the AuNP applies to this explanation. Overproduction of $^{\bullet}OH$ radicals in the presence of AuNPs has been reported only under radiation exposure.[32–34] In some works, 4.5 fold-increase in $^{\bullet}OH$ formation was reported. It was explained by the special properties of interface water which has a lower level of ionization leading to a higher radiolytic yield of $^{\bullet}OH$ radical formation as well as solvated electrons.[33,34] A similar phenomenon, namely the effect of AuNP on the ionization potential of molecules, was demonstrated in two other works but using DNA molecules. The works were discussed elsewhere.[23] First, it was shown that 10 eV electrons produce the most significant DNA

damage in the presence of AuNPs. DNA damage induced by 10 eV electrons was examined for two DNA-AuNP complexes prepared with positively charged 5 nm nanoparticles and negatively-charged 15 nm nanoparticles.[35] Tight binding of the small, positive AuNPs to the PO_4 groups of DNA led to significant damage, reaching an enhancement factor of 4.5 at a 1:1 ratio of DNA: AuNP.[36] Important to say that these experiments utilizing DNA-AuNPs complex cannot be compared with those reporting •OH radical overproduction because •OH radicals were measured in a homogenous solution. The amount of interface water molecules is negligible compared to bulk water molecules. Meanwhile, in the experiment with DNA, DNA: AuNP ratio was 1:1. Thus, the mechanism of •OH radical overproduction in the presence of AuNPs remains unclear.

1.4.3. Biological

In contrast to chemical effects, the biological effects of gold nanoparticles are more studied. Such effects as DNA repair inhibition, cell cycle disruption and oxidative stress caused by nanoparticles are usually highlighted in works devoted to radiosensitization.[9,22,23,37] Moreover, in a recent review entitled "Gold Nanoparticles as a Potent Radiosensitizer: A Transdisciplinary Approach from Physics to Patient", a large amount of data on the toxicity of nanoparticles have been reviewed in the context of radiosensitization.[12] There is a lot of evidence that AuNPs affect gene expression and can change the activity of proteins. The molecular basis of any biological process is complex and lies in the field of biochemistry, which is outside the scope of research presented here. Nonetheless, the proposed biological effects of AuNP will be taken into account in the discussion of our experimental results.

1.4.4. Summary

Summarizing the most often reported effects of AuNPs in the context of radiosensitization, the chemical effect can be placed in the centre as a bridge between physical and biological effects (Figure 1.12). Because among all the discussed effects, ROS production, which is a chemical process, can be associated with physical and biological effects. The physical way to increase ROS concentration is clear: ionizing radiation causes ROS production via water radiolysis. Therefore, the dose enhancement by AuNPs will increase ROS concentration homogenously by Photoelectric and Compton effects or locally by low-energy Auger electrons. The problem is that ROS concentration measured in the presence of AuNPs under radiation is almost often higher than can be explained by the physical effects. At the same time, higher ROS concentration in the presence of AuNPs

agrees with observed oxidative stress, which is a disbalance between antioxidants and prooxidants, such as ROS, in cells. However, oxidative stress was also observed without radiation. Thus, AuNPs should also produce ROS independently from radiation, which has not been studied yet.

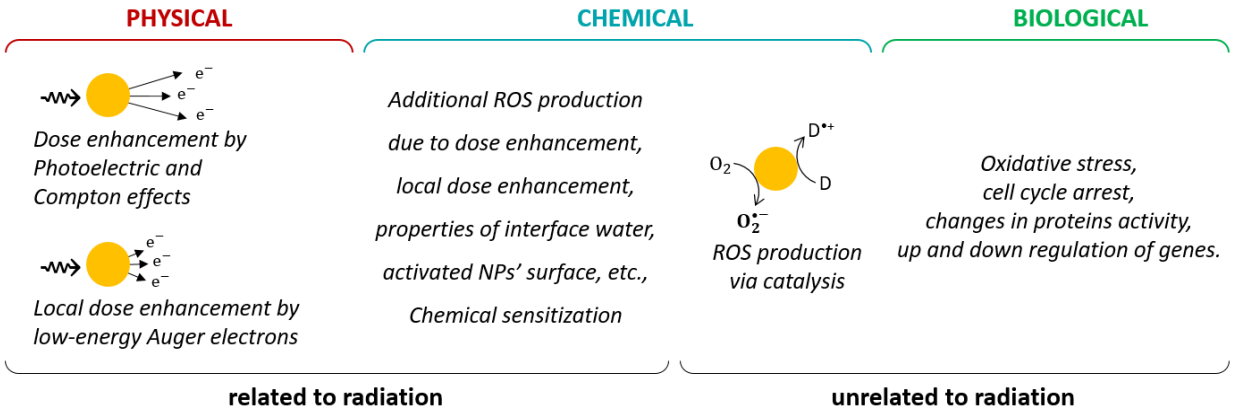

Figure 1.12. Summary of the effects of gold nanoparticles thought to be responsible for the radiosensitizing effect.

The proposed chemical ways for increasing the concentration of ROS in the presence of AuNPs both under the action of irradiation and without it do not have sufficient evidence and require verification. Moreover, as discussed in the sub-section of biological effects, there is a lot of evidence that AuNPs affect gene expression and can change the activity of proteins. The basis of these processes is the chemical activity of AuNPs. Therefore, more investigation of the chemical reactivity of AuNPs in the context of radiosensitization is needed.

1.5. Research objectives

The current work is devoted to studying the chemistry of the radiosensitizing effect of AuNPs. Therefore, to examine the effects of AuNPs proposed in the literature, we will consider them with respect to processes that are induced by ionizing radiation.

Radiation-induced processes include energy absorption followed by water radiolysis and ROS formation. ROS react with organic compounds in a cell, forming secondary organic radicals, which finally are transformed into stable products (Figure 1.13). Even though energy absorption is a physical process, its modification affects all other chemical steps.

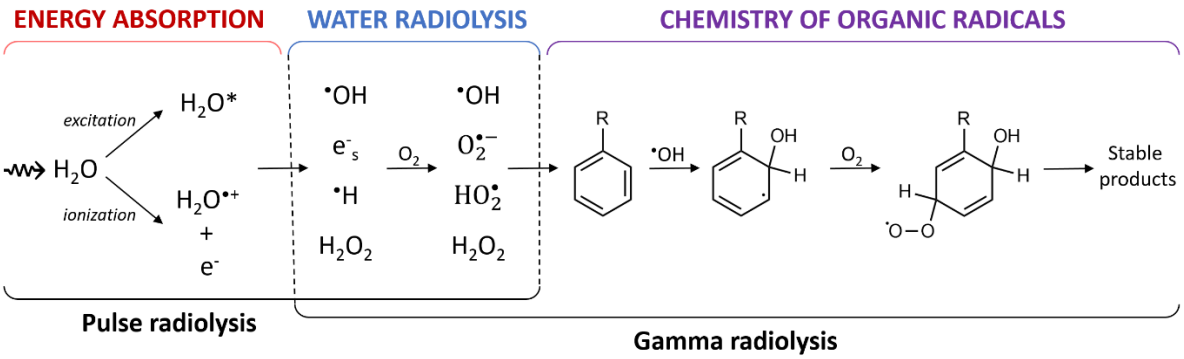

Figure 1.13. Processes induced by ionizing radiation and methods for their study, pulse and gamma radiolysis coupled with spectroscopy measurements.

In the following chapters, we will focus on each step of radiation-induced processes separately to examine the proposed effects of AuNPs by different techniques such as pulse and gamma radiolysis. Most of the attention will be paid to the effect of AuNPs on water radiolysis and radical chemistry since they are less understood. Additionally, we will present preliminary results of AuNPs' effect on biomolecules oxidation in the absence of radiation.

CHAPTER 2. SYNTHESIS AND CHARACTERIZATION OF GOLD NANOPARTICLES

Contents

2.1. INTRODUCTION

This chapter contains information about gold nanoparticles used in the current research work. Nowadays, methods to synthesize metal nanoparticles, such as gold, are well established. Salt solutions undergo the action of reducing agents leading to the formation of metallic nanoparticles. Different sizes and shapes can be obtained by varying chemical composition, reduction rate and surfactants. In this work, nanoparticles of various sizes were prepared using three methods: Turkevich method, reduction with sodium borohydride, and radiolytic method utilizing gamma rays. The goal was to prepare AuNPs with the highest possible concentration of gold without washing and concentrating them. It was necessary to be sure of the exact composition of the samples. Apart from synthesized nanoparticles, we used one type of commercial nanoparticles, 1.9 nm AuroVist™ AuNPs purchased from Nanoprobes Ink.

Gold nanoparticles have distinct plasmon band absorption spectra in the visible range. The broad and intense absorption band is attributed to plasmon oscillation – a collective free electron movement in gold nanoparticles in the presence of the electric field of light. Since the position and shape of the plasmon absorption band are related to the nanoparticles' size and shape, optical absorption spectroscopy – UV-Visible spectrophotometry is an important tool to study metallic colloids. In this work, the spectra of prepared samples were measured by Hewlett Packard 8453 UV-spectrophotometer using quartz cuvettes. Some samples were also analyzed by transmission electron microscopy (TEM) (STEM 1400, JEOL Ltd.), dynamic light scattering (DLS) and Zeta-potential (Zetasizer Nano ZS, Malvern) measurements for more detailed characterization. The size of at least 100 particles was measured to determine the particle size distribution by TEM images.

2.2. GOLD NANOPARTICLES

2.2.1. Synthesized by Turkevich method

Turkevich method is the most common and simple method of metal nanoparticles synthesis. The widely used strategy (classical) of AuNPs synthesis by the Turkevich method consists of the following steps: the gold salt water solution is boiled, and sodium citrate is quickly added under vigorous stirring to reduce gold ions. After a few minutes, the wine-red gold colloidal suspension is obtained with AuNPs' size of about 20 nm.[38] As well, there is an inverse method, when a gold salt solution is added rapidly to a boiling citrate

solution. During AuNPs synthesis, citrate (Ctr) is oxidized to dicarboxy acetone (DCA),[39] which works as a stabilizer (Figure 2.1). When the citrate concentration is in excess, citrate molecules also stabilize AuNPs.

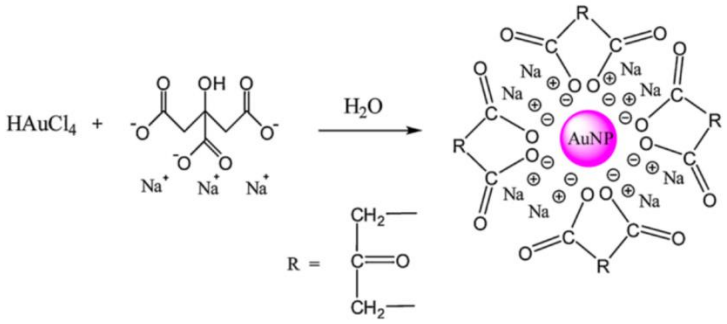

Figure 2.1. The scheme of Turkevich method for AuNPs preparation.[40]

In recent work, step by step reduction of Ag^{I} and Au^{III} by citrate with further nucleation of silver and gold atoms were studied by means of pulse and gamma radiolysis.[41] The results of the study are summarized in Figure 2.2.

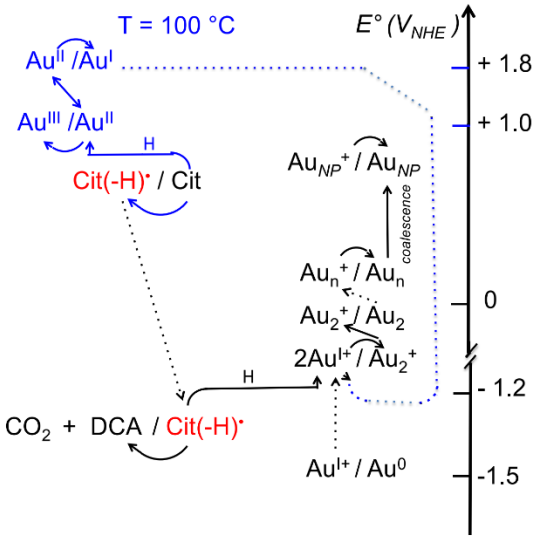

Figure 2.2. General mechanism of transient steps in the Turkevich synthesis of gold nanoparticles. The citrate radical Cit(-H)• (in the text Ctr•) initiates the nucleation.[41]

Briefly, citrate is able to reduce Au^{III} to $Au^{II,}$ forming citrate radical Ctr• with releasing of H^+ (reaction 2.1).[42] Since this reaction is slow at room temperature, the synthesis is usually carried out at 100°C.

$$Au^{III}Cl_4^- + Ctr \xrightarrow{100\,^{\circ}C} [Au^{III}Cl_3\ Ctr]^- + Cl^- \xrightarrow{100\,^{\circ}C} Au^{II}Cl_3^- + Ctr^{\bullet} + H^+ + Cl^- \quad (R.\,2.1)$$

Then, Au^{II} undergoes rapid dimerization[43] with further dimer disproportionation into $Au^{III}Cl_4^-$ and $Au^{I}Cl_2^-$ (reaction 2.2).[44]

$$\mathrm{Au^{II}Cl_3^- + Au^{II}Cl_3^- \rightarrow [Au^{II}Cl_3^-]_2 \rightarrow Au^{I}Cl_2^- + Au^{III}Cl_4^-} \ (\mathrm{R.\,2.2})$$

Citrate radical $Ctr^{\bullet}$ and Au^{I} can form $Au^{I}Ctr^{\bullet}$ complex (reaction 2.3),[41] which can reduce another Au^{I} ion to atoms (reaction 2.4).[41]

$$\mathrm{Au^{I} + Ctr^{\bullet} \rightarrow Au^{I}_{Ctr}Ctr^{\bullet}} \ (\mathrm{R.\,2.3})$$

$$\mathrm{Au^{I}Ctr^{\bullet} + Au^{I} \rightarrow Au_2^+ + DCA + CO_2} \ (\mathrm{R.\,2.4})$$

The nucleation and growth of particles occur by coalescence of atoms and oligomers or in situ reduction by $Cit^{\bullet}$ of ions adsorbed on particles (reactions 2.5 and 2.6).[41]

$$\mathrm{Au_2^+ + Ctr^{\bullet} \rightarrow Au_2 + DCA + CO_2} \ (\mathrm{R.\,2.5})$$

$$\mathrm{Au_2 \rightarrow \cdots \rightarrow} \mathit{AuNP} \ (\mathrm{R.\,2.6})$$

According to the overall reaction 2.7, the complete reduction of all gold ions by citrate requires at least the molar ratio Au: Citrate of 1:1.5.[39,45]

$$\mathrm{2AuCl_4^- + 3Ctr^{3-} \rightarrow 2Au + 3DCA^{2-} + 3CO_2\uparrow + 8Cl^- + 3H^+} \quad (\mathrm{R.\,2.7})$$

Previous studies also suggested that dicarboxy acetone and its degradation product (acetone) could take part in additional redox reactions with gold ions if citrate concentration is less than 1.5 of gold salt concentration (reaction 2.8 and 2.9).[45]

$$\mathrm{DCA^{2-} + 2H_2O \xrightarrow{100\,^{\circ}C} acetone + 2CO_2\uparrow + 2OH^-} \quad (\mathrm{R.\,2.8})$$

$$\mathrm{4AuCl_4^- + 6H_2O + 3\,acetone \xrightarrow{100\,^{\circ}C} 4Au + 9CH_2O + 12H^+ + 16Cl^-} \quad (\mathrm{R.\,2.9})$$

We tried to make the sample's composition as simple as possible. Therefore, heating was stopped immediately after AuNPs formation to avoid the formation of acetone, and we did not use citrate concentration less than 1.5 of gold concentration.

The size of nanoparticles is controlled by the rate of nucleation and crystal growth rate, which in turn can be controlled by varying the ratio between gold cations and citrate anions.[46] The size dependence of AuNPs from Au: Citrate ratio is shown in Figure 2.3 for both classical and inverse Turkevich methods.[47] The smallest particles can be prepared using Au: Citrate ratio of 1:4; further decrease of gold salt concentration does not affect the size of nanoparticles.

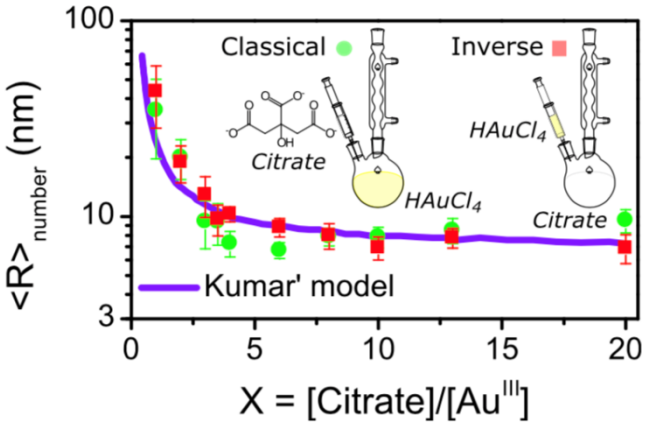

Figure 2.3. The averaged radius of AuNPs as a function of Ctr^{3-}: Au^{3+} molar ratio.[47]

To obtain particles of different sizes by Turkevich synthesis, Au: Citrate ratios of 1:1.5 and 1:4 were used. For the used Au: Citrate ratio of 1:1.5 and 1:4, the maximum possible concentration of gold salt was 3 and 2 mM, respectively. Further increase in gold concentration led to rapid particles aggregation. In both cases, the pH of the AuNPs solutions was around pH 4, which was adjusted with NaOH to the required value for specific experiments. The exact pH value of the samples will be indicated in the description of each experiment.

The synthesis of AuNPs with Au: Citrate ratio of 1:1.5 and the final gold atomic concentration of 3 mM included the following steps: 3 mL of 100 mM stock solution of potassium gold (III) chloride ($K[AuCl_4]$, 98%, Sigma-Aldrich) was diluted with 82.5 mL of deionized water (Milli-Q, 18 MΩ.cm). The solution was heated up to 100 °C, 4.5 mL of 100 mM sodium citrate (>99%, Sigma-Aldrich) was added to the solution under stirring by magnet stir bar with high speed. The sample was named TM1.

The synthesis of AuNPs with Au: Citrate ratio of 1:4 and the final gold atomic concentration of 2 mM included the following steps: 2 mL of 100 mM stock solution of potassium gold (III) chloride ($K[AuCl_4]$, 98%, Sigma-Aldrich) was diluted with 90 mL of deionized water (Milli-Q, 18 MΩ.cm). The solution was heated up to 100 °C, 8 mL of 100 mM sodium citrate was added to the solution under stirring by magnet stir bar with high speed. The sample was named TM2.

For both samples, heating was stopped when the solutions had turned red. The solutions were cooled down under stirring. The complete reduction of gold ions was verified by the total disappearance of the absorption at 220 nm. Samples were characterized by UV-vis absorption measurements and analysis by TEM. The results are presented in Figures 2.4 - 2.5 and Figures 2.6 - 2.7 for samples TM1 and TM2, respectively.

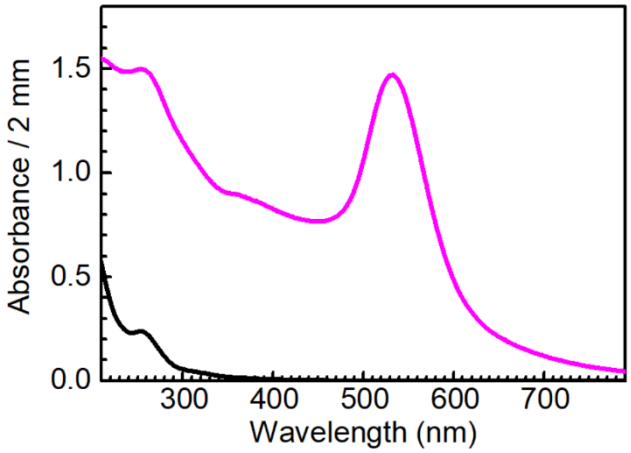

Figure 2.4. Absorption spectra of TM1 sample - AuNPs prepared by Turkevich method with Au: Citrate of 1:1.5 containing 3 mM of gold atoms (pink) and its supernatant (black). AuNPs' suspension was diluted with deionized water 1.5 times before measurement.

To exclude the influence of other chemical species on processes of interest, we used supernatant as an appropriate reference in some experiments. The supernatant of the TM1 sample was obtained by centrifugation of AuNPs suspension, eliminating AuNPs to a large degree but leaving other chemical substances. Centrifugation was done in 2 mL Eppendorf microtubes utilizing an Eppendorf MiniSpin centrifuge with an F-45-12-11 rotor at a speed of 13400 rpm for 30 min. We controlled by absorption measurement that at least 99% of AuNPs were removed from the supernatant solution (Figure 2.4). TM1 sample had the maximum plasmon band absorption at 533 nm. The peak at 260 nm in Figure 2.4 is due to dicarboxy acetone (DCA), a citrate oxidation product.

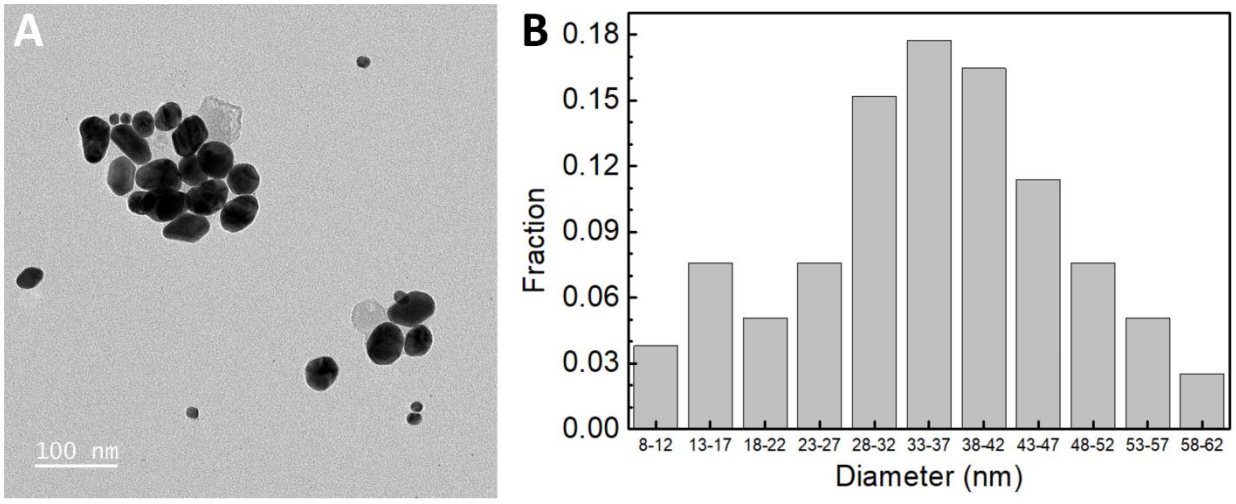

Figure 2.5. TEM image (**A**) and size distribution histogram (**B**) of TM1 sample - AuNPs prepared by Turkevich method with Au: Citrate of 1:1.5 containing 3 mM of gold atoms (λ_{max} = 533 nm).

TM1 sample had a mean AuNPs' diameter of 35 ± 13 nm with a broad particle size distribution, possibly due to low citrate concentration. Moreover, not all particles had spherical shape. The mean hydrodynamic diameter measured by the DLS technique was 45 nm. The sample had a zeta-potential of -35 mV.

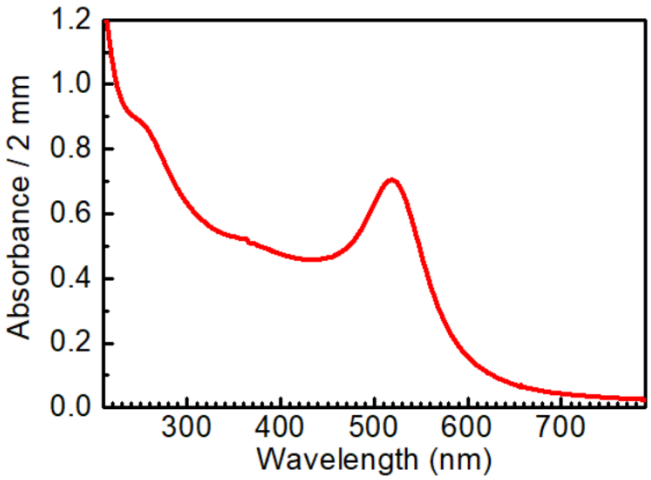

Figure 2.6. Absorption spectra of TM2 sample - AuNPs prepared by Turkevich method with Au: Citrate of 1:4 containing 2 mM of gold atoms. AuNPs' suspension was diluted with deionized water two times before measurement.

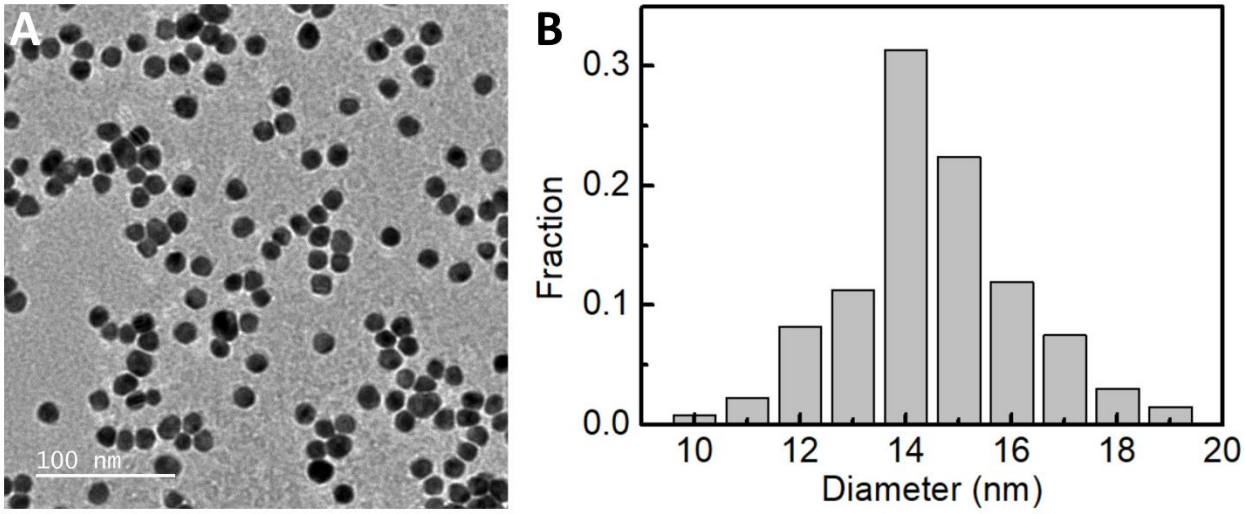

Figure 2.7. TEM image (**A**) size distribution histogram (**B**) of TM2 sample - AuNPs prepared by Turkevich method with Au: Citrate of 1:4 containing 2 mM of gold atoms (λ_{max} = 520 nm).

TM2 sample had the maximum plasmon band absorption at 519 nm and a mean diameter of 15 ± 2 nm determined by TEM. Due to the higher citrate concentration, the particle size distribution of the TM2 sample was more narrow than TM1. All information about two samples prepared by the Turkevich method is summarized in Table 2.1.

Table 2.1. Information about AuNPs prepared by Turkevich method.

Name	**[Au],**			**Au: Citrate**	**λ_{max}, nm**	**D_{TEM}, nm**	**D_{DLS}, nm**	**ζ, mV**
	mM	µg/ml	wt.%					
TM1	3	600	0.06	1:1.5	533	35 ± 13	45	−35
TM2	2	400	0.04	1:4	519	15 ± 2	-	-

2.2.2. Synthesized by sodium borohydride reduction

Sodium borohydride is a common reducing agent used in organic and inorganic chemistry. It is more powerful than sodium citrate. Therefore, reducing gold cations by sodium borohydride does not require heating. Usually, in AuNPs synthesis by reduction with sodium borohydride surfactants such as citrate or thiols are used to stabilize nanoparticles.[40] However, AuNPs can be synthesized without the utilization of additional surfactants. In this case, particles are stabilized by an electron double layer made of Na^+, K^+ and BO_3^{3-}.[48]

In this work, the AuNPs sample prepared by reduction with sodium borohydride (BH1) contained 3 mM of gold salt. It was the maximum possible gold concentration to prepare stable nanoparticles. The synthesis included the following steps: 3 mL of 100 mM potassium gold (III) chloride ($K[AuCl_4]$, 98%, Sigma Aldrich) solution was diluted with 87.7 mL of deionized water (Milli-Q, 18 MΩ.cm). Then 9.3 mL of 100 mM $NaBH_4$ (98%, Sigma Aldrich) was quickly added to the solution while actively stirring with a magnetic stirrer for 15 min. The absorption spectrum of the sample is presented in Figure 2.8.

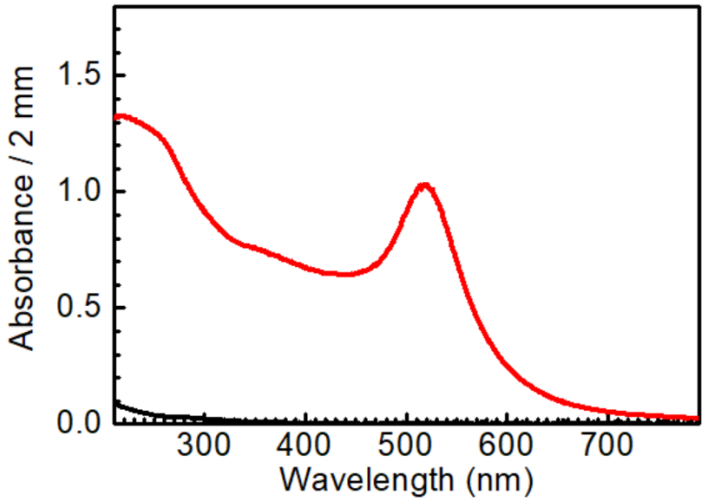

Figure 2.8. Absorption spectra of BH1 sample - AuNPs prepared by reduction with sodium borohydride containing 3 mM of gold atoms (red) and its supernatant (black). AuNPs suspension was diluted with deionized water two times before measurement.

Since it is not easy to precipitate small 20 nm particles just by centrifugation, the supernatant of the BH1 sample was prepared as the following: 3 mL of 100 mM $K[AuCl_4]$ solution were mixed directly with 9.3 mL of 100 mM $NaBH_4$ without dilution. Such a high concentration of gold ions and BH_4^- leads to fast aggregation of formed particles, which can be easily precipitated by centrifugation. Thus, the supernatant solution contains all chemical species left after the reaction except gold. Centrifugation was done in 2 mL Eppendorf microtubes utilizing an Eppendorf MiniSpin centrifuge with F-45-12-11 rotor at a speed of 13400 rpm for 30 min. Then, the transparent liquid above solid precipitate was gently taken and diluted with Milli-Q water to have the same concentration of chemical species as in AuNPs suspension. TEM image and size distribution histogram are presented in Figure 2.9.

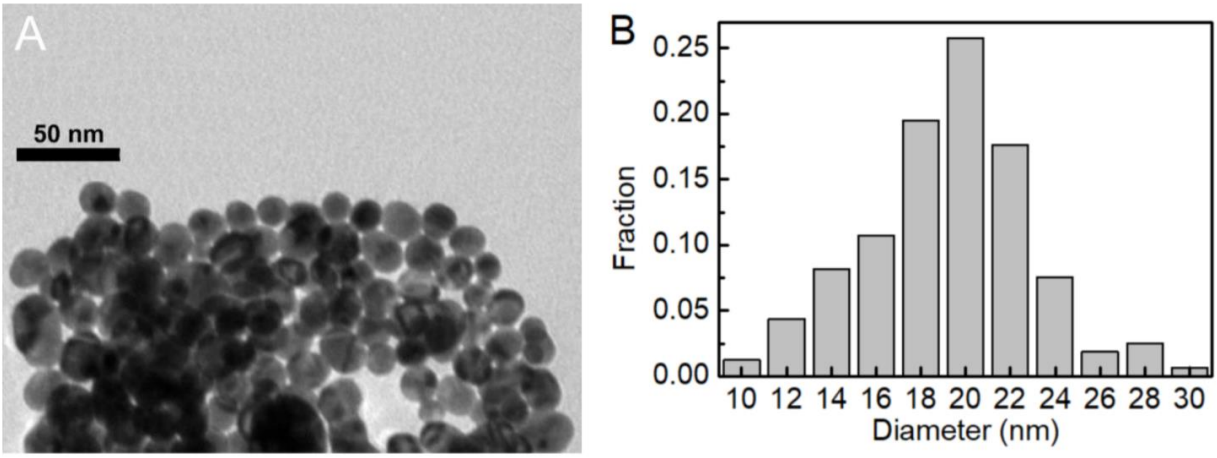

Figure 2.9. TEM image (**A**) size distribution histogram (**B**) of BH1 sample - AuNPs prepared reduction with sodium borohydride containing 3 mM of gold atoms (λ_{max} = 520 nm).

BH1 sample had the maximum plasmon band absorption at 520 nm and a mean diameter of 20 ± 4 nm determined by TEM. The zeta potential of the sample was -20 mV. Information for the sample is summarized in Table 2.2 below.

Table 2.2. Information about AuNPs prepared by $NaBH_4$ reduction.

Name	**[Au],**			**λ_{max}, nm**	**D_{TEM}, nm**	**ζ, mV**
	mM	μg/ml	wt.%			
BH1	3	600	0.06	520	20 ± 4	−20

2.2.3. Synthesized by radiolytic method

The principle of metal nanoparticles synthesis by γ-radiolysis is based on metal cations reduction by reducing species produced during water radiolysis. The most powerful reducing species are solvated electrons (e_s). The metal cation is reduced step by step to a

metal atom. Reduced metal atoms eventually coalesce to form atom clusters, which start to work as centres of nucleation for further growth of metal nanoparticles, as depicted by the following reactions 2.10 - 2.12:[49]

$$e_s^- + M^{m+} \rightarrow M^{(m-1)+} \quad (R\ 2.10)$$

$$e_s^- + M^{m+} \rightarrow M^0 \quad (R\ 2.11)$$

$$nM^0 \rightarrow M_2 \rightarrow \cdots M_n \cdots \rightarrow M_{agg} \quad (R\ 2.12)$$

The oxidizing species such as •OH radical and •H atom can be converted to reducing ones by adding 2-propanol to the solution. Both species subtract hydrogen atoms mostly from alpha-carbon forming α-hydroxyisopropyl radical (reactions 2.13 and 2.14). The radical of 2-propanol has RedOx potential of -1.5 V, sufficient for reduction of gold cations like gold and silver.[50]

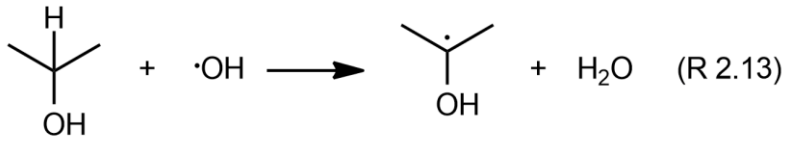

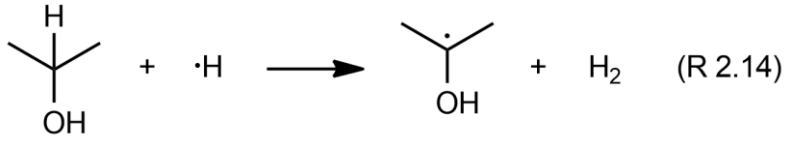

The overall radiolytic yield (G) of reducing species in the presence of 2-propanol can be calculated based on the yield of the primary products of water radiolysis (scheme 2.1 and equation 2.1 below).

$$H_2O \xrightarrow{\gamma} e_s^-(2.8),\ H_3O^+, {}^\bullet H(0.6), {}^\bullet OH(2.8), H_2O_2(0.7) \quad (S.\ 2.1)$$

$$G(\text{reducing species}) = G(e_{aq}^-) + G({}^\bullet OH) + G({}^\bullet H) = 6.3 \times 10^{-7} \text{mol J}^{-1} \quad (Eq.\ 2.1)$$

As the concentration of formed species (C, mol L^{-1}) depends on the deposited dose, it can be calculated by equation 2.2.

$$C = D \times G \times \rho \quad (Eq.\ 2.2)$$

Thus, 1 kGy deposited in an aqueous solution of 2-propanol produces 0.63 mmol L^{-1} of reducing species. The stationary concentration of produced species depends on the dose rate. The higher the dose rate, the greater the stationary concentration of radicals. In turn, the concentration of radicals affects the reduction rate of metal cations. Thus, increasing the dose rate makes it possible to obtain smaller nanoparticles.

In this work, AuNPs were prepared by γ-radiolysis technique using PVA (99+%, Mw = 85000 – 124000, Sigma-Aldrich) as a surfactant agent and 2-propanol (99.5%, Sigma-Aldrich) as a scavenger of •OH and •H radicals. Aqueous solutions containing 4 mM of $K[AuCl_4]$, 100 mM of PVA and 100 mM of 2-propanol after deoxygenation by bubbling with Ar (Alpha Gaz, Air Liquide) were irradiated using ^{60}Co γ-source. The total dose of irradiation was 20 kGy (5 kGy per 1 mM of gold salt solution) with a changing dose rate from 1 to 3.5 kGy h^{-1}.

The absorption spectra of three prepared samples (RM1-3) are presented in Figure 2.10. The change in the dose rate allowed to obtain particles with the maximum plasmon band at different wavelengths. Samples RM1, 2 and 3 had the maxima at 530, 539 and 567 nm, respectively. The more to the right the peak, the larger the nanoparticle size. All samples absorb light even at 800 nm, which means large or non-spherical particles are present.

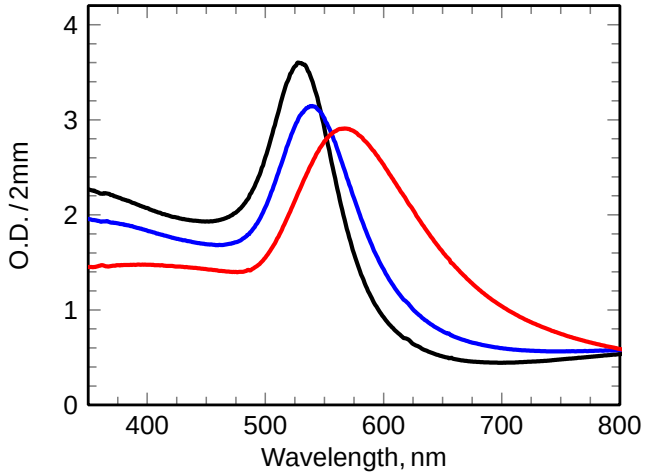

Figure 2.10. Absorption spectra of samples RM1-3 - AuNPs suspensions prepared by radiolytic method All samples have the same chemical composition (4 mM of gold salt, 100 mM of PVA and 100 mM of 2-propanol). The dose rate was 3, 2 and 1 kGy h^{-1} for black, blue, and red curves, respectively.

TEM images are presented in Figures 2.11-2.13. TEM analysis confirmed the presence of non-spherical particles. The shape of the particles is very diverse. In addition to spherical particles, there are also rods, disks, triangles and polygons of gold. Therefore, samples were additionally characterized by DLS measurements, which showed hydrodynamical diameters from 127 to 187 nm. The reason is that long molecules of PVA stabilize these AuNPs. Shape heterogeneity also affects the mean diameter measured by DLS. Thus, the best way to characterize these AuNPs is to use the position of the plasmon band maximum.

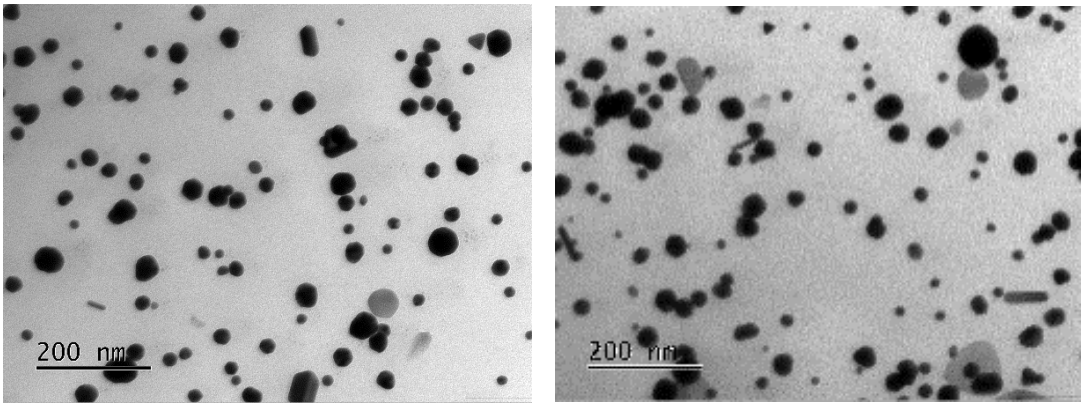

Figure 2.11. TEM images of RM1 sample – AuNPs (λ_{max} = 530 nm) prepared by the radiolytic method using dose rate of 3 kGy/h.

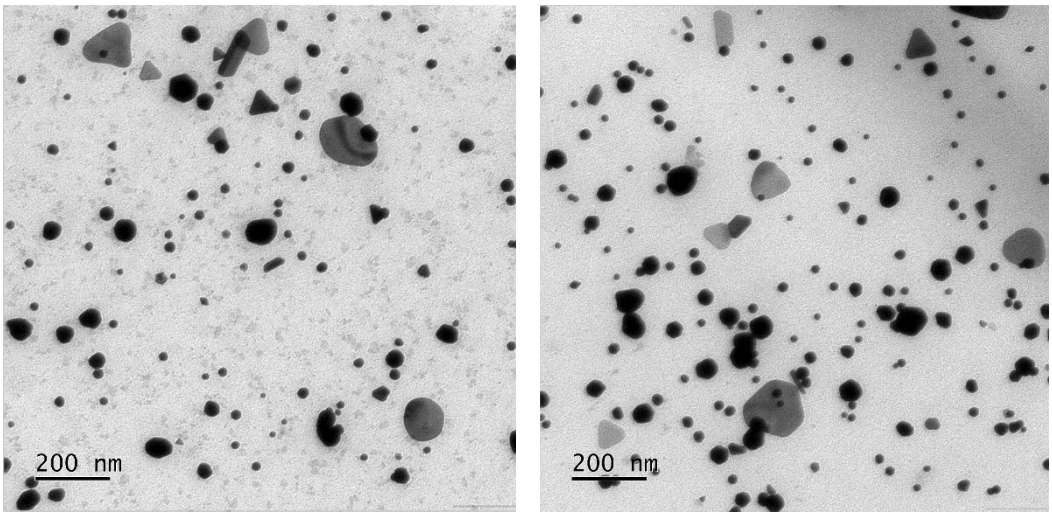

Figure 2.12. TEM images of RM2 sample – AuNPs (λ_{max} = 539 nm) prepared by the radiolytic method using dose rate of 2 kGy/h.

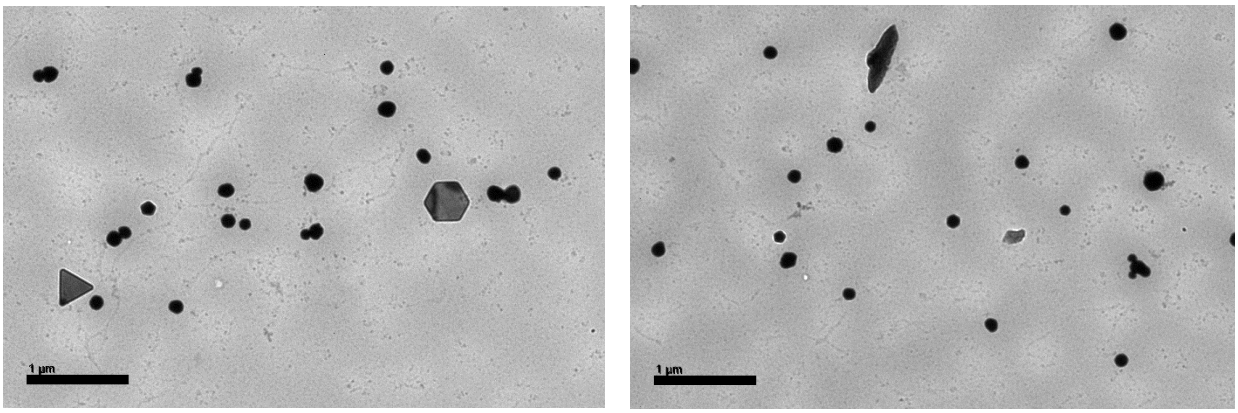

Figure 2.13. TEM images of RM3 sample – AuNPs (λ_{max} = 567 nm) prepared by the radiolytic method using dose rate of 1 kGy/h.

All information about three samples prepared by the radiolytic method is summarized in Table 2.3.

Table 2.3. Information about AuNPs prepared by the radiolytic method.

Name	**[Au],**			**Dose rate, kGy/h**	**λ_{max}, nm**	**D_{DLS}, nm**
	mM	μg/ml	wt.%			
RM1	4	800	0.08	3	530	127
RM2				2	539	166
RM3				1	567	187

2.2.4. AuroVist™ 1.9 nm

AuroVist™ is an X-ray contrast agent for micro-CT produced by Nanoprobes, Inc. (Yaphank, New York).[51] AuroVist™ 1.9 nm nanoparticles show significant CT image enhancement compared to the iohexol contrast agent (trade name Omnipaque). Tumour image enhancement is also obtained due to nanoparticle extravasation across tumour capillary pores. Such small NPs show a much higher diffusion coefficient than larger NPs.[52] These nanoparticles have been used in the seminal work of J. Hainfeld et al.[20] and in many other subsequent studies.[53–55]

Due to the small nanoparticles size of 1.9 nm, the plasmon band is absent (Figure 2.14).

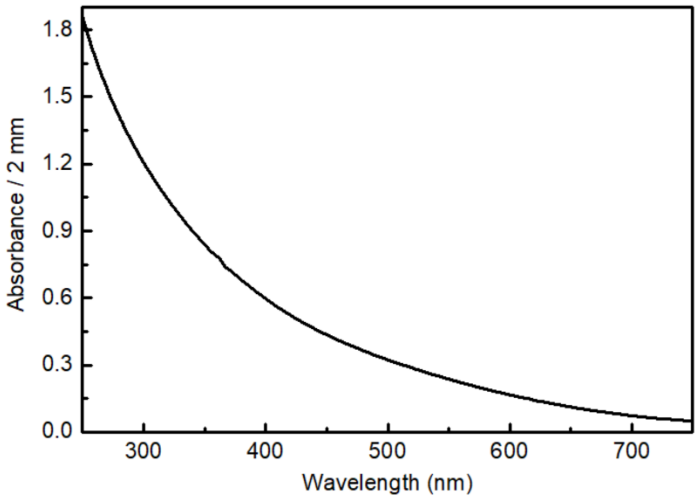

Figure 2.14. Absorption spectra of AuroVist™ nanoparticles in water at 1.5 mM of gold (0.03 wt.% or 300 μg/ml).

The manufacturer states the following features of AuroVist™: low toxicity (LD50 >1.4 g Au/kg); low osmolality even at high concentrations; low viscosity: inject even into small vessels; nanoparticles are excreted through the kidney; 1.9 nm gold core, ~50,000 Da.

The nanoparticles size is confirmed by TEM analysis (Figure 2.15).[53] However, there is no information about surfactant composition. Only an overall mass of ~50,000 Da is given.

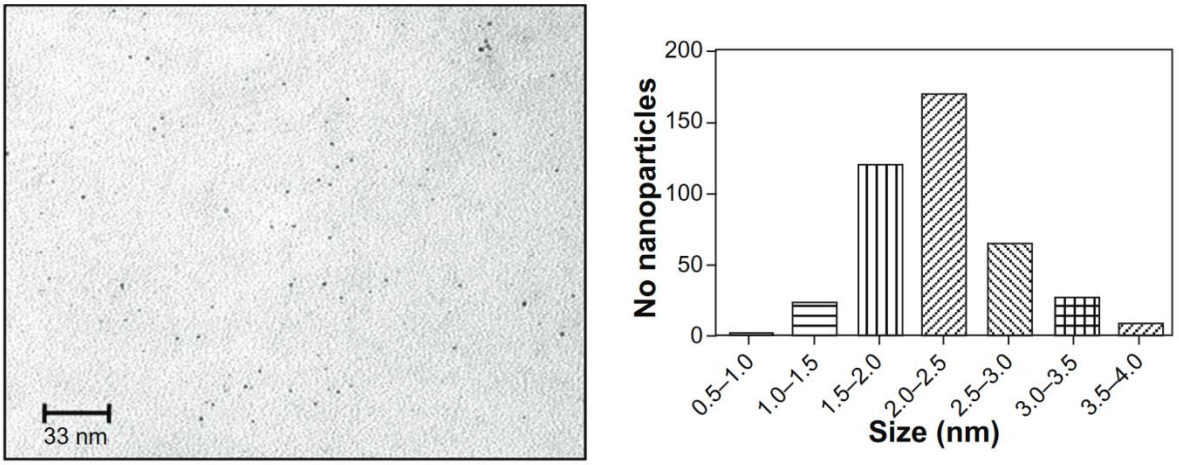

Figure 2.15. Transmission electron microscopic image of monodispersed 1.9 nm Aurovist™ gold nanoparticles and size distribution histogram.[53]

2.3. SUMMARY

For the reader's convenience, all nanoparticles used in this work are listed in Table 2.4, indicating the chapters in which they are mentioned. Please note that gold atomic concentration are used, not nanoparticles concentration in all experiments described in the following chapters. This is more appropriate because not all samples have spherical particles, and some have a pretty broad size distribution.

Table 2.4. List of all used AuNPs.

Method	**Name**	**[Au]**			**Stabilizer**	**λ_{max}, nm**	**D, nm** TEM / *DLS*	**ζ,** mV	**Chapter**
		mM	wt.%;	µg/ml					
Turkevich	TM1	3	0.06	600	Ctr, DCA	533	35 ± 13	-35	3
	TM2	2	0.04	400		519	15 ± 2	-	5
Reduction bu $NaBH_4$	BH1	3	0.06	600	Na^+, K^+, BO_3^{3-}	520	20 ± 4	-20	3, 4, 5
Radiolytic	RM1	4	0.08	800	PVA	530	*127*	-	3
	RM2					539	*166*	-	
	RM3					567	*187*	-	
Comercial AuNPs	AuroVist™	1.5	0.03	300	Molecules of ~50kDa	-	1.9	-	5

CHAPTER 3. PULSE-RADIOLYSIS STUDY OF NANOPARTICLES SUSPENSIONS

Contents

3.1. INTRODUCTION

Pulse radiolysis is an efficient technique for generating radical species and studying their reactivity. Electron accelerators are the most common facilities used in pulse radiolysis experiments. They are usually combined with time-resolved spectroscopy measurements to study processes from picosecond to second time scale.

3.1.1. Solvated electron kinetics

Among other species produced during radiolysis of pure water, direct detection by spectroscopy measurement is easier for the solvated electron since it has a high molar absorption coefficient (Figure 3.1).[8,56]

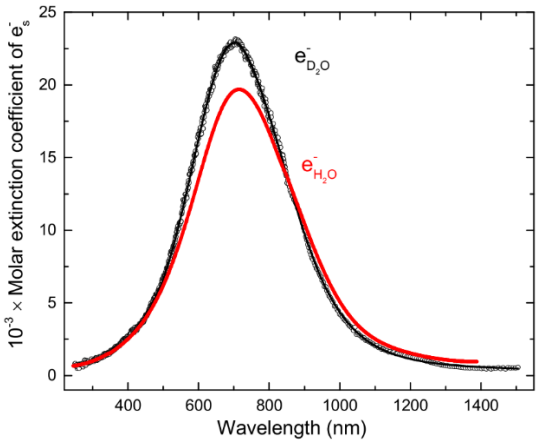

Figure 3.1. Absorption spectra of e^-_s in neat H_2O (from 250 to 850 nm from Ref[56] and from 850 to 1400 nm from Ref[8]) and in D_2O.[8]

Even in pure water, solvated electrons disappear due to radical-radical reactions, mainly due to reactions between two solvated electrons and the reaction of an electron with a hydroxyl radical or with H_3O^+. However, if the solution contains a solute that can react with solvated electrons or hydroxyl radicals, the kinetics will accordingly accelerate or decelerate. Examples of solvated electron kinetics measured by pulse radiolysis are presented in Figure 3.2 A.

Suppose the electron accelerator has a short pulse duration in the order of picoseconds. In that case, pre-solvated electrons reactivity can be studied quasi-directly by the decrease in the initial yield of solvated electrons (Figure 3.2 B). This method was used to study e^-_{pre} attachment to DNA nucleo-bases/sides/tides.[57] Despite the high reactivity of pre-solvated electrons, the solute concentration should be in the order of tens of mM to observe the reaction with pre-solvated electrons.[57–61]

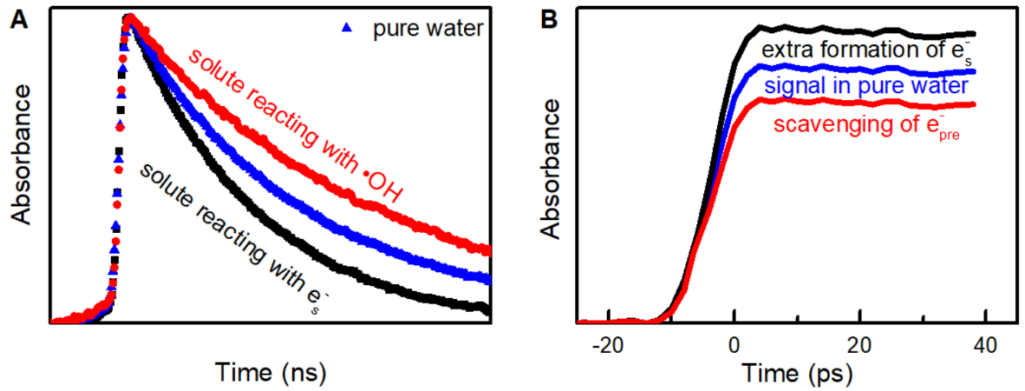

Figure 3.2. Examples of solvated electron kinetics measured by pulse radiolysis. *Not experimental data, used for illustration.*

When the reactivity of pre-solvated electrons is excluded, the initial concentration of solvated electrons is proportional to the absorbed dose. Therefore, the dose enhancement effect can be directly studied by pulse radiolysis following the initial solvated electron concentration increase.

3.1.2. Influence of solid-phase on water radiolysis

The water radiolysis occurs differently at the solid/liquid interface than in bulk liquid. The most studied effect is an increase in H_2 formation.[62] It has great importance for nuclear energy research for safety reasons. Water radiolysis always occurs in the cooling systems of nuclear reactors, and molecular hydrogen formation must be controlled due to its explosive properties.

The pulse radiolysis technique has been used to study the radiolysis of water in the presence of solid phases. For example, the presence of SiO_2 and ZnO nanoparticles increases solvated electron formation. The results are presented in Figure 3.3.[63] Note that the concentration of SiO_2 and ZnO is in order of mole per litre.

It is difficult to reach a high concentration of nanoparticles in water, avoiding their precipitation. Therefore, porous materials can be used to perform experiments with higher solid/water ratios. Porous glass is transparent enough for spectroscopy measurements. Pulse radiolysis measurements were performed in glass with pours sizes of 1 and 57 nm (Figure 3.4).[64] The smaller the pore size, the higher the solid:water ratio. Therefore, the initial concentration of solvated electrons in glass with a pore size of 1 nm is grated than in 57 nm porous glass and water. At the same time, the lifetime of solvated electrons is shorter in small pores due to their recombination and reaction with SiO_2.

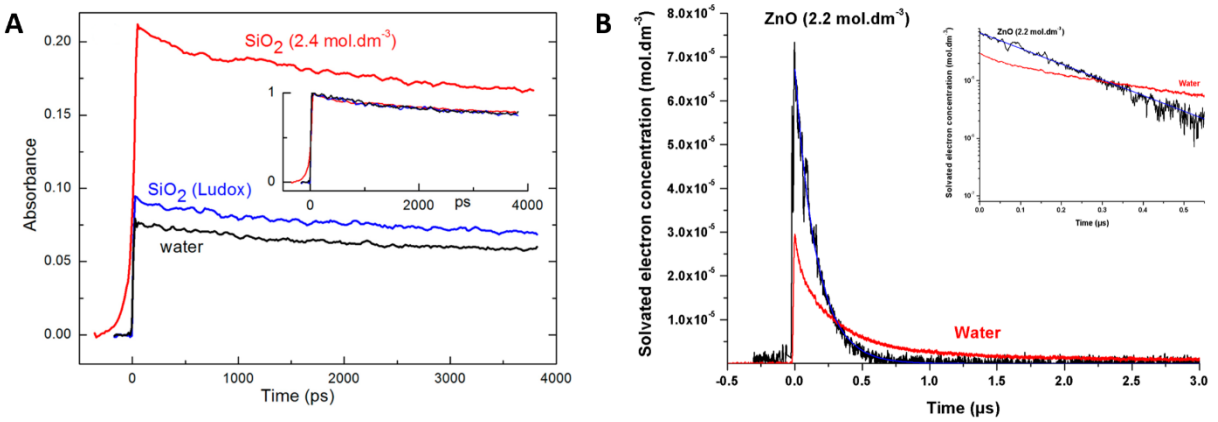

Figure 3.3. The evolution of the absorbance displayed at 720 nm in the 0−4 ns time scale range in water (black), Ludox (blue), and a 2.4 mol·dm^{-3} silica nanoparticle suspension (red). The three kinetics, normalized at their initial absorbance value, are shown in the inset, revealing that the three decays are the same (**A**). Solvated electron concentration decay recorded after 10 ns of electron pulse absorption at 633 nm in a 1 mm optical path cell in water (red) and in a 16 wt % ZnO suspension (black). The decays are represented with a logarithmic scale in the inset (**B**).[63]

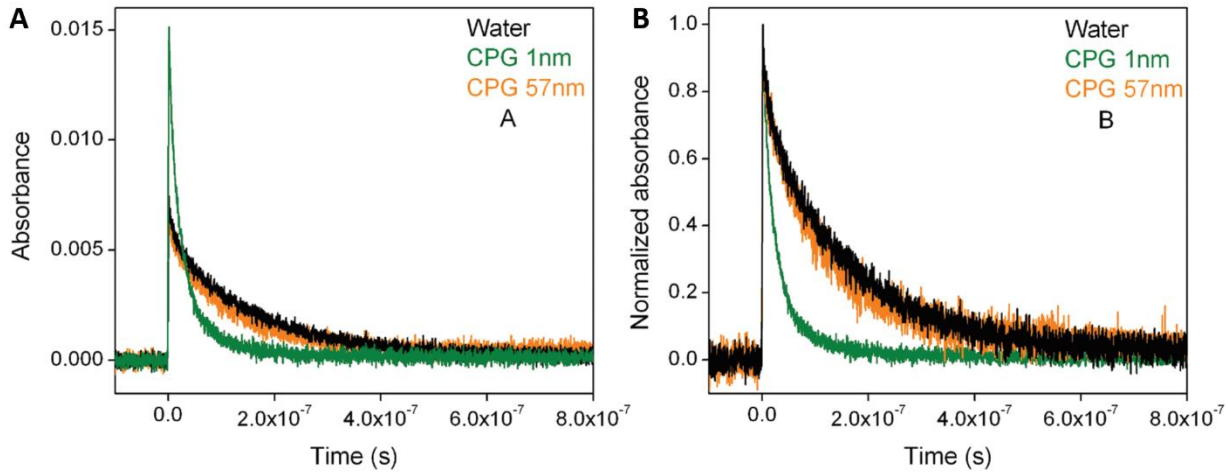

Figure 3.4. Evolution of the solvated electron in bulk water (black) and water confined in controlled porous glass (CPG) with 1 nm (orange) and 50 nm (green) pore diameter: normalized to the absolute dose (**A**) and normalized at 20 ns (**B**).[64]

In both cited works, radiation (electrons and gamma photons) of MeV energies was used. Despite the same cross-section of water and used materials at the MeV energy range, the dose enhancement (higher initial concentration of solvated electrons) was observed. It was explained by charge transfer from the solid phase to water (Figure 3.5).[63] Thus, all energy absorbed by both phases is eventually deposited in water. Note that this effect is significant only at a very high solid:water ratio.

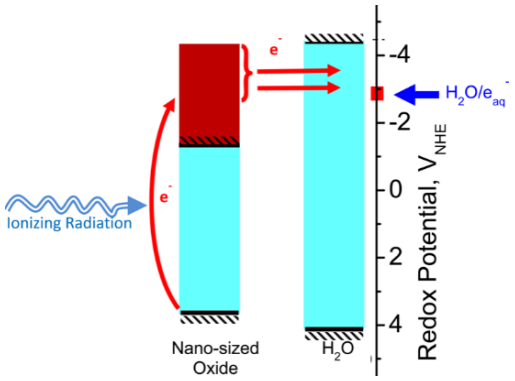

Figure 3.5. Scheme of charge transfer from solid to liquid phase.[63]

3.1.3. Gold nanoparticles effects on water radiolysis

There are a lot of works in the field of radiosensitization research stating the increase in •OH radicals formation in the presence of gold nanoparticles.[23,24] However, there is no clear explanation for such a phenomenon.

The radiolysis of water after energy deposition undergoes two pathways (Scheme 3.1). The main path is ionization, and the minor one is excitation. After ionization, the survived water-cation radical loses a proton, leaving behind •OH radical.[65] A secondary electron thermalizes within a few femtoseconds, followed by its solvation within 1 ps. Dissociation of the excited water molecule leads to the formation of the •H atom and •OH radical. The formed species in ionization spurs react with each other and solutes present in the solution. Thus, to increase the formation of •OH radicals, gold nanoparticles should influence at least one of the two ways. In any case, it will affect the formation of solvated electrons or the kinetic of solvated electrons. Therefore, pulse radiolysis is an appropriate tool to examine the idea of •OH radical overproduction.

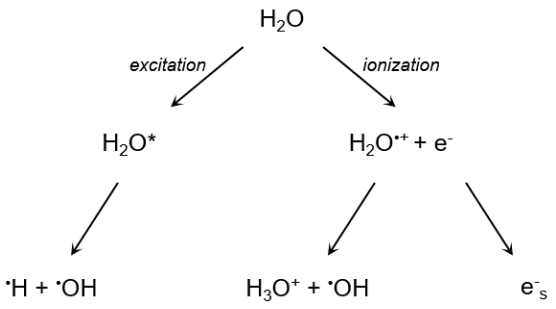

Reaction	Rate constant
$e^-_s + e^-_s + 2H_2O \rightarrow H_2 + 2OH^-$	0.55
$e^-_s + H_3O^+ \rightarrow {}^\bullet H + H_2O$	2.30
$e^-_s + {}^\bullet H + H_2O \rightarrow H_2 + OH^-$	2.50
$e^-_s + {}^\bullet OH \rightarrow OH^-$	3.00
$^\bullet OH + {}^\bullet OH \rightarrow H_2O_2$	0.55
$^\bullet OH + {}^\bullet H \rightarrow H_2O$	2.00

× 10^{10} ($M^{-1}s^{-1}$)

Scheme 3.1. First steps of water radiolysis within 1 ps and some reactions of hydrated electron (e^-_s) and hydroxyl radical (•OH) and their constant rates.[5]

There is only one article on pulsed radiolysis of AuNPs suspensions of gold nanoparticles, which reports on the reaction of gold nanoparticles with solvated and even pre-solvated

electrons (Figure 3.6).[66] This article was preceded by a work in which a rate constant $k_e \sim 5 \times 10^{14}$ M^{-1} s^{-1} was reported for the reaction of pre-solvated electrons and gold nanoparticles, studied by muon spectroscopy.[67] These works conclude that AuNPs can scavenge the pre-solvated electrons.

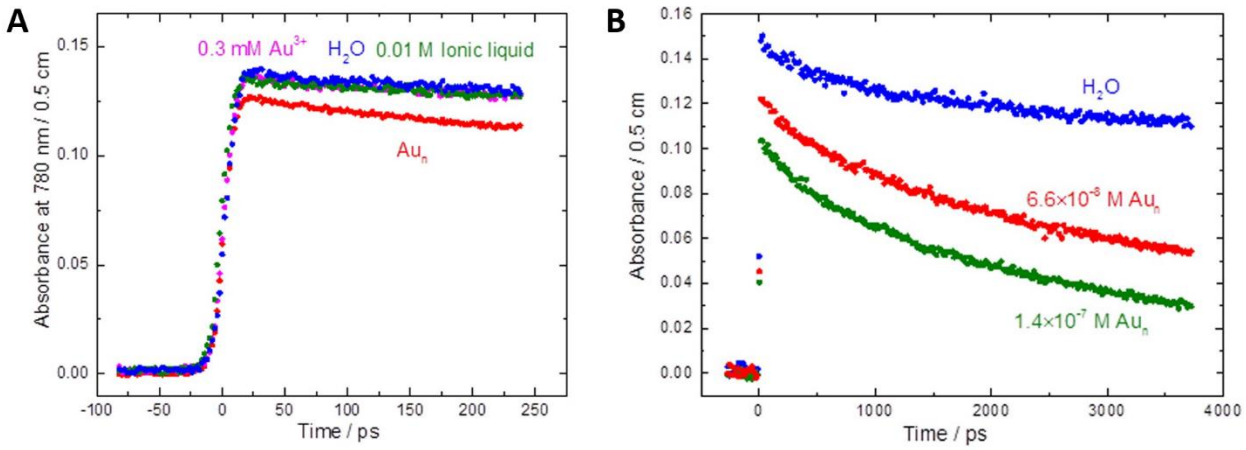

Figure 3.6. Recorded kinetics at 780 nm in water up to 250 ps for a solution of ionic liquid in water at the same concentration used to stabilize gold nanoparticles, solution of 3.3×10^{-8} M naked 15 nm gold nanoparticles in water (Au_n), and solution of 0.3 mM Au^{3+} in water (Au^{3+} was used as a precursor of gold nanoparticles) at 23 °C (**A**). Recorded kinetics at 800 nm in water up to 4 ns for the solution of 6.6×10^{-8} M (blue circles) and 1.4×10^{-7} M naked 15 nm gold nanoparticles in water (Au_n) at 23 °C (**B**).[66]

3.2. RESEARCH OBJECTIVES

Research objectives were to study AuNPs effect on water radiolysis utilizing pulse-radiolysis coupled with time-resolved spectroscopy. Suppose AuNPs increase ROS concentration in a homogenous solution due to energy absorption processes. In that case, it can be detected directly by measuring solvated electrons concentration at 10 ps after energy deposition and the full kinetic of solvated electrons (Figure 3.7).

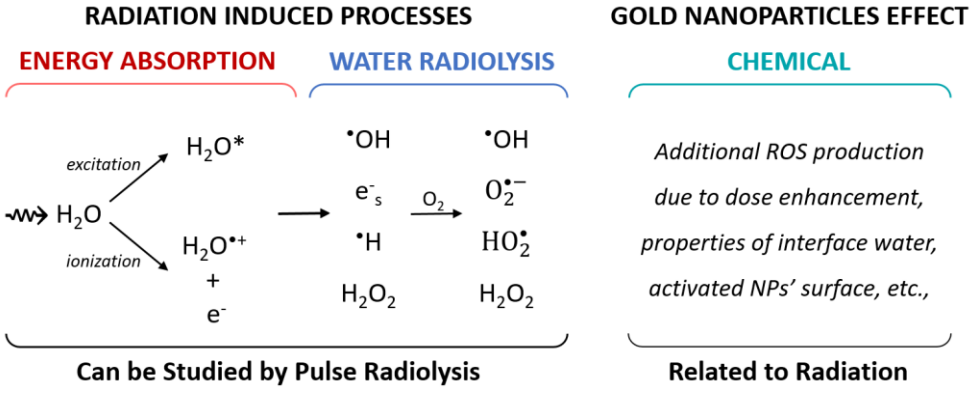

Figure 3.7. Schematic presentation of research objectives of Chapter 3.

3.3. EXPERIMENTAL PART

3.3.1. ELYSE – an electron accelerator coupled with time-resolved spectroscopy

ELYSE is a linear electron accelerator located in the Institute of Chemical Physics in Université Paris-Saclay in France.[68] The principle scheme of ELYSE is presented in Figure 3.8. In our work, electron pulses of ~4 nC with 5 ps duration and electron energy around 8 MeV delivered at a repetition frequency of 5 or 10 Hz were used.

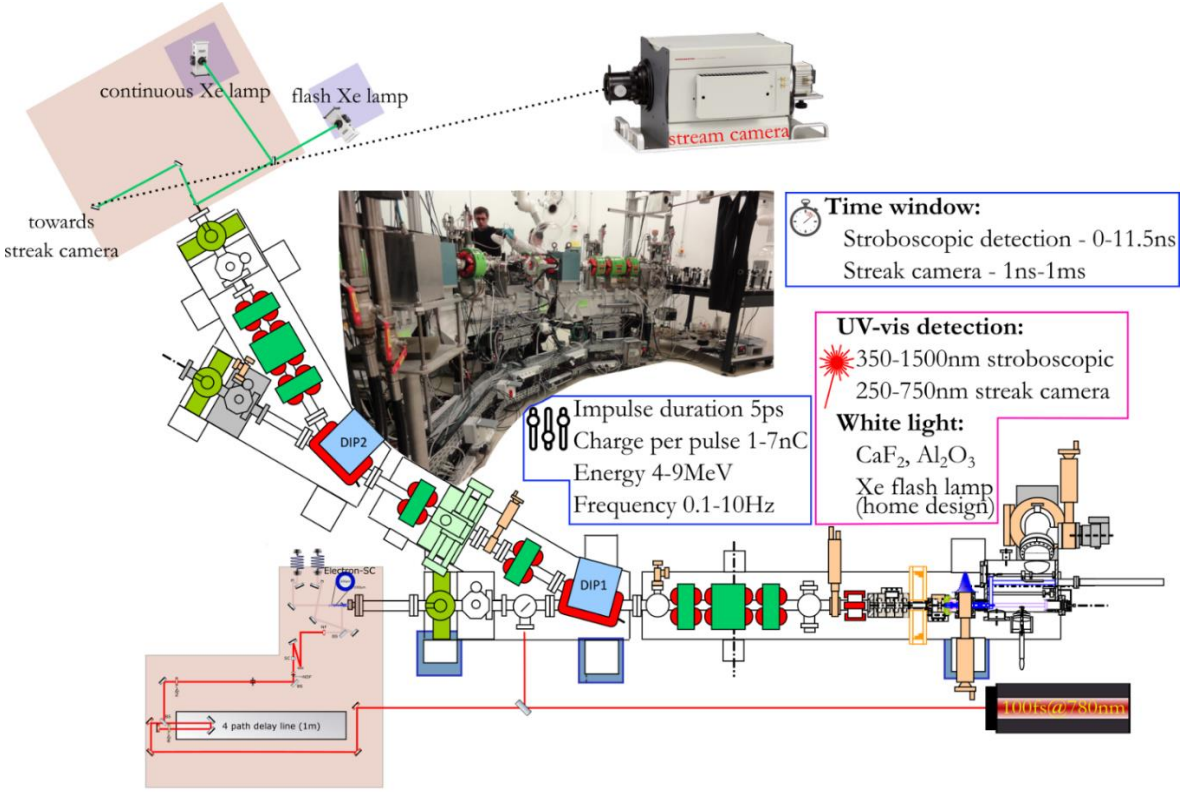

Figure 3.8. Principle scheme of ELYSE with its main characteristics.

The accelerator has three lines. Two of them are dedicated to time-resolved optical absorption spectroscopies. The detection systems are synchronized with electron pulses brought by the accelerator. The optical paths are collinear to the electron pulse propagation.

The first detection system is a classical pump-probe experiment. The pump is the pulse of 8 MeV electrons, and the probe is a supercontinuum generated by focusing ~1 µJ of the laser source into a 6-mm-thick CaF_2 disk. The optical probe covers a broad spectral range from 360 to 790 nm. A mechanical delay line is used to record kinetics up to 10 ns after the electron pulse. A reference signal was split off from the broadband probe before the optical cuvette. Both probe and reference beams pass into the optical fibres, transmitted

to a spectrometer (Andor™ SR-303i-B), and dispersed onto a CCD camera (Andor™ Newton). Combining the broadband probe and the multichannel detector allowed the entire transient spectrum to be recorded in one shot.

Another detection system is capable of registering signals on longer time scales up to milliseconds. In our work, it was used to record kinetics up to several microseconds. The system consists of a xenon flash-lamp as a source of light and Kymera 328i-B2 spectrophotometer coupled with Hamamatsu C7700 streak camera as a signal recording system. The flash lamp has pulses of < 5 μs. The spectrum of light pulses can be reordered from 240 to 800 nm. Unlike pump-probe measurements, with a streak camera, all spectral changes are recorded in one pulse of the lamp. Therefore, a satisfying signal-to-noise ratio requires a large number of repetitions (~400-1000), which are then averaged.

3.3.2. Experimental conditions

The deposited dose per pulse was deduced from solvated electrons absorbance measurements in pure water and verified before each set of scans. The stroboscopic detection with a mechanical delay line was used for time-resolved studies in the range of 10 ns. For longer timescales, a transient absorption setup with a streak camera detection was used. The optical quartz cells of 5 mm length were used with thin (100 μm) optical windows for all experiments. Optical detection during pulse radiolysis measurements of AuNPs suspensions has some limitations. The gold nanoparticles suspensions strongly absorb in the UV–vis range. Thus, only the red light >600 nm could penetrate the samples. The solutions of 30 mL were circulated using a peristaltic pump with a flow rate of 40 mL min^{-1} for measurements in microsecond timescales, whereas, for subnanosecond scales, static quartz cuvettes were used.

Utilizing pulse radiolysis coupled with time-resolved spectroscopy requires a correct reference. In the study of AuNPs suspensions, pure water may not be suitable. The time evolution of radical species in AuNPs suspensions can be affected by the presence of nanoparticle stabilizers. Thus, supernatants of the samples are more appropriate references. Although for picosecond and nanosecond timescales, where bimolecular reactions are not significant, pure water could be appropriate as a reference. Our experimental setup allows easily for the determination of optical density within 1 mO.D. accuracy for a nanosecond and shorter timescales, and 5 mO.D. for a microsecond one. Thus, the solvated electron concentration could be determined with 50 nM and 250 nM accuracy, respectively.

3.4. RESULTS AND DISCUSSION

3.4.1. Artifacts in pump-probe measurements of highly scattering samples

Usually, pulse radiolysis experiments are performed for transparent samples because the light absorption and scattering obstruct spectroscopy measurements. This was a problem for all AuNPs samples prepared by the radiolytic method. These samples were almost opaque, so we had to use light with a wavelength of more than 700 nm. We found a decrease in the initial signal of solvated electrons at 10 ps for all samples prepared by the radiolytic method (Figure 3.9).

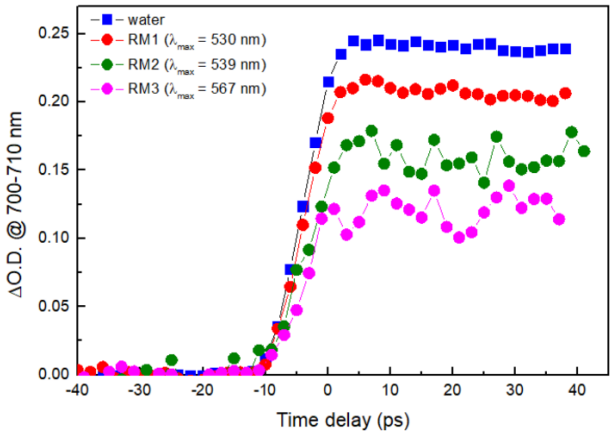

Figure 3.9. The recorded kinetics of solvated electrons in the RM1-3 samples - AuNPs prepared by the radiolytic method, containing 4 mM of gold atoms,100 mM of PVA and 100 mM of 2-propanol. All samples were light scattering. For more details, see Chapter 2.

Note that the drop in solvated electron concentration means scavenging of pre-solvated electrons. This scavenging process must be very effective since it competes with electron solvation with a time constant of 300 fs. Usually, it requires hundreds of mM of solute, which can react with solvated electrons. It was astounding to find the increase in pre-solvated electron scavenging with the increase in nanoparticle size at the same concentration of gold atoms. If we assume that the average size of nanoparticles in the samples RM1-3 is between 100 and 200 nm, it corresponds to the nanoparticle concentration lower than 150 pM. The pre-solvated electron scavenging in the RM3 sample is approximately 50%. We did not find any reasonable explanation for such a fast interaction between pre-solvated electrons and AuNPs. However, we found a correlation of the decrease in solvated electron signal at 10 ps after electron pulse with light absorption/scattering by AuNPs samples, presented in Figure 3.10.

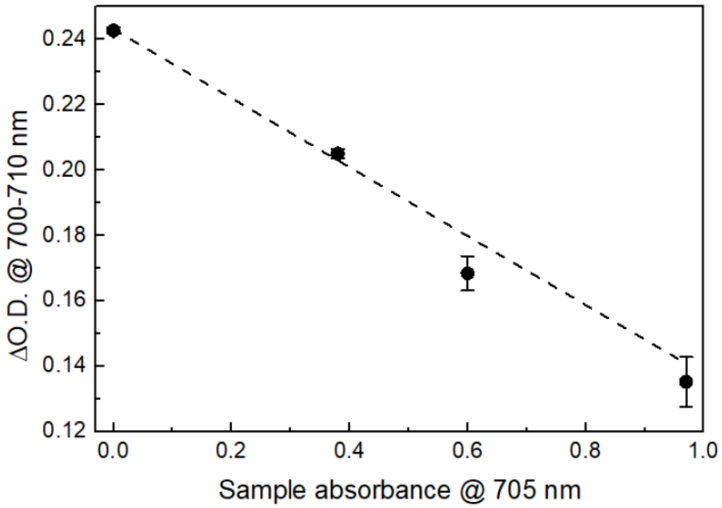

Figure 3.10. Correlation of decrease in solvated electron signal at 10 ps after electron pulse with light absorption/scattering by AuNPs samples. Signals of solvated electrons are taken from Figure 3.9, light absorption/scattering by AuNPs samples is taken from Figure 2.10.

Eventually, we found an instrumental problem to measure highly scattering samples. In reality, the correlation presented in Figure 3.10 depends on the amount of light passing through the samples, which is linearly correlated with the samples' light absorption. In our pump-probe measurements, one pulse of light is divided into two. One goes to the reference channel, another goes through the sample and comes to the optic fibre of the signal channel. Then both light pulses enter one 256 x 1024 pixel CCD camera, which has two areas of 128 pixels each (Figure 3.11).

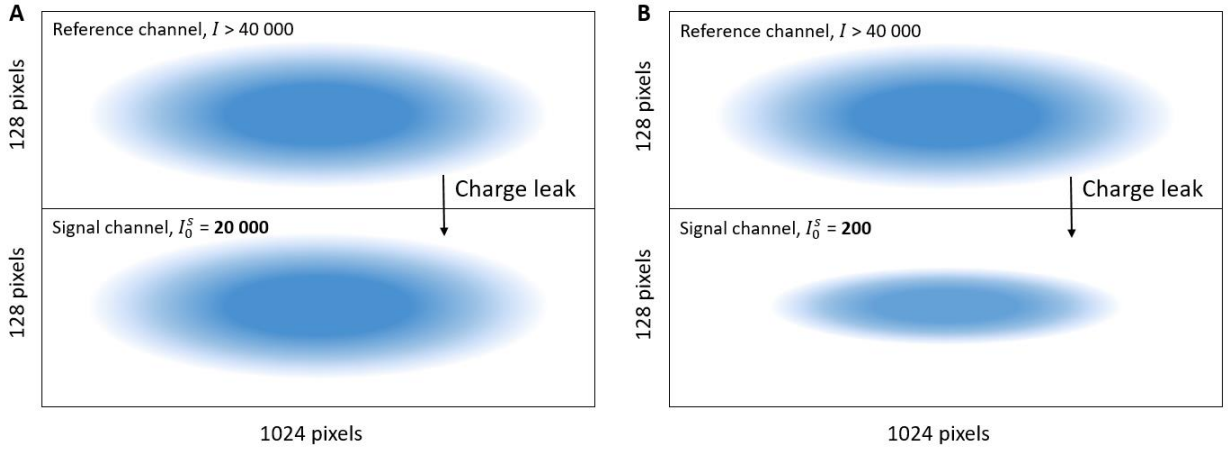

Figure 3.11. Simplistic representation of CDD camera for two experimental cases. The signal channel has a number of counts comparable with the reference one (**A**). The signal channel has a very low number of counts due to light absorption/scattering by the sample (**B**).

The optical density in kinetic measurements presented in Figure 3.9 is calculated by equation 3.1, where I^s and I^R are light intensity in signal and reference channels, I_0 and I_e are light intensity in the absence and presence of electron pulse. Thus, there are four different intensity signals. Bg and ε are background and error, respectively. Note that ε is relatively small compared to intensities. For simplicity, we will consider only the signal channel because the reference one passes through the air and is not affected by the sample.

$$log\frac{(I_0^s - Bg + \varepsilon)(I_e^R - Bg - \varepsilon)}{(I_e^s - Bg + \varepsilon)(I_0^R - Bg - \varepsilon)} = log\frac{I_0^{s'} + \varepsilon'}{I_e^{s'} + \varepsilon'} \quad (eq.\ 3.1)$$

The problem of the measurements was a small charge leak from the part of CCD where photons from the reference channel come to the area of the signal channel. It is not a problem for ordinary experiments with transparent solutions. Usually, there are approximately 20 000 counts in the signal channel in the absence of electron pulse and around 10 000 counts in the presence of electrons, which gives absorption of 0.301 (eq. 3.2).

$$log\frac{I_0^{s'}}{I_e^{s'}} = \log\left(\frac{20000}{10000}\right) = \log\left(\frac{200}{100}\right) = 0.301 \quad (eq.\ 3.2)$$

For example, the charge leak adds about 10 counts to the signal channel, almost not changing the result (eq. 3.3). However, if the amount of light in the signal channel is decreased to 200 counts due to light absorption and scattering by the sample, the same charge leak of 10 counts will significantly affect the measurement (eq. 3.4).

$$log\frac{I_0^{s'} + \varepsilon'}{I_e^{s'} + \varepsilon'} = \log\left(\frac{20000 + 10}{10000 + 10}\right) = 0.3008 \quad (eq.\ 3.3)$$

$$log\frac{I_0^{s'} + \varepsilon'}{I_e^{s'} + \varepsilon'} = \log\left(\frac{200 + 10}{100 + 10}\right) = 0.28 \quad (eq.\ 3.4)$$

Thus, the results presented in Figure 3.9 are artefacts due to the opacity of samples prepared by the radiolytic method. We could not increase enough the amount of light passing through the samples for an appropriate measurement even by significant dilution. The high light scattering by these samples is due to the presence of large nanoparticles of non-spherical shape. We suppose that previously reported pre-solvated electron scavenging by AuNPs can also be explained by the artefacts of spectroscopy measurements since a similar detection system was used.[66]

3.4.2. Gold nanoparticles effect on the yield of solvated electrons

Correct pump-probe measurements were possible for all samples prepared by reduction with sodium borohydride and Turckevich method. Enough number of photons even at 650 nm could pass through these samples, which allowed to perform proper measurements avoiding a previously described issue. In Figure 3.12, the results of pulse radiolysis measurements are presented for two samples, BH1 and TM1, with the gold atomic concentration of 3 mM prepared by two different methods. We found no difference in solvated electrons production for the samples BH1, TM1 and TM2 compared to water on a time scale of a few tens of picoseconds, where radical–radical reactions do not occur. Similar results for the TM2 sample can be found in Appendix 1 at the end of the manuscript (Figure S1 A).

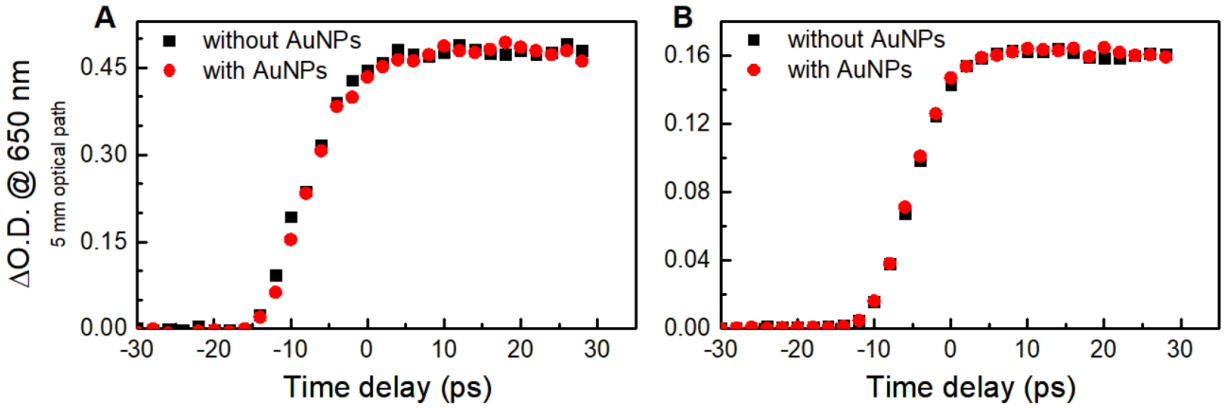

Figure 3.12. Kinetics of solvated electrons within tens of picoseconds after a 5 ps electron pulse in water (black squares) and AuNPs suspensions containing 3 mM of gold atoms (red dots) prepared by **A** – reduction with sodium borohydride (BH1, λ_{max} = 520 nm, d_{TEM} = 20 ± 4 nm) and **B** – Turkevich method (TM1, Au: citrate ratio is 1:1.5, λ_{max} = 533 nm, d_{TEM} = 35± 13 nm).[69]

The solvated electron concentration just after the 5 ps electron pulse correlates with all •OH radicals produced by the ionization path of water radiolysis (see Scheme 3.1). These results show that the presence of AuNPs at a concentration up to 3 mM (600 µg/ml or 0.06 wt.%) does not affect the ionization path of water radiolysis, and any interaction of pre-solvated electrons with AuNPs does not occur.

3.4.3. Gold nanoparticles effect on the yield of hydroxyl radicals

The yield of •OH radicals at 10 ps after energy deposition is greater than those of solvated electrons, 0.52 µmol/J and 0.44 µmol/J, respectively.[8,65] Higher formation of •OH radicals is due to their formation from the dissociation of excited water molecules (Scheme 3.1). Any change in •OH radical concentration will affect the kinetic of solvated electrons.

Therefore, to study the effect of AuNPs on the water dissociation channels, we measured solvated electron kinetics in nanosecond and microsecond time scales in suspensions of AuNPs and compared them with appropriate references.

For the nanosecond time scale, water could be used as a reference. We also did not find any effect of AuNPs on solvated electron kinetics. These observations indicate that the radical–radical reactions occurred in the radiation track in the same way as in the solution without AuNPs (Figure 3.13). Similar results for TM2 samples can be found in Appendix 1, Figure S1 B.

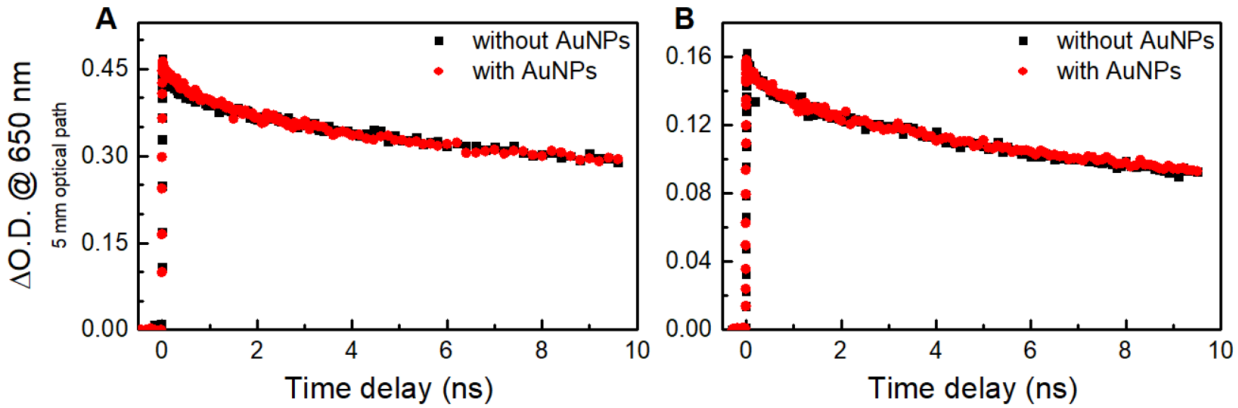

Figure 3.13. Kinetics of solvated electrons within ten nanosecond time scale after a 5 ps electron pulse in water (black squares) and AuNPs suspensions containing 3 mM of gold atoms (red dots) prepared by **A** – reduction with sodium borohydride (BH1, λ_{max} = 520 nm, d_{TEM} = 20 ± 4 nm) and **B** – Turkevich method (TM1, Au: citrate ratio is 1:1.5, λ_{max} = 533 nm, d_{TEM} = 37 ± 13 nm).[69]

We selected supernatants as references for a microsecond range because they contained most of the solutes, which could react with e^-_s and/or •OH radicals. In the case of AuNPs prepared by the borohydride reduction method, the decay of hydrated electrons was slower in AuNPs suspension and its supernatant than in neat water with the same pH (Figure 3.14 A). It is explained by the fact that anions BO_3^{3-} and BH_4^- react with the •OH radical,[70] suppressing the •OH radical-solvated electron interaction, which increases the lifetime of e^-_s. In contrast to the AuNPs solution prepared by the Turkevich method, the decay in the supernatant and AuNPs suspension was faster than in water (Figure 3.14 B) because hydrated electrons reacted with acetone dicarboxylic acid (DCA) generated during the synthesis as a byproduct of citrate oxidation.[41] Absorption at 260 nm in the supernatant verified the presence of DCA (Figure 2.4). The rate constant of the hydrated electron reaction with DCA is expected to be similar to the acetone reaction (6.5×10^9 $M^{-1}s^{-1}$).[70] The same solvated electrons kinetics in AuNPs suspensions and

supernatants demonstrate the absence of any primary radical overproduction reported for similar AuNPs by indirect measurements.[24,33]

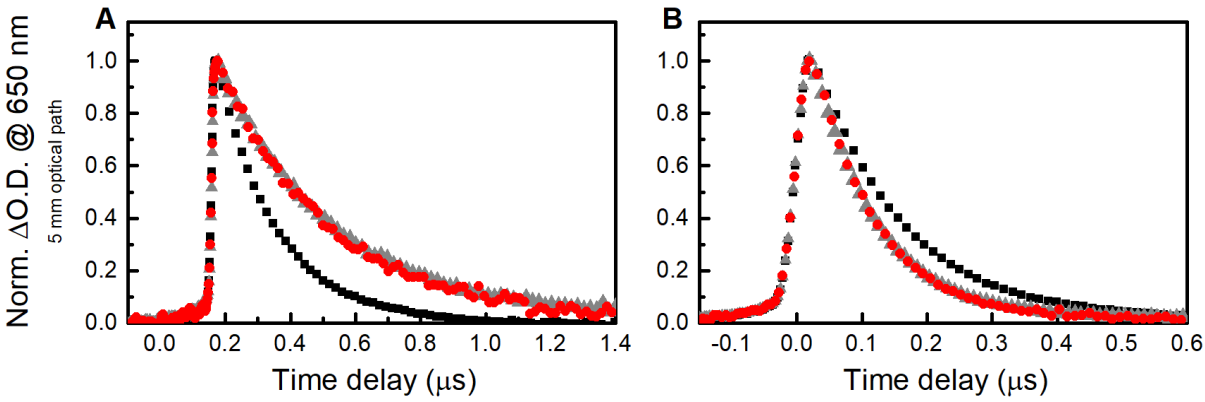

Figure 3.14. Kinetics of solvated electrons within a microsecond time range after a 5 ps electron pulse in water (black squares), AuNPs suspensions containing 3 mM of gold atoms (red dots), and their supernatants (grey triangle). (**A**) AuNPs were prepared by the borohydride reduction method (BH1, λ_{max} = 520 nm, d_{TEM} = 20 ± 4 nm). The BH1 sample, supernatant, and water had pH 8. (**B**) AuNPs were prepared by the Turkevich method (TM1, Au: citrate ratio is 1:1.5, λ_{max} = 533 nm, d_{TEM} = 37 ± 13 nm). The TM1 sample, supernatant and water had pH 6.[69]

The conducted experiments are different from those in vitro and in vivo due to extreme dose rates exceeding 10^{13} Gy s^{-1} (100 Gy per pulse of 5 ps). At such high dose rates, the lifetime of radicals was significantly reduced, e.g. the solvated electrons were entirely disappearing within ca. 1 μs (Figure 3.14) due to a high concentration of later and •OH radicals in the order of micromoles per litre. The concentration of AuNPs lay in the range of 12 nM (for 20 nm AuNPs with the gold atomic concentration of 3 mM). Thus the interaction between radicals and particles, which is discussed elsewhere,[71,72] was a statistically rare event in our conditions. Therefore, observed decays of solvated electrons in the microsecond range were explained by radical chemistry mainly within the radicals' spurs and diffusion into the volume of the solution.

We stress that the conditions of our experiments are comparable with some works stating •OH radical overproduction. Some of these works report a 4.5-fold enhancement of •OH radical production even for 1.25 MeV gamma rays, which have a similar linear energy transfer as 8 MeV electrons used in our work.[33] Another critical point is that •OH radical overproduction was measured in a homogenous solution. Therefore, it should be possible to detect such effects by pulse radiolysis measurement. Our direct measurements by pulse radiolysis contradict indirect ROS detection by a fluorescent method. Therefore, published

results on ROS overproduction measured by indirect techniques will be revised in the next chapter.

3.4.4. Importance of controlling sample composition

To prepare AuNPs by the radiolytic method (samples RM1-3), 2-propanol was used as •OH radical scavenger. In reactions of 2-propanol with •OH radicals and •H atoms (reaction 2.10 and 2.11 in section 2.2.3), the radical of 2-propanol is formed by H atom abstraction from alpha carbon. Since this radical has a RedOx potential of -1.5 V, it transforms to acetone reducing gold cations. Acetone is an effective electron scavenger due to carbon-oxygen double bound. Therefore, the decay of solvated electrons occurs faster in AuNPs suspensions and their supernatants than in water at the same pH (Figure 3.15 A). Unlike other samples discussed above, water could not be used as a reference even at the nanoscale time for all samples prepared by the radiolytic method. Note that the initial signal of solvated electrons is lower in AuNPs suspension than in water and in the supernatant because of the low number of photons that can pass through the sample due to light scattering. This problem of artefacts in pump-probe measurements of highly scattering samples was discussed in section 3.4.1.

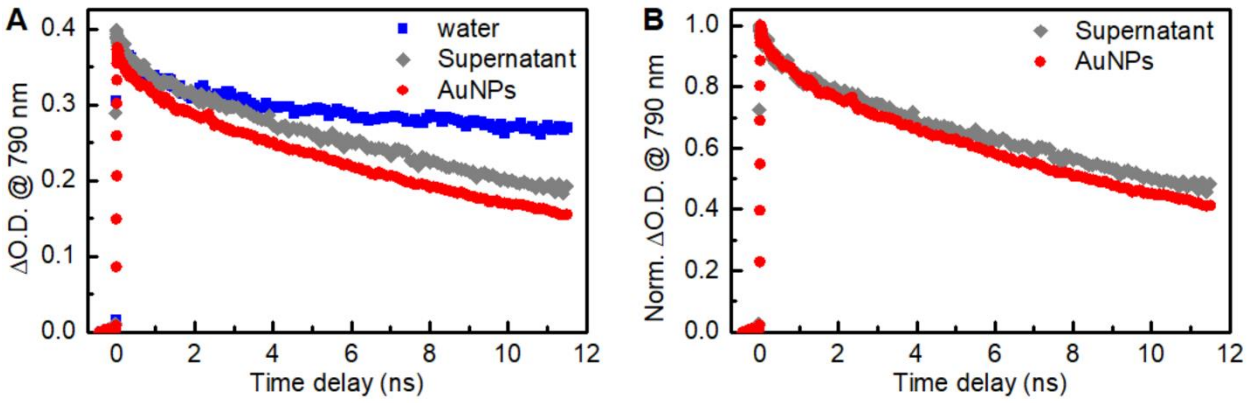

Figure 3.15. Kinetics of solvated electrons within nanosecond time scale after a 5 ps electron pulse in water (blue squares), AuNPs suspension (red dots) prepared by the radiolytic method and its supernatant at pH 8. AuNPs – RM1 (4 mM of gold atoms, λ_{max} = 530 nm). The supernatant was prepared by AuNPs precipitation by centrifugation. **A** – original data; **B** – normalized data.

We encountered poor reproducibility of solvated electron kinetics in AuNPs suspensions obtained by the radiolytic method and in their supernatants. We have always observed the acceleration of solvated electron decay with repeated use of samples. The reason for that is the formation of acetone from 2-propanol under irradiation. Interestingly, this

effect was stronger in the presence of AuNPs. Therefore, in Figure 3.15 B solvated electron decay is slightly faster in AuNPs suspension compared to the supernatant. This effect was observed for all AuNPs obtained by other methods with the addition of 2-propanol before pulse radiolysis measurement. These results showed that the presence of AuNPs increases acetone formation in an irradiated solution containing 2-propanol. This phenomenon will be discussed in detail in the next chapter.

3.5. CONCLUSIONS

We did not detect any increase in primary water radicals' formation in the presence of AuNPs at concentrations comparable to those used in radiosensitization studies (up to 3 mM of gold atoms, 600 µg/ml or 0.06 wt.%). On the one hand, such results are expected because physical dose enhancement is insignificant due to the low concentration of nanoparticles and high electron beam energy of 8 MeV. On the other hand, the direct measurements of solvated electrons showed that even if nanoparticles increase ROS production, this is unrelated to energy absorption and water radiolysis.

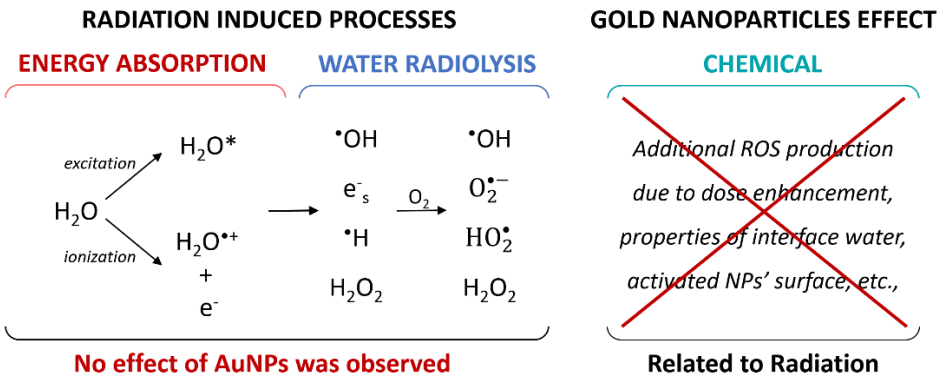

Figure 3.16. Schematic presentation of the results of pulse radiolysis experiments in relation to understanding AuNPs radiosensitizing effect.

Moreover, our results contradict previously reported pre-solvated electron scavenging by AuNPs stabilized by the ionic liquid.[66] We believe that two aspects of pulse radiolysis experiments coupled with spectroscopy measurements were not considered in that work: the light scattering problem and the utilization of an appropriate reference.

In addition, we observed that if samples contained 2-propanol, then kinetics of solvated electrons were gradually accelerated with the accumulation of the absorbed dose. Surprisingly, this effect was stronger in the presence of AuNPs. This is a preliminary result on the AuNPs' effect on the sample composition, probably, due to their catalytic properties, which will be discussed in the next chapter.

CHAPTER 4. CATALYSIS OF REACTIONS INVOLVING ORGANIC RADICALS

Contents

4.1. INTRODUCTION

As mentioned in the previous chapter, in all the studies reporting an increase in ROS production in the presence of nanoparticles, ROS were measured by indirect methods. Our direct measurements of the formation and kinetics of solvated electrons by pulsed radiolysis did not confirm any additional formation of primary water radicals. In this chapter, we will discuss methods for measuring ROS concentration in the presence of nanoparticles used in radiosensitization studies. We will also review the knowledge of radiation chemistry and the catalysis of reactions involving radicals. Finally, using two test systems, we will study in detail the catalytic effect of AuNPs on radical chemistry to explore the applicability of the methods used to quantify ROS concentration in the presence of nanoparticles in radiosensitization studies.

4.1.1. Methods for reactive oxygen species detection

Reactive oxygen species (ROS) such as $^{\bullet}OH$, $O_2^{\bullet-}$ have a short lifetime. Therefore, they are detected using sacrificial molecules that form more stable and easily detectable products when reacting with ROS. There are two common types of ROS detection: using spin traps and fluorescent dyes.

Spin traps are molecules that act as free radical scavengers to form new radicals with a much longer lifetime. Due to unpaired electrons, radicals can be detected by measuring electron paramagnetic resonance (EPR). Examples of $^{\bullet}OH$ and superoxide ($O_2^{\bullet-}$) radicals' detection by 5,5-dimethyl-1-pyrroline-N-oxide spin trap is presented in Figure 4.1.[73]

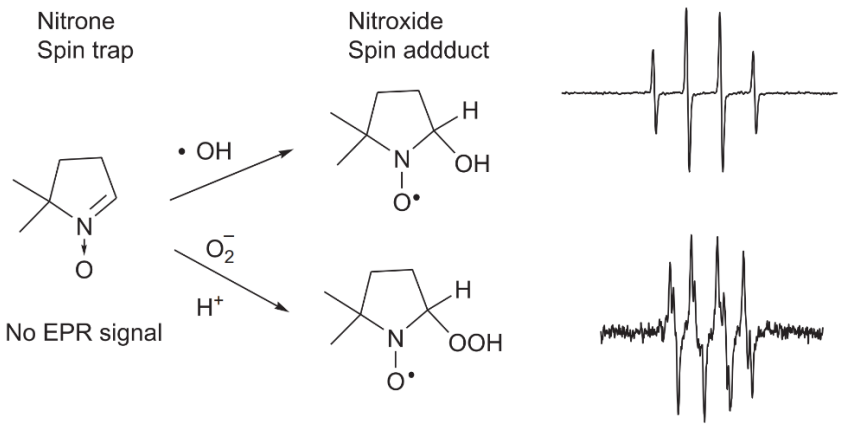

Figure 4.1. EPR signals of reaction products of hydroxyl and superoxide radicals with 5,5-dimethyl-1-pyrroline-N-oxide (DMPO) spin trap.[73]

ROS detection by fluorescent dyes is the most common method in biological experiments.[74,75] This method is based on converting a non-fluorescence molecule into a fluorescent one in reaction with ROS. It is assumed that the increase in fluorescent intensity is proportional to the increase in ROS concentration. For example, detection of •OH radicals is based on hydroxylation of aromatic compounds producing fluorescent products (Figure 4.2).[76] There are various dyes based on benzoate, coumarin and phenoxazinone systems.[74]

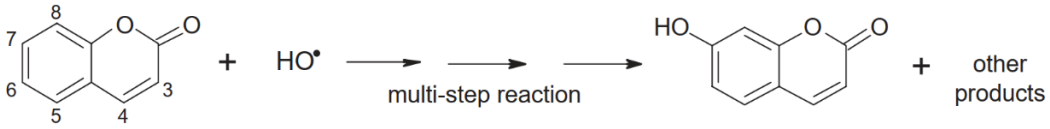

Figure 4.2. Coumarin hydroxylation forming fluorescent 7-hydroxycoumarin.[76]

In contrast to using a paramagnetic probe formed as from a one-step reaction of the initial molecule with a free radical, a fluorescent probe formation mechanism is more complex. The first step is the same in both methods, the formation of an adduct. However, fluorescent dyes are complex molecules. For example, the coumarin molecule has six sites for the •OH radical attack (Figure 4.2). We will consider only one site to discuss the mechanism of coumarin hydroxylation (Figure 4.3).

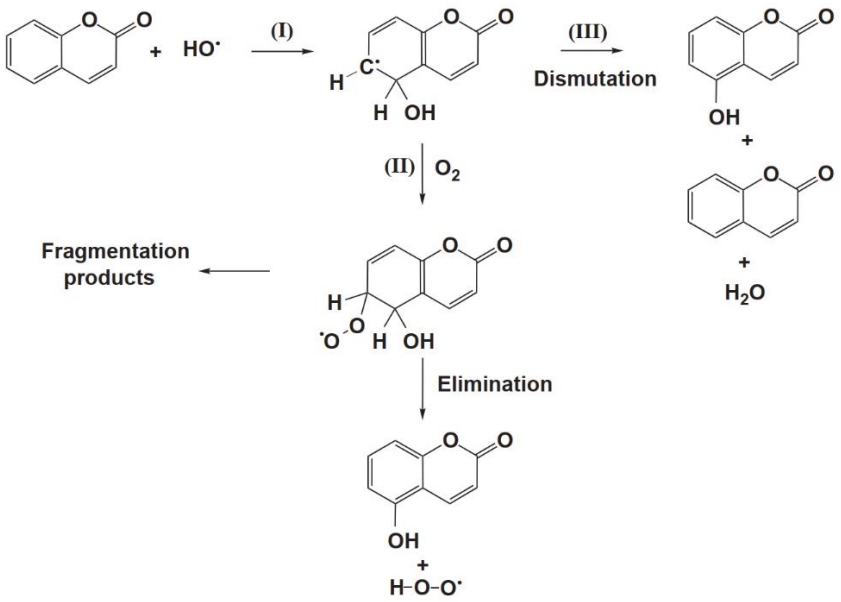

Figure 4.3. Reaction mechanism of coumarin hydroxylation. Note that only one site of •OH radical attack is considered.[76]

The adduct is formed after the attachment of •OH radical to the molecule (Figure 4.3 reaction I). Then, the adduct must be oxidized to form hydroxycoumarin. In the absence

of oxidizers, it occurs by disproportionation reaction between two adducts (Figure 4.3 reaction III). In the presence of oxygen, the yield of hydroxylation reactions is increased due to oxygen attachment to the adduct forming peroxyl-type radical with further elimination of $HO_2^{\bullet}$ radical. The reaction yield of hydroxylation is low, and many other products are formed in addition to the fluorescent product. The main concern about the fluorescent method is that it is assumed that the reaction mechanism of fluorescent product formation remains the same under different experimental conditions.

4.1.2. Hydroxyl radical-induced oxidation of aromatic compounds

In radiation chemistry, the reactivity of hydroxyl radicals towards organic compounds has been extensively studied. Much attention has been paid to studying radical-induced reactions of amino acids, DNA and RNA bases to understand processes occurring in living systems under exposure to ionizing radiation.[18,19,57,77–82] We will consider a few examples of hydroxyl radical reactions with simple aromatic compounds. Benzene is the simplest aromatic molecule. It has six equivalent sites for •OH radical attachment. The main product of benzene oxidation by hydroxyl radical is phenol (Figure 4.4).[83] However, even for so simple molecule reaction mechanism in the presence of oxygen is complex, more than fifteen different ring-opened and fragment products are formed.

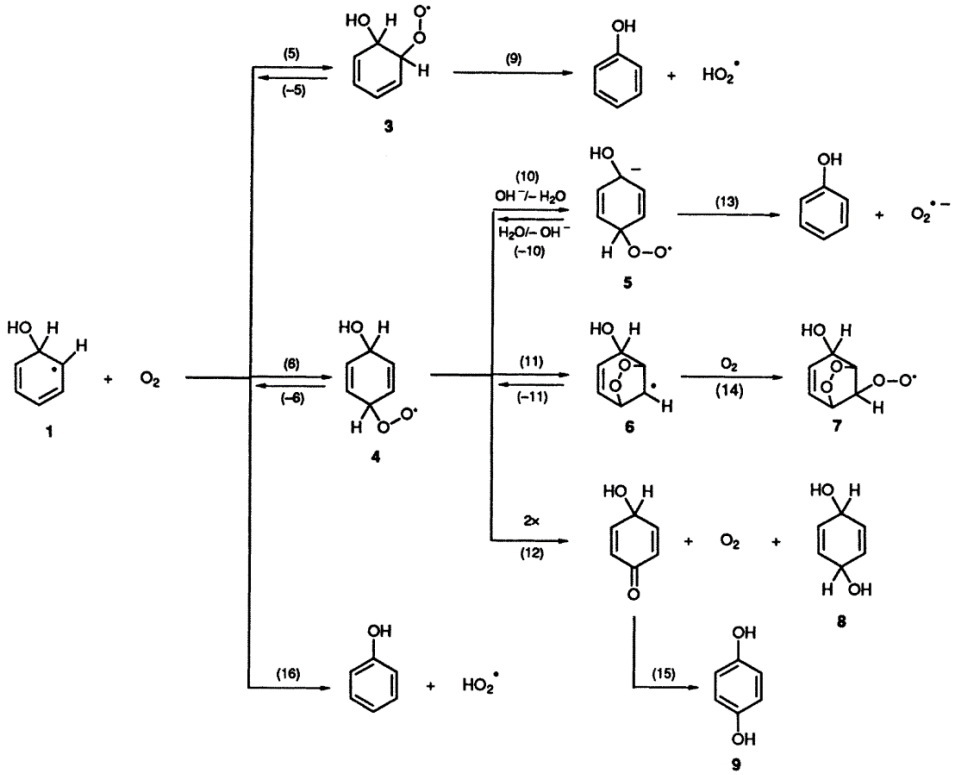

Figure 4.4. Benzene oxidation induced by hydroxyl radical in the presence of oxygen.[83]

The effect of the experimental condition was well demonstrated for phenylalanine oxidation by •OH radicals.[84] Similar to benzene oxidation, •OH radical reacts with phenylalanine by attachment forming adducts. Phenylalanine has one functional group; therefore, there are five sites for •OH radical attack (Figure 4.5). However, an adduct with OH group in *ipso* position (1 in Figure 4.5) and •H atom abstraction from carbon in the functional group (5 in Figure 4.5) are minor and account for about 20% of •OH radicals. Further oxidation of adducts (2-4 in Figure 4.5) with OH group in *ortho*, *meta* and *para* positions leads to the formation of tyrosines, which are the main products.

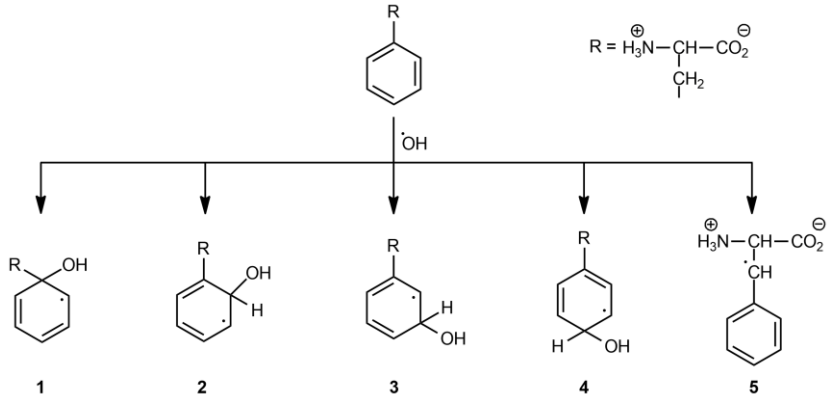

Figure 4.5. Phenylalanine reaction with hydroxyl radical.[84]

An aqueous solution of phenylalanine at millimolar concentration was irradiated by gamma rays under N_2O atmosphere. N_2O was used to convert solvated electrons to hydroxyl radicals. The influence of molecular oxidizers such as O_2 and $Fe(CN)_6^{3-}$on tyrosines' formation was investigated. As discussed above, oxygen attaches to OH adducts of aromatic compounds, forming peroxyl type radicals (Figure 4.6). Eventually, it increases the formation of hydroxylated products. In the case of phenylalanine oxidation, tyrosines formation was increased more than five times in the presence of O_2 (Table 4.1).

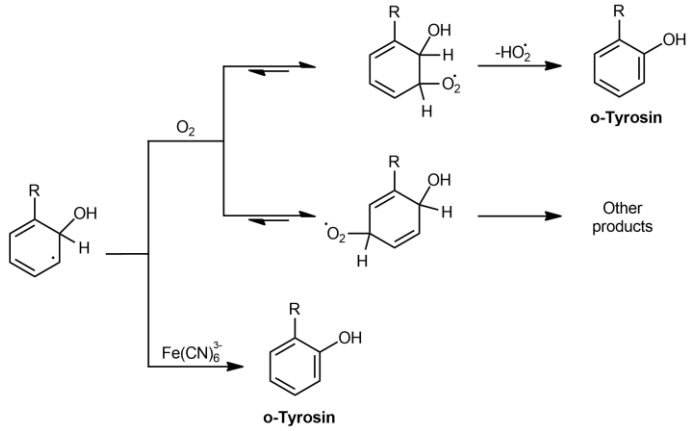

Figure 4.6. Phenylalanine adduct oxidation to tyrosin by oxygen and $Fe(CN)_6^{3-}$.[84]

$Fe(CN)_6^{3-}$ showed an even stronger effect on tyrosines formation. It was increased eight times compared to the absence of additional oxidants in the solution. Such effect was explained by direct oxidation of the adducts by $Fe(CN)_6^{3-}$. Thus, it is possible to convert all adducts to hydroxylated products in the presence of oxidants.

Table 4.1. γ-Radiolysis of phenylalanine in neutral aqueous solutions, with various additives.[84]

	N_2O	**N_2O/O_2***	**$N_2O/Fe(CN)_6^{3-}$****
Product	**G(Product)/G(•OH)**		
Total Tyrosine	10%	52%	80%

* mixture 4:1 (v/v) saturated, ** $[Fe(CN)_6^{3-}]$ = 2 × 10^{-4} mM.

These results showed that hydroxylation of aromatic compounds by •OH radicals strongly depends on experimental conditions such as oxygen concentration. It is also important that other oxidants can increase the yield of hydroxylation by adducts oxidation.

4.1.3. Hydroxyl radical detection in the presence of nanoparticles

In the field of radiosensitization research, the idea of ROS overproduction in the presence of nanoparticles has been reported by many scientific groups. A lot of works has been summarized in a recent review.[24] Below, we will consider a couple of works reporting an increased •OH radical formation in the presence of AuNPs, discussing the used approach and proposed explanations.

As previously discussed, •OH radical detection is based on a hydroxylation reaction forming a fluorescent product. It is very important to note that it is the fluorescent signal measured in the experiments, which is then used to calculate the concentration of the product, which is used to calculate the concentration of •OH radicals. The radiolytic yield (G, mol J^{-1}) of the fluorescent product of •OH radicals is found from the slope of the linear approximation of the dependence of the species concentration on the applied dose. An example of such measurements is presented in Figure 4.7. In this work,[32] 2-[6-(4-amino)phenoxy-3H-xanthen-3-on-9-yl]benzoic acid (APF) was used for •OH radicals detection in the presence of 20 nm AuNPs at different concentrations. The slope on the fluorescent signal versus applied dose graph corresponds to the radiolytic yield of a fluorescent product, which is assumed to be proportional to the radiolytic yield of hydroxyl radicals. An increase in the fluorescent signal by 1.46 times was observed in the presence of 50.8 μM of AuNPs. It was explained by additional •OH radicals generation by the secondary water radiolysis possibly caused by the photoelectrons and fluorescent X-rays in the presence of AuNPs. However, the concentration of gold was 50.8 μM, which

corresponds to 0.001 wt.%. Thus, the physical dose enhancement cannot explain the observed results.

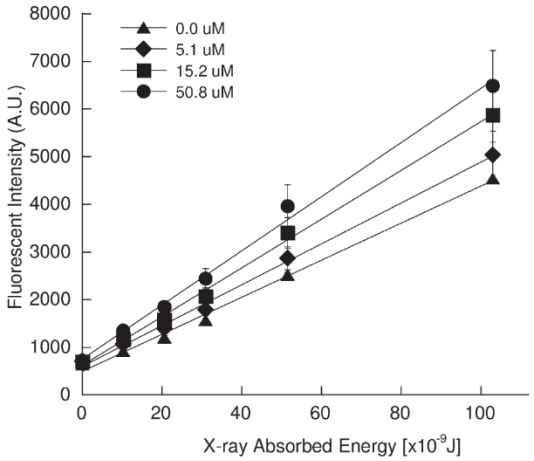

Figure 4.7. Fluorescent intensities of APF fluorescent probe for 0.0, 5.1, 15.2 and 50.8 μM of 20 nm AuNPs' solutions under x-ray irradiation.[32]

In another work,[34] •OH radicals were measured by coumarin fluorescent dye. A product of coumarin hydroxylation with OH group at position 7 (7OH coumarin) has intense fluorescence. In that work, a radiolytic yield of 7OH coumarin was measured in the presence of 32.5 nm AuNPs with different concentrations (graph in Figure 4.8).

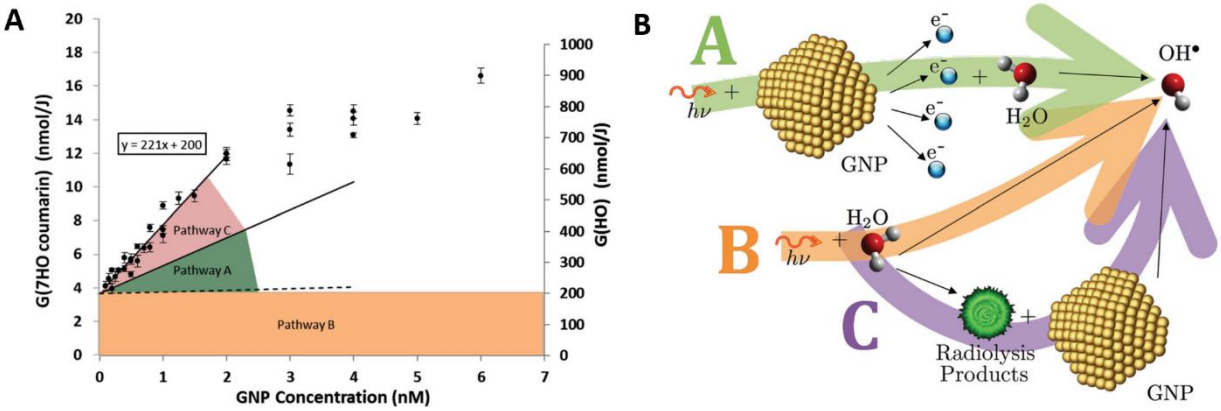

Figure 4.8. Measurements showing the yield of 7-hydroxycoumarin per Joule of radiation deposited in the sample (left y-axis) and calculated yield of •OH radical as functions of AuNPs concentration (**A**). Proposed pathways of •OH radical production in the presence of AuNPs (**B**).[34]

From 0 to 2 nM of AuNPs, a linear increase in radiolytic yield of 7OH coumarin was observed. 1 nM of 32.5 nm AuNPs corresponds to 1.05 mM of gold atoms or 0.021 wt.% of gold, which is comparable to the concentration of gold used in experiments *in vitro* and *in vivo*. The radiolytic yield of •OH radicals was calculated based on the concentration

of 7OH coumarin and presented on the right Y-axis (Figure 4.8 A). According to the experimental results at 1 nM of AuNPs, the radiolytic yield of •OH radicals is enhanced more than two times. The maximum 4.5-fold increase was achieved with 6 nM AuNP. The authors considered a few mechanisms of •OH radical production to explain the results (Figure 4.8 B).

Pathway B is a "normal" way of •OH radical production due to energy deposition in water leading to water radiolysis. Since 20 keV monochromatic X-rays were used as a radiation source, the dose enhancement effect was considered. Considering the difference in mass-energy absorption coefficient between water and gold at 20 keV energy, the dose enhancement of 1.025 was estimated. The dashed line shows it in the graph in Figure 4.8. Such a slight increase in dose could not explain the observed results, so other routes were proposed. It was proposed that apart from negligible dose enhancement, Pathway A also includes more efficient •OH radical production by photons, electrons, and holes leaving the nanoparticle and causing the reaction H_2O + Energy → •OH + ½ H_2, either in one step or a set of steps. In pathway C, the water-nanoparticle interface is thought to play a major role. It is assumed that interface water is structured on the AuNP surface, which weakens the H-OH bond, potentially making water radiolysis more efficient near the AuNP. The authors highlight the importance of the water-nanoparticle interface when nanoparticle solutions are exposed to ionizing radiation.

There is one more paper that should be mentioned here. In that work,[85] coumarin carboxylic acid (3CCA) was oxidized to 7-hydroxycoumarin-3-carboxylic acid (7-OH-CCA) by •OH radicals under X-ray radiation. An increased 7-OH-CCA formation was observed for AuNPs of 3, 7, and 30 nm at different concentrations. The lowest concentration to observe a 10% enhancement in 7-OH-CCA formation was less than 20 nM for the 3 nm AuNPs, 2.4 nM for 7 nm AuNPs, and 0.15 nM for 30 nm AuNPs. Moreover, the same effect was observed for platinum nanoparticles (PtNPs). In contrast to previously discussed work, increased formation of the fluorescent product was mainly explained by reactions of radical intermediates 3-OH-CCA• with superoxide-activated AuNPs or PtNPs. The nanoparticles could become negatively charged upon reaction with superoxide radicals, and the negatively charged particles would enhance the reaction between 3-OH-CCA• and one of the O_2 molecules around the negatively charged AuNP to form 7-OH-CCA (Figure 4.9).

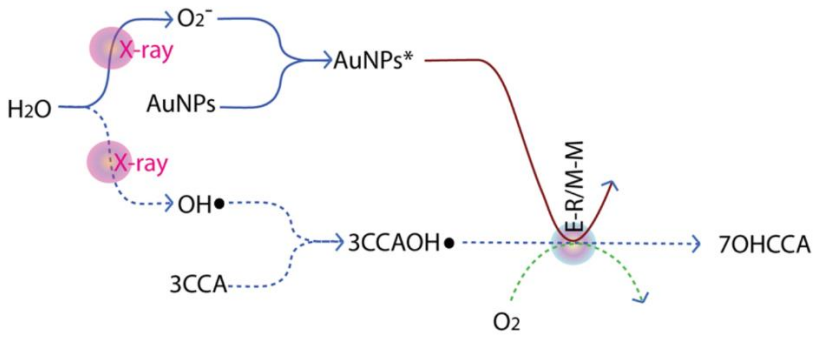

Figure 4.9. Two possible reaction pathways are shown: pathway 1 (dashed lines) is the previously established mechanism of formation of 7-OH-CCA, and pathway 2 (solid lines) displays the proposed superoxide-activated AuNP pathways. Pathway 2 employs •OH produced from AuNPs, but •OH from water would also be possible.[85]

Later, the same group demonstrated by ESR measurements that AuNPs are able to catalyze the conversion of intermediate radicals into final products.[86] The authors discuss the significance of this discovery for detecting ROS in the presence of AuNP. However, this work has not received much attention from the radiosensitization research community. Perhaps because the work only qualitatively demonstrated the ability of AuNP to catalyze reactions involving organic radicals without revealing the reaction mechanism.

4.1.4. Catalysis of radical reactions

Some works discussed in the previous section mentioned catalysis in different ways. In work utilizing coumarin, it was stated that gold nanoparticles enhance the radiolysis of water near the nanoparticles. In work utilizing coumarin carboxylic acid, it was stated that gold nanoparticles increase the conversion of the intermediate radical into stable products, but this requires activation of the nanoparticle's surface by the superoxide radical. Also, in section 1.4.2 devoted to the chemical effects of gold nanoparticles potentially responsible for the radiosensitizing effect, the catalytic production of superoxide radical on the surface of nanoparticles was mentioned. Therefore, it is important to discuss the catalytic activity of AuNP, focusing on reactions involving radicals.

In early studies, gold showed lower catalytic activity compared to platinum (Pt) and palladium (Pd) for hydrogenation and dehydrogenation reactions widely used in chemical synthesis.[87,88] Considering the high price of gold, it was not considered a promising catalyzer. This view changed in 1987 when it was found that small gold particles on Co_3O_4,

α-Fe_2O_3, or NiO supports efficiently catalyze CO oxidation at low temperatures.[89] However, the catalytic activity of metal nanoparticles, including gold, under normal conditions was demonstrated earlier by radiation chemistry and electrochemistry communities.[90–92] Nevertheless, the work on CO oxidation provoked great interest in studying the catalytic properties of gold nanoparticles (AuNPs).[93] Perhaps, the works in radiation and electrochemistry gold colloids were unnoticed due to the use of gold colloids, which are not suitable for industrial applications. Unsupported nanoparticles are still less studied for catalysis than supported ones.[94]

In 1979, it was discovered that silver and gold nanoparticles increase hydrogen production in an irradiated aqueous solution containing 2-propanol.[90,91] This was explained by the fact that metal nanoparticles in solution work as microelectrode taking carbon-centred unpaired electrons of 2-propanol radicals (reaction 4.1) and then reducing water yielding molecular hydrogen (reaction 4.2).[50] Since then, a lot of work has been done to study the ability of various nanoparticles to increase the formation of hydrogen in the presence of alcohol radicals.[95–103]

$$(CH_3)_2C^{\bullet}OH + AuNP \rightarrow (CH_3)_2CO + 2H^+ + AuNP^- \quad (R.4.1)$$

$$AuNP^- + H^+ \rightarrow AuNP + \frac{1}{2}H_2 + OH^- \quad (R.4.2)$$

Oxidation of 2-propanol radical leads to acetone formation. In this process, nanoparticles behave as an oxidant towards 2-propanol radicals. Obviously, acetone formation is affected by the presence of AuNPs, similarly as tyrosine formation was increased in the presence of $Fe(CN)_6^{3-}$ (see section 4.1.2). However, such experimental data are absent because the attention of researchers was focused only on the formation of H_2.

Apart from the research on the reduction of water, there are other works involving radicals and different NPs: ESR studies of unpaired electrons of the organic radicals interaction with gold nanoparticles (AuNPs),[104] the oxidation of organic free radicals initiated by AuNPs,[105] and place-exchange reactions catalyzed by AuNPs;[106] as well as alkyl radicals interaction with Pt, Ag, and AuNPs.[107–113] Even though cells always contain organic radicals formed by metabolic ROS present in cells, the catalytic activity of nanoparticles in reactions involving organic radicals has not been singled out as an independent research topic. In general, we would like to attract attention to the catalytic effect of NPs' in biomedical applications. To our knowledge, such discussion was being carried out only in a few studies. In the works of Zidki et al., it was proposed that the therapeutic properties of silver and gold NPs might be due to their ability to scavenge alkyl-radicals.[107] Narode

et al. studied the role of AuNPs in the degradation of tyrosine intermediates formed in the reaction with hydroxyl radical.[114]

4.2. Research objectives

The research objective is to study the catalytic effect of AuNPs on the oxidation of organic radicals produced by hydroxyl radical attack (Figure 4.10). The reactivity of •OH radical includes two types of reaction: •H atom abstraction and •OH radical attachment. Therefore, the results of two corresponding systems will be presented: α-hydroxyisopropyl radical oxidation to acetone (this radical is produced by •H atom abstraction from α carbon of 2-propanol), and acetanilide adducts oxidation forming *ortho*-, *meta*-, and *para*-acetaminophen (the adducts are formed by •OH radical attachment to the benzene ring of acetanilide molecule).

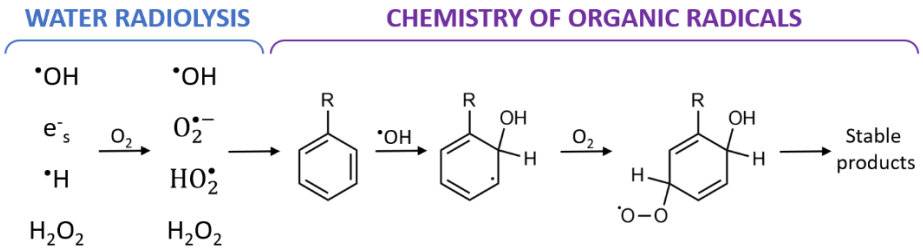

Figure 4.10. Radiation-induced processes that can be studied in steady-state experiments using gamma radiolysis

4.3. Experimental part

In all experiments presented below, we used only the BH1 sample – AuNPs prepared by reduction with sodium borohydride because it had the simplest composition, which was convenient for product analysis after irradiation. AuNPs' suspension and its supernatant had pH 7.

4.3.1. Gamma radiolysis

^{60}Co panoramic gamma source was used as a source of ionizing radiation. The values of the dose rates were verified by Fricke dosimetry and ranged from 20 to 70 Gy min^{-1}. Samples were irradiated in glass bottles closed with silicone corks under different atmospheres: air, O_2 (Alpha Gaz, Air Liquide), Ar (Alpha Gaz, Air Liquide), or N_2O (Alpha Gaz, Air Liquide) depending on experimental conditions. Samples of 2 or 4 ml were bubbled with a chosen gas at least for 10 min. AuNPs were aggregated right after

irradiation by adding NaCl (99.9%, VWR) up to 0.5 wt.% concentration and then precipitated by centrifugation.

Under N_2O atmosphere, solvated electrons are converted to hydroxyl radicals by reaction 4.3, giving the radiolytic yield of $^{\bullet}OH$ radicals of 5.6×10^{-7} mol J^{-1} in the homogeneous step of water radiolysis.

$$N_2O + e_s^- + H_2O \rightarrow {}^{\bullet}OH + OH^- + N_2 \quad (R.4.3)$$

4.3.2. Pulse radiolysis

The effect of the dose rate was investigated by using a picosecond electron (8 MeV) accelerator ELYSE (see section 3.3.1) as a source of extremely high dose rate radiation of 100 Gy per pulse with 5 ps pulse duration. The deposited dose per pulse was deduced from solvated electrons absorbance measurements in pure water and by Fricke dosimetry. The solutions of 30 mL were circulated using a peristaltic pump with a flow rate of 70 ml min^{-1}.

4.3.3. 2-propanol oxidation

4 ml of AuNPs' suspension (BH1 sample), the supernatant or water containing 100 mM of 2-propanol (99.5%, Sigma Aldrich) and 20 mM of acetone (99.8%, Sigma Aldrich) were irradiated at different doses. Acetone concentration formed during irradiation was measured by UV-vis absorption. The extinction coefficient 15.4 M^{-1} cm^{-1} at 265 nm was determined in the laboratory, which agrees with the literature data.[115] In experiments performed under N_2O atmosphere, samples did not initially contain acetone.

4.3.4. Acetanilide hydroxylation

2 ml of AuNPs' suspension and the supernatant containing 0.5 mM of acetanilide (≤100%, Jeulin, Évreux, France) were irradiated at different doses up to 200 Gy. Irradiated samples were analysed by high-performance liquid chromatography (Agilent Technologies 1260 infinity). A diode-array detector was used to record the light intensity in the range from 200 to 500 nm. The HPLC column was EC 50/4.6 Nucleoshell RP 18plus, 2.7 µm. The mixture of 97% water and 3% acetonitrile was used for isocratic elution at a 1.5 ml min^{-1} flow rate. The products of acetanilide hydroxylation (acetaminophen) were determined by comparing their absorption spectra and retention time with commercial standards: 2-acetaminophen (97%, Acros Organics) and 3-acetaminophen (99+%, Acros Organics) and 4-acetamidophen (>99%, Sigma-Aldrich).

4.3.5. Determination of radiolytic yields

To calculate radiolytic yields of formed or consumed species, we used standard values of radiolytic yields (G × 10^7, mol J^{-1}) of primary radicals for the homogenous step of water radiolysis, which are given in brackets below in scheme 4.1:[5,70]

$$H_2O \xrightarrow{\gamma} e_s^-(2.8),\ H_3O^+, {}^\bullet H(0.6), {}^\bullet OH(2.8), H_2O_2(0.7) \quad (S.4.1)$$

Dependencies of formed or consumed molecules during radiation versus applied dose are assumed to have a linear trend if the accuracy of the linear fit of all experimental points does not exceed 10%.

4.4. Results and discussion

4.4.1. Mechanism of α-hydroxyisopropyl radical oxidation

The first step of 2-propanol (ROH) oxidation in irradiated aqueous solution is a hydrogen atom abstraction mainly from the α carbon by ˙OH (reaction 4.4, k_1 = 1.9 × 10^9 M^{-1} s^{-1}) and ˙H (reaction 4.5, k_2 = 7.4 × 10^7 M^{-1} s^{-1}) radicals forming α-hydroxyisopropyl radical (R˙OH).[116] In the presence of acetone (20 mM), hydrated electrons (e^-_{aq}) are entirely scavenged, forming the same R˙OH radical (reaction 4.6, k_3 = 6.5 × 10^9 M^{-1} s^{-1}).

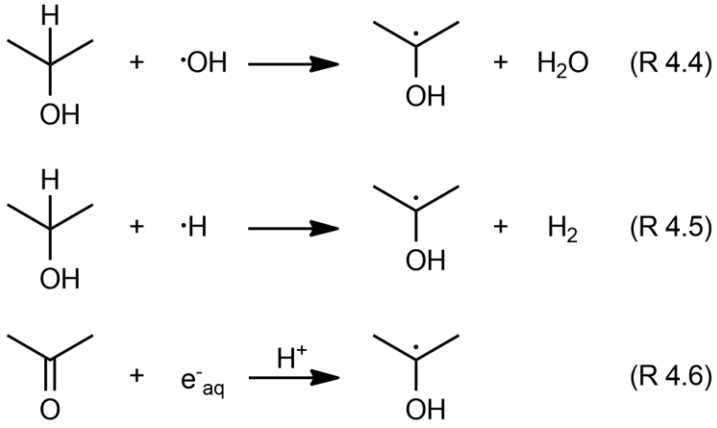

The radiolytic yield of R˙OH in an irradiated aqueous solution of 2-propanol/acetone can be calculated based on radiolytic yields of water radiolysis products (see Scheme 4.1 in section 4.3.5) giving the value of 6.2 × 10^{-7} mol J^{-1} (eq. 4.1).

$$G(R^\bullet OH) = G\left(e_{aq}^-\right) + G({}^\bullet OH) + G(H^\bullet) = 6.2 \times 10^{-7} \text{mol J}^{-1} \quad (eq.4.1)$$

The oxidation of R˙OH radicals leads to acetone formation, which was detected by absorption measurements (Figure 4.10). Then, acetone concentration was determined spectroscopically (@265nm, 15.4 M^{-1} cm^{-1})

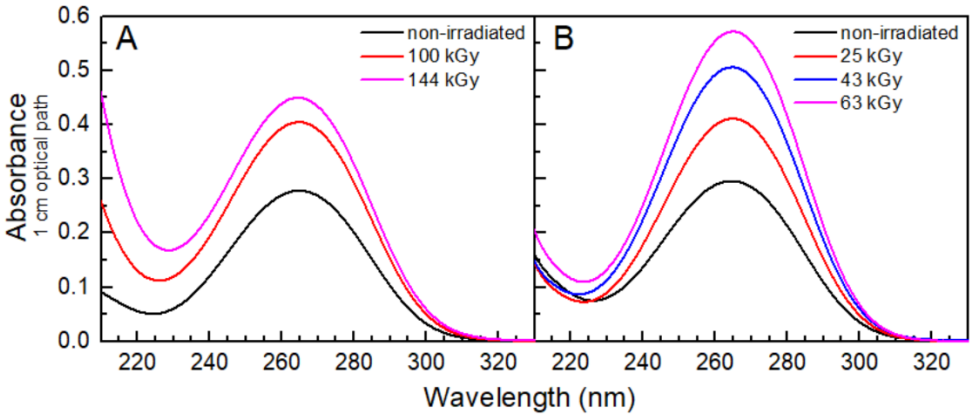

Figure 4.10. Evolution of UV-vis absorption spectra after different dose deposition. Samples contained 100 mM of 2-propanol and 20 mM of acetone in the supernatant (**A**) and in the BH1 sample - AuNPs prepared by reduction with sodium borohydride containing 3 mM of gold atoms (**B**). Both solutions were deoxygenated with Ar.

To find acetone formation yield, its concentration measured after irradiation was plotted versus applied dose considering the initial acetone concentration in the samples. All experimental points were fitted with a linear fit. The slopes (Figure 4.11) represent radiolytic yield in 10^{-7} mol J^{-1} units.

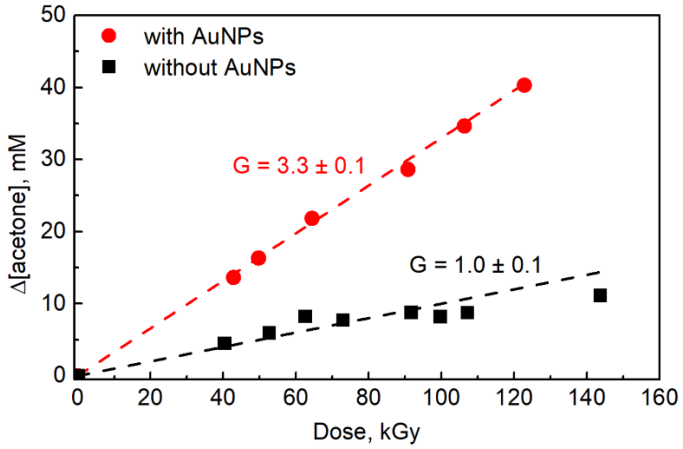

Figure 4.11. Acetone formation in AuNPs' suspension containing 3 mM of gold atoms (red dots) and supernatant (black squares) under gamma radiation. Both solutions contained 100 mM of 2-propanol, 20 mM of acetone and were deoxygenated by Ar.[117]

The acetone formation yield in the absence of AuNPs can be explained assuming that the oxidation of R•OH to acetone occurs through two reactions: disproportionation of two R•OH radicals (reaction 4.7) and oxidation of R•OH by hydrogen peroxide (reaction 4.8). One electron reduction of H_2O_2 produces an additional •OH radical. Therefore, H_2O_2 does not consume R•OH radicals because the additionally produced •OH radical (reaction 4.8) will oxidize 2-propanol forming the R•OH radical again (reaction 4.4).

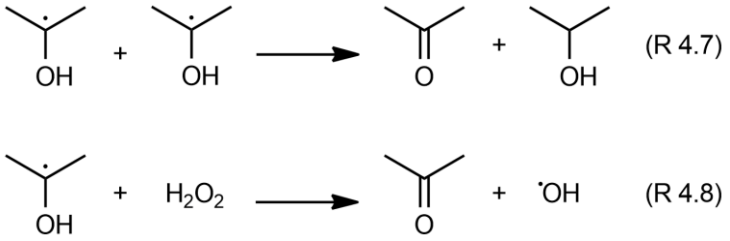

Overall radiolytic formation yield of acetone in the absence of AuNPs can be calculated using equation 4.2, where the yield of hydrated electrons is subtracted because acetone is consumed through reaction 4.6. The proposed reaction mechanism of R•OH oxidation to acetone in the absence of AuNPs explains well the experimental results presented in Figure 4.11.

$$\mathrm{G(acetone)} = \frac{1}{2}\mathrm{G(R^{\bullet}OH)} + \mathrm{G(H_2O_2)} - \mathrm{G}\left(\mathrm{e_{aq}^-}\right) = \ 1.0 \times 10^{-7}\mathrm{mol\,J^{-1}}\ (\mathrm{eq.\,4.2})$$

The acetone formation was increased more than three times in the presence of AuNPs. The direct oxidation of R•OH radicals can explain the higher formation yield of acetone in the presence of AuNPs to acetone. This catalytic reaction (reaction 4.9) should compete with the disproportionation (reaction 4.7). However, even at 0.1 mM (ca. 0.002 wt.%) of gold concentration, which corresponds to 0.4 nM of AuNPs, the same acetone radiolytic yield of 3.1 ± 0.1×10^{-7} mol J^{-1} was obtained (Figure 4.12).

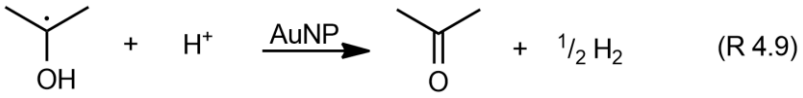

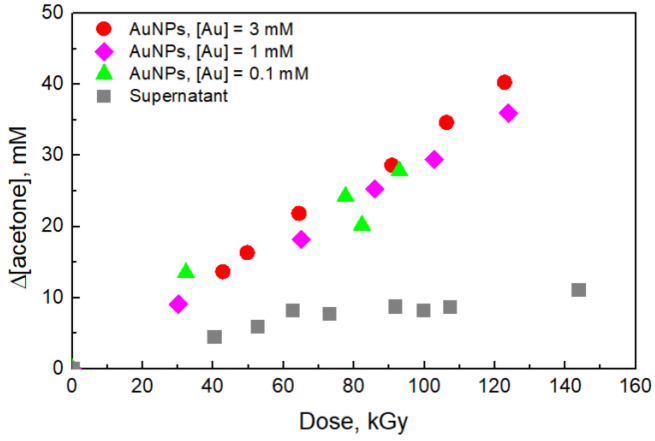

Figure 4.12. Acetone formation in AuNPs' suspension at different gold concentrations. The BH1 sample was diluted with deionized water. All solutions contain 100 mM of 2-propanol, 20 mM of acetone and deoxygenated by Ar gas.

Applying the reaction mechanism discussed above for the solution without AuNPs but substituting the disproportionation reaction by direct R•OH oxidation catalysed by AuNPs (reaction 9), the acetone yield should be equal to 4.1 × 10^{-7} mol J^{-1} (eq. 4.3).

$$\mathrm{G(acetone) = G(R^{\bullet}OH) + G(H_2O_2) - G(e_{aq}^-) = \ 4.1 \times 10^{-7} mol\ J^{-1}} \ \mathrm{(eq.\ 4.3)}$$

However, the experimental value of acetone yield in the presence of AuNPs equals 3.3 ± 0.1 × 10^{-7} mol J^{-1} (Figure 4.11). The difference between predicted and experimental values is close to the yield of H_2O_2 (0.7 × 10^{-7} mol J^{-1}). We can assume that H_2O_2 in the presence of AuNPs does not participate in the oxidation of R•OH and does not produce additional •OH radicals. Our assumption agrees with the proposition that H_2O_2 into water and oxygen in contact with nanoparticles.[50,118] Thus, the acetone formation yield can be calculated by equation 4.4. In this case, experimental and predicted values fit each other well within the experimental error (Figure 4.11).

$$\mathrm{G(acetone) = G(R^{\bullet}OH) - G(e_{aq}^-) = \ 3.4 \times 10^{-7} mol\ J^{-1}} \ \mathrm{(eq.\ 4.4)}$$

The competition between the catalytic oxidation of R•OH and the disproportionation reaction was not easy to demonstrate by varying AuNPs' concentrations. Therefore, in addition to the steady-state irradiation (^{60}Co) of the solutions, another approach was applied where the picosecond electron accelerator was used as a source of radiation with an extremely high dose rate (100 Gy per pulse of 5 ps duration, Table 4.2). The drastic increase of the dose rate from 1 Gy s^{-1} for gamma rays and 10^{13} Gy s^{-1} for electron pulse increases the transient concentration of R•OH, allowing disproportionation reaction of R•OH to compete with its oxidation at the surface of AuNPs. In this case, the presence of AuNPs should not affect the acetone formation yield.

For these experiments, irradiated solutions contained only 100 mM of 2-propanol, and N_2O was used to scavenge hydrated electrons instead of acetone. In this case, all hydrated electrons were converted to •OH radicals within 3 ns.[70,119] In this condition, G(R•OH) can still be calculated by equation 4.1 (6.2 × 10^{-7} mol J^{-1}) as in the previous experiments.

Table 4.2. Dose rate effect on acetone formation yields in the absence (water) and presence of AuNPs (3 mM). Irradiated solutions contained 100 mM of 2-propanol under N_2O atmosphere.

Dose rate, Gy s^{-1}	**G(acetone), × 10^7 mol J^{-1}**	
	with AuNPs	*without AuNPs*
~1 (^{60}Co)	6.1 ± 0.1	4.3 ± 0.2
~10^{13} (ELYSE)*	4.4 ± 0.1	4.4 ± 0.1

*ELYSE is an electron accelerator (dose rate = 100 Gy/pulse with pulse duration of 5 ps)

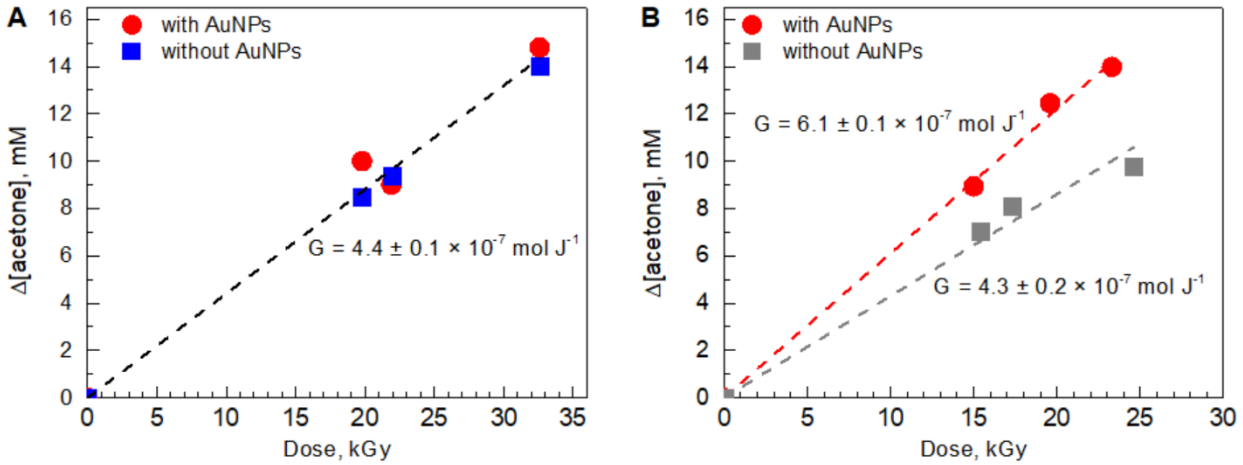

Figure 4.13. (**A**) Acetone formation in aqueous solutions containing 100 mM of 2-propanol under N_2O atmosphere irradiated by (**A**) electron accelerator ELYSE (dose rate ~10^{13} Gy s^{-1}), (**B**) gamma rays (^{60}Co). Red dots represent the BH1 sample – AuNPs prepared by reduction with sodium borohydride containing 3 mM of gold. Blue and grey squares represent water and the supernatant, respectively.

We found that in the case of gamma irradiation where the concentration of R•OH is low, the experimental value of acetone formation yield in the presence of AuNPs equals the yield of R•OH within the experimental error (Table 4.2). This result confirms that only the direct oxidation of 2-propanol radical to acetone catalyzed by AuNPs is involved (eq. 4.5).

$$\mathrm{G(acetone) = G(R^{\bullet}OH) = \ 6.2 \times 10^{-7} mol\ J^{-1}}\ \mathrm{(eq.\ 4.5)}$$

In the absence of AuNPs, but in all other things being equal (^{60}Co), the acetone formation mechanism should include disproportionation and oxidation of R•OH by H_2O_2 reactions (eq. 4.6).

$$\mathrm{G(acetone) = \frac{1}{2} G(R^{\bullet}OH) + G(H_2O_2) = \ 3.8 \times 10^{-7} mol\ J^{-1}}\ \mathrm{(eq.\ 4.6)}$$

We found a slightly higher value of 4.3 ± 0.2 × 10^{-7} mol J^{-1} than that given by equation 4.6. The possible explanation for higher yield is that reaction 4.8 becomes more competitive due to the higher concentration of H_2O_2 formed in the ionizing spurs by •OH radicals (reaction 4.10). The higher concentration of •OH radicals is explained by the fact that N_2O dissolved in water reacts with hydrated electrons within 3 ns (k = 9.1 × 10^9 M^{-1} s^{-1}), favouring reaction 4.10 in the non-homogenous step of water radiolysis.

$$\mathrm{^{\bullet}OH + {}^{\bullet}OH \rightarrow H_2O_2}\ \mathrm{(R.\ 4.10)}$$

At high dose rates (Table 4.2), in the presence and absence of AuNPs the formation yields of acetone equal 4.4 ± 0.1 × 10^{-7} mol J^{-1}. This can be explained that at high dose rates

when the concentration of R•OH is higher compared to gamma radiolysis, the disproportionation reaction is the dominant one, and the catalytic oxidation by AuNPs is negligible.

Our results clearly show that the presence of AuNPs changes the mechanism of acetone formation by catalyzing the oxidation of R•OH into acetone.

4.4.2. Catalysis of acetanilide hydroxylation

The •OH radical not only can cause H-abstraction, but it also could form •OH adduct. Therefore, to study the catalytic effect of AuNPs on such a type of reaction, we chose acetanilide hydroxylation by •OH, which is similar to aromatic systems discussed in the introduction to this chapter. It includes the following steps: attachment of •OH to benzene ring forming an adduct and the loss of an electron, followed by the loss of H^+, forming a stable hydroxylated molecule (Scheme 4.2).[83,84] In this reaction, numerous products are formed. Herein, we focused on three main products: hydroxyacetanilide with a hydroxyl group in ortho, meta, para positions, and acetanilide consumption (Figure 4.14 A).

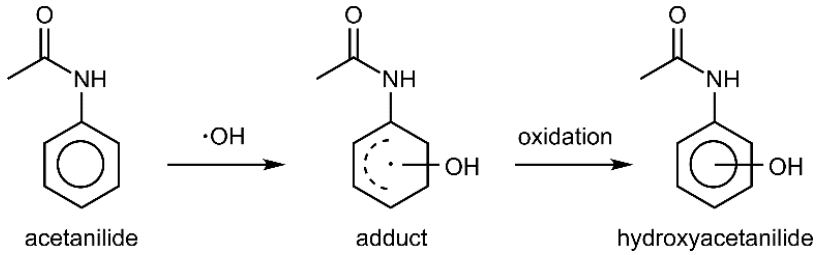

Scheme 4.2. Acetanilide hydroxylation by hydroxyl radical.

Aqueous solutions of 0.5 mM acetanilide with and without AuNPs (BH1 samples diluted two times, [Au] = 1.5 mM) were irradiated (^{60}Co) under the N_2O atmosphere to convert all hydrated electrons to •OH radicals (reaction 4.3 in section 4.3.1).

The first observation consists of a drastic decrease in the number of products in the presence of AuNPs. Products numbered from 1 to 5 in Figure 4.14 A are not detected in the presence of AuNPs. Secondly, acetanilide consumption is slightly different for samples with and without AuNPs (Figure 4.14 B). In the absence of AuNPs, the yield of the acetanilide disappearance equals to 5.0×10^{-7} mol J^{-1}, which is lower than •OH radicals of 5.6×10^{-7} mol J^{-1} (see section 4.3.1). Probably, the reason for that is the disproportionation reaction between two adducts that re-form acetanilide. In the presence of AuNPs, the absolute value of acetanilide disappearance is equal to the yield of •OH radicals. It means that direct oxidation of acetanilide adducts by AuNPs dominates over the

disproportionation reaction. Moreover, this result also indicates that AuNPs do not induce higher •OH radicals production in contrast to the previously reported statement.[24]

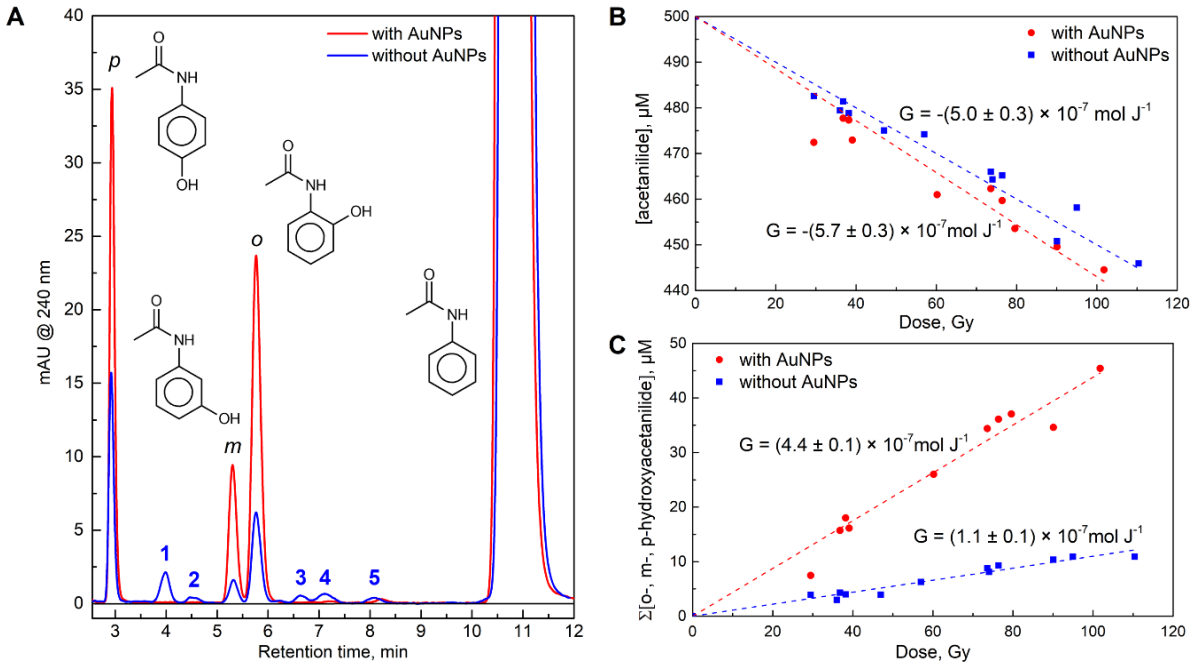

Figure 4.14. Results of acetanilide (0.5 mM) hydroxylation during water radiolysis without (blue) and with (red) AuNPs (BH1 sample diluted two times, [Au] = 1.5 mM) under N_2O atmosphere. (**A**) Chromatograms after 90-Gy dose deposition by gamma rays. (**B**) The disappearance of acetanilide; (**C**) the formation of ortho, meta, para-hydroxyacetanilide. Radiolytic yields (G) were determined from linear slopes.[117]

The total hydroxylation yield was increased 4 times from 20% to 79% (Table 4.3) in the presence of AuNPs (Figure 4.14 C). The results are similar to phenylalanine hydroxylation in the presence of $Fe(CN)_6^{3-}$discussed in section 4.1.2. As in the case of 2-propanol, acetanilide adducts were selectively oxidized in the presence of AuNPs.

Table 4.3. Acetanilide hydroxylation

	Reaction yield*		Ratio
	With AuNPs	Without AuNPs	
p-hydroxyacetanilide	22.5%	7%	3.2
m-hydroxyacetanilide	8.9%	1.3%	6.9
o-hydroxyacetanilide	46.6%	11.6%	4
Total	**78.6%**	**19.6%**	**4**

*Reaction yield is calculated based on the concentration of •OH radicals produced during water radiolysis, G(•OH) = 5.6 × 10^{-7} mol J^{-1}- at the homogeneous stage of water radiolysis.

4.4.3. Oxygen influence on the catalytic oxidation of organic radicals

We also examined the effect of oxygen on the studied systems. This was motivated by the fact that oxygen is present in cells and can react with many organic radicals, usually by attachment, to form peroxyl-type radicals. Herein, the oxygen effect on acetanilide hydroxylation in the presence and absence of AuNPs was studied for two oxygen concentrations: ca. 0.25 mM (air-saturated solution) and ca. 1.22 mM (O_2-saturated solution). Experiments in the presence of oxygen were similar to the experiment performed under the N_2O atmosphere described above. Aqueous solutions of acetanilide (0.5 mM) were irradiated by gamma rays in the absence and presence of AuNPs (BH1 sample, [Au] = 1.5 mM). Irradiated samples were analyzed by HPLC (Figure 4.15).

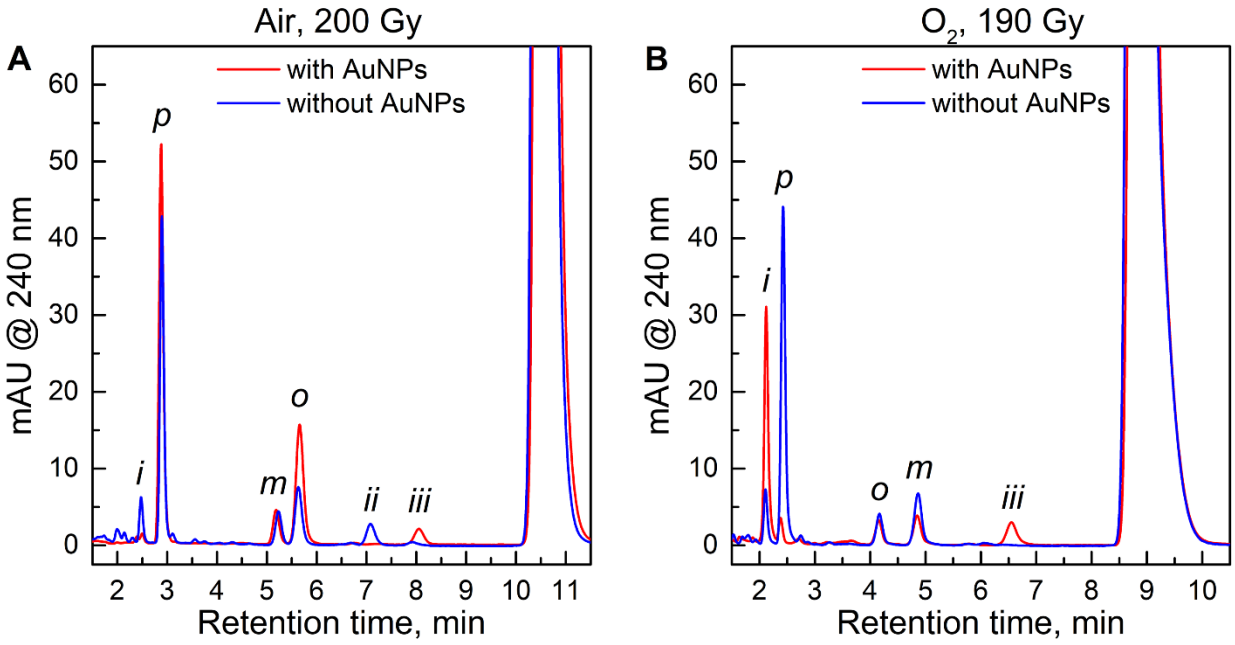

Figure 4.15. Chromatograms of aqueous solutions of acetanilide (0.5 mM) irradiated by gamma rays (^{60}Co) in the absence (blue) and presence (red) of AuNPs (BH1 sample, [Au] = 1.5 mM) under air (**A**) and oxygen (**B**) atmoshperes.

A qualitative analysis of the chromatograms showed that the presence of oxygen in the sample reduces the number of reaction products. Apart from products of hydroxylation (o, m, p), only two sub-products (i and iii) were found in the sample without nanoparticles saturated with oxygen (Figure 4.15 B) compared to 5 sub-products in the sample saturated with N_2O (Figure 4.14 A). Sub-product ii was only detected in air-saturated solutions without AuNPs but not in oxygen-saturated ones. We observe two sub-products i and iii, in the presence of AuNPs and oxygen (Figure 4.15), which was not the case for

deoxygenated solutions (Figure 4.14 A). Interestingly, an increase in oxygen concentration in samples with AuNPs increases the formation of sub-products i and iii.

Radiolytic yields of acetanilide consumption and hydroxylated products formation are presented in Figure 4.16. In the presence of AuNPs, for the two oxygen concentration solutions, the radiolytic yield of acetanilide consumption is equal to the yield of •OH radicals (2.8×10^{-7} mol J^{-1}), while in the absence of AuNPs it is slightly higher (3.1 and 3.3×10^{-7} mol J^{-1} for air and oxygen saturated solution, respectively) (Figure 4.16 A and B). The higher yield of acetanilide consumption can be explained by an additional route of •OH radicals' formation through the H_2O_2 reaction with the adducts, similar to results discussed above for α-hydroxyisopropyl radical.

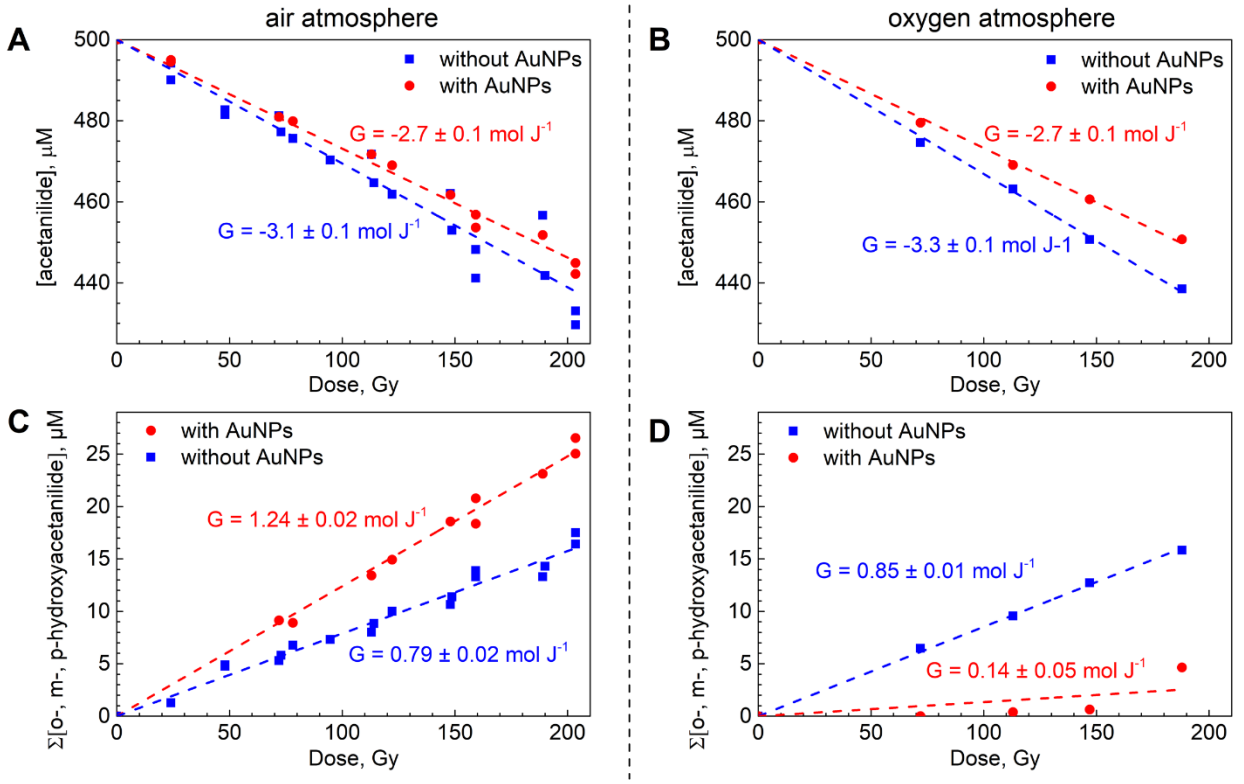

Figure 4.16. Results of acetanilide (0.5 mM) hydroxylation during water radiolysis without (blue) and with (red) AuNPs (BH1 sample diluted two times, [Au] = 1.5 mM) under air and oxygen atmospheres. Acetanilide consumption (**A** and **B**). Formation of hydroxyacetanilide (**C** and **D**).[120]

In the absence of AuNPs, the presence of oxygen slightly increases the reaction yield of acetanilide hydroxylation (Figure 4.16 C and D), as it was observed for similar molecules.[83,84] However, we found that in the presence of both oxygen and AuNPs, the yield of hydroxylation drops down. In the oxygen saturated solution, the formation of hydroxyacetanilide almost does not occur (Figures 4.16 C and D).

All results of oxygen effect on acetanilide hydroxylation in the absence and presence of AuNPs are summarized in Figure 4.17, representing reaction yield as a function of oxygen concentration. In the absence of nanoparticles, an increase in the oxygen concentration leads to an increase in the yield of the hydroxylation reaction. However, in the presence of nanoparticles, an increase in the oxygen concentration reduces the yield of the hydroxylation reaction. Nevertheless, AuNPs increase the hydroxylation yield at oxygen concentration below 0.25 mM. Since oxygen concentration in cells is lower than in air-saturated solution, it is expected that AuNPs will increase the yield of hydroxylation reaction during water radiolysis in cells exposed to ionizing radiation.

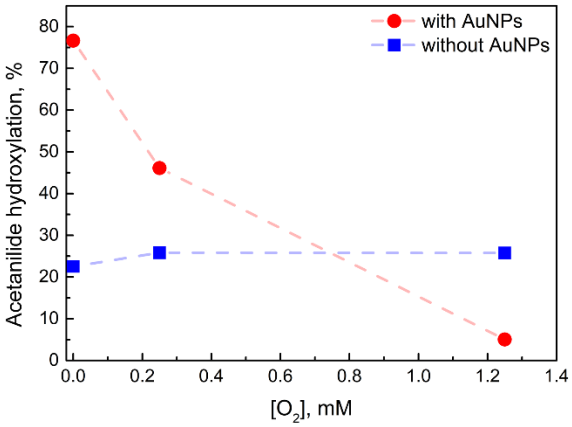

Figure 4.17. Reaction yield of acetanilide hydroxylation versus oxygen concentration in the presence and absence of AuNPs. The reaction yield was estimated based on radiolytic yields of acetanilide consumption and hydroxyacetanilide formation (Figures 4.14 and 4.16).

The reaction mechanism should include the following reaction: as discussed previously, •OH radical attaches to a benzene ring of acetanilide, forming an adduct (scheme 4.3, reaction 9). Adducts are oxidized to hydroxylated products by a disproportionation reaction without oxidizers (reaction 10). In addition, many other ring-opening products can be formed. As we showed, the presence of AuNPs increases the yield of hydroxylation by the adducts oxidation (reaction 11). It is known that oxygen reversible attaches to such types of organic radicals forming peroxyl radical (reaction 12). Eventually, it increases hydroxylation yield by eliminating hydroperoxyl radicals (reaction 13).[83,84] The explanation of the drop in the yield of hydroxylation reaction in the presence of both AuNPs and oxygen (Figure 4.17) could be that reaction 12 is faster than reaction 11, and AuNPs catalyse the oxidation of peroxyl type radicals, which does not lead to hydroxyacetanilide formation (reaction 14). Additionally, we observed a similar effect for 2-propanol oxidation to acetone (Figure S2 in Appendix 2).

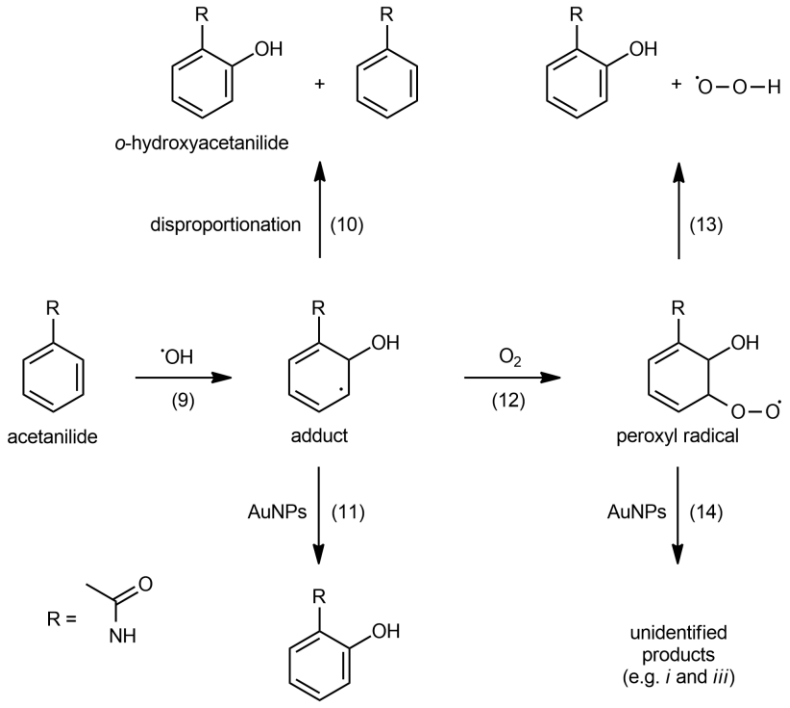

Scheme 4.3. Reaction scheme of acetanilide hydroxylation by ˙OH radical in the presence of O_2 and AuNPs (the scheme presents only the case of ˙OH radical attachment to *ortho* position and *o*-hydroxyacetanilide formation). Unidentified products i and iii are found by HPLC (Figure 4.15).

Amide functional group is an ortho-, para- director; consequently, the significant products of hydroxylation are ortho- and para-hydroxyacetanilide (Figure 4.18). An interesting effect of AuNPs catalysis is that it affects the ratio between products. For example, in the case of a deoxygenated solution, the formation of o- and p-hydroxyacetanilide is increased 4 and 3.2 times, respectively. At the same time, the formation of m-hydroxyacetanilide is increased seven times.

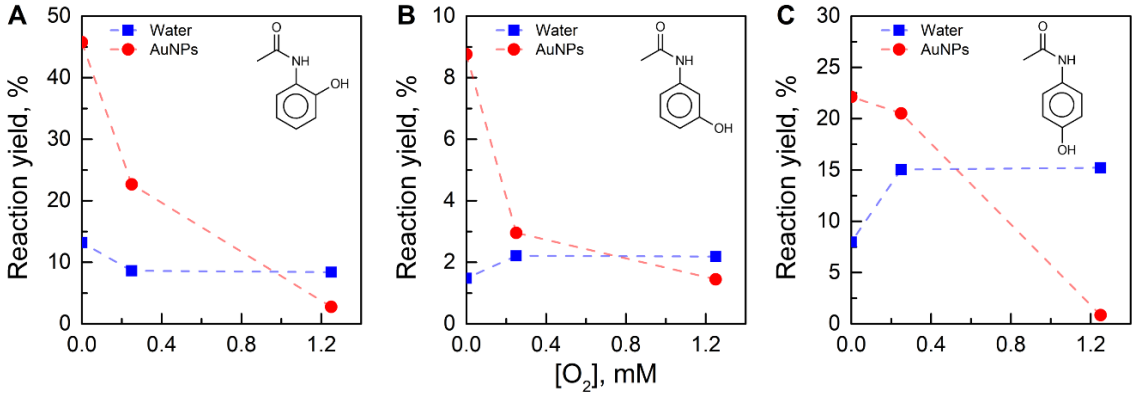

Figure 4.18. Reaction yield of (**A**) ortho-, (**B**) meta-, and (**C**) para-hydroxyacetanilide formation. Reaction yield was estimated based on radiolytic yields of acetanilide consumption (Figure 4.14 and 4.16) and o, m, p- hydroxyacetanilide formation (Figures S3 in Appendix 2).

4.5. CONCLUSIONS

A detailed reaction mechanism of α-hydroxyisopropyl radical oxidation to acetone was presented, explaining an increase of acetone formation 3.4 times in the presence of AuNPs. These results complete our knowledge about processes occurring in an aqueous solution containing 2-propanol and metal nanoparticles exposed to ionizing radiation, which was studied first time more than 40 years ago for the increase in H_2 production during water radiolysis.

Utilizing acetanilide as a test system got hydroxylation aromatic compounds by $^{\bullet}OH$ radicals in the presence of AuNPs, we showed that OH-adducts are selectively oxidized to hydroxylated products on the surface of AuNPs. Thus, hydroxylation reactions cannot be used for $^{\bullet}OH$ radicals detection in the presence of metal nanoparticles. We also demonstrated the competition between oxygen attachment to OH-adducts and their catalytic oxidation on the nanoparticle's surface. Thus, the mixture of both oxygen and AuNPs decreases hydroxylation's reaction yield. However, even at oxygen concentration in air-saturated solution ($[O_2] \sim 0.25$ mM), the presence of AuNPs increases the formation of hydroxylated products. It is important because oxygen concentration in living cells is much lower than 0.25 mM. Therefore, catalysis on the AuNP surface is expected to predominate.

We would like to stress that the oxidation of organic free radicals to stable products has important consequences for the bio-chemistry of the cells. First of all, it fixes radiation damage, which prevents molecules attacked by free radicals, such as $^{\bullet}OH$, from being repaired by antioxidants and other repair processes in cells. Moreover, if some molecules formed in cells by radiation are signal molecules (e.g. molecules that start cellular apoptosis), their increased formation due to redox catalysis will cause higher cell death. On the other hand, capturing the unpaired electron of an organic radical by NPs can have a positive effect, for example, stopping radical chain reactions, such as lipid peroxidation in cell membranes. At the moment, we see a lack of communication between the field of catalysis research and biomedical research using NPs. However, the results we obtained are essential to consider in all biomedical applications of NPs. Most of them exhibit catalytic properties, and free radicals are always present in living cells due to natural metabolic processes. Great attention should be applied to the cases when the NPs are combined with ionizing radiation, such as imaging and radiation therapy.

CHAPTER 5. CATALYTIC OXIDATION OF BIOMOLECULES (*preliminary results*)

Contents

5.1. INTRODUCTION

All experimental results presented in the previous two chapters show that using low LET ionising radiation, the presence of AuNPs does not affect the radiolysis of water at concentrations up to 3 mM of gold (0.06 wt.%), which is comparable with those used in radiosensitization studies. In the previous chapter, it was quantitatively demonstrated on two systems that gold nanoparticles catalyze the oxidation of organic radicals, which in particular leads to an increase in the yield of the hydroxylation reaction involving •OH radicals. Thus, the use of a fluorescent method for the detection of •OH radicals, which is based on hydroxylation reaction, is not applicable in the presence of catalytically active nanoparticles, if we do not consider the change of chemical pathway.

Catalysis of reactions involving organic radicals has been discussed in the context of RedOx catalysis,[121] where radicals act as electron donors, and water plays the role of an acceptor. Reactions with oxygen reduction also belong to the group of redox reactions. And there are many works demonstrating the ability of AuNPs to catalyze the aerobic oxidation of organic compounds.[93] Perhaps one of the most interesting reactions catalyzed by gold nanoparticles, which in my opinion should be taken into account when using nanoparticles in cells, is the aerobic oxidation of glucose to gluconate.[122] In this reaction, AuNPs showed an efficiency comparable to that of the enzymatic catalyst Hydrase.[123,124]

The factor decreasing the catalytic activity of unsupported (colloidal) nanoparticles is utilising surfactants to improve nanoparticle stability in the solution. Nonetheless, even polymer-stabilized AuNPs can catalyze aerobic oxidation of alcohols.[94] A large amount of evidence for the catalytic activity of gold nanoparticles with different stabilizers is summarized in this review.[94]

All of the above leads us to two ideas: in the presence of stronger oxidizing agents, such as oxygen, nanoparticles can catalyze the oxidation of antioxidants and other electron donors contained in cells and involved in protecting cells from radiation damage. Thus, nanoparticles could influence the chemical processes in cells even before applying ionizing radiation, which is consistent with research on the toxicity of nanomaterials and their interaction with different proteins and genes. The second idea is that the claim that nanoparticles can enhance the production of other active forms of oxygen such as peroxide or superoxide should also be tested considering the catalytic properties of the nanoparticles, similarly as was done for the hydroxyl radical.

In this chapter, we will present some preliminary results of Vitamin C oxidation catalyzed by AuNPs. We choose Vitamin C because it does not cause aggregation of nanoparticles, unlike glutathione. Moreover, ascorbic acid has strong absorption in the UV range, unlike its oxidation product dehydroascorbic acid. Thus, it is easy to study Vitamin C oxidation by absorption measurement. At the same time, the presence of Vitamin C is essential for cell functioning. Lowering of Vitamin C concentration in a cell disrupts the defence mechanisms, protein metabolism, ability to synthesize neurotransmitters, regenerate Vitamin E, etc. Please note that the experimental results presented in this chapter are preliminary and require further investigation. However, even at this stage of the study, this is enough to contribute to our understanding of the action of AuNPs as radiosensitizers.

5.2. EXPERIMENTAL PART

The ability to catalyze the oxidation of vitamin C with oxygen was studied for three types of AuNPs: uncovered 20 nm AuNPs prepared by reduction with sodium borohydride (sample BH1, table 2.2 in section 2.2.2), citrate stabilized 20 nm AuNPs prepared by Turkevich method (sample TM2, see table 2.1 in the section 2.2.1) and commercial AuNPs of 1.9 nm in diameter (AuroVist™, see section 2.2.5). Absorption spectra of AuroVist™ and BH1 AuNPs are presented in Figure 5.1.

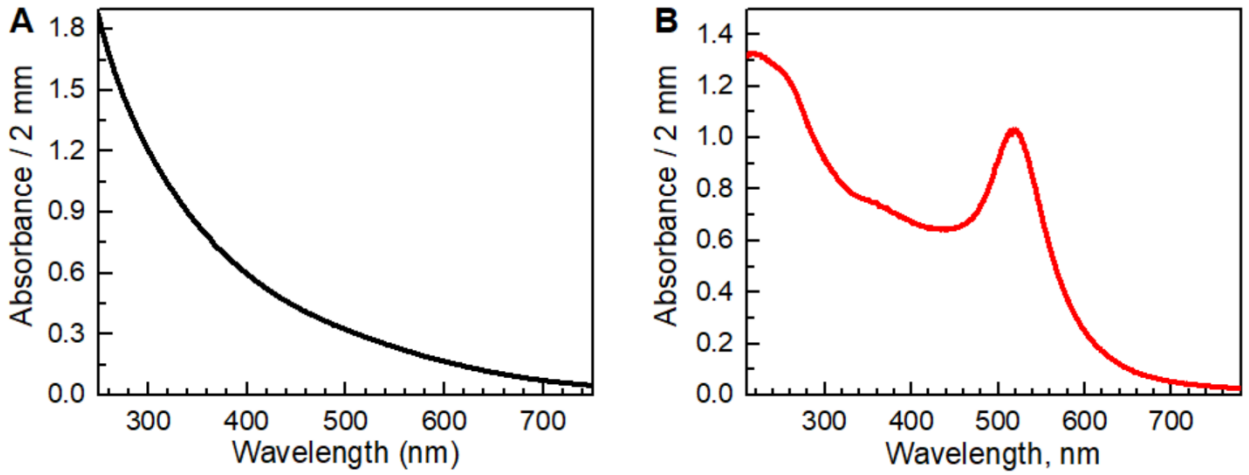

Figure 5.1. Absorption spectra of AuNPs. (**A**) AuroVist™ (1.5 mM of gold). (**B**) BH1 sample – AuNPs prepared by reduction with sodium borohydride (1.5 mM of gold).

The absorption maximum of L-ascorbic acid is sensitive to pH. Therefore, we used sodium salt of L-ascorbic acid (99%, Alfa Aesar) to avoid changing the pH with the concentration of the molecule. The concentration of sodium ascorbate was measured by UV-vis

absorption spectroscopy (Hewlett Packard 8453) using an extinction coefficient of 14.6×10^3 $M^{-1}cm^{-1}$ at 265 nm. The extinction coefficient was measured in our laboratory.

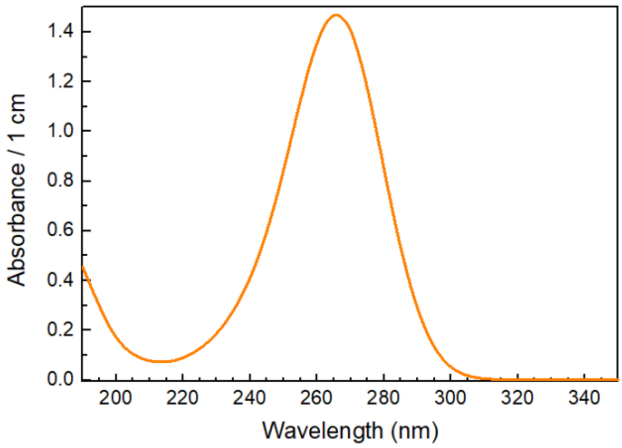

Figure 5.2. The absorption spectrum of 100 μM of sodium ascorbate.

The kinetics of Vitamin C oxidation in the presence of AuNP was measured by the disappearance of the absorption band at 265 nm (Figure 5.2). Experiments were performed at three concentrations of oxygen: ~0 (Ar saturated solution), 0.256 mM (under air) and 1.2 mM (O_2 saturated solution). In all experiments, pH was adjusted to 7.

Experiment 1. For BH1 and TM2 AuNPs samples under air. 2 ml solution of sodium ascorbate (200 μM) were mixed with 2 ml solution of AuNPs containing 200 μM of gold, directly in 1 cm quartz cuvette. The final solution of 4 ml placed in 1 cm optical cuvette contained 100 μM of sodium ascorbate and AuNPs (BH1 or TM2) with 100 μM of atomic concentration of gold.

Experiment 2. For BH1 and TM4 AuNPs samples under Ar atmosphere ($[O_2]\sim0$)[125]. Solutions of sodium ascorbate and AuNPs were saturated with Ar gas in closed communicating vessels. A 2 ml solution of nanoparticles containing 200 μM of gold was placed in a glass bottle closed with a rubber cork with two connected plastic tubes (gas input and output). The gas output from the glass bottle was connected to 1 cm optical cuvette closed with a rubber cork also having a gas output. The cuvette contained 2 ml of 200 μM solution of sodium ascorbate. After 15 minutes of bubbling, the gas output tube of the glass bottle containing AuNPs solution was immersed in the nanoparticle solution to transfer it to the cuvette with sodium ascorbate under the flow of Ar.

Experiment 3. For AuroVist™ nanoparticles under O_2 atmosphere ($[O_2]$ = 1.2 mM). 400 μl solution of AuNPs with the gold concentration of 3 mM were mixed with 400 μl solution

of sodium ascorbate in 2 mm quartz cuvette, then bubbled with oxygen for 10 min covered with Parafilm M to avoid gas exchange.

Experiment 4. For BH1 and TM2 AuNPs samples under O_2 atmosphere ([O_2] = 1.2 mM). 4.6 mM sodium ascorbate solution and suspension of AuNPs containing 3 mM of gold atoms were bubbled with O_2 for 15 min. Then solutions were rapidly mixed with a ratio of 2 to 1 directly in 1 mm quartz cuvette.

5.3. Results and discussion

The results of experiments 1 and 2 are presented in Figure 5.3. We observed a rapid and complete disappearance of the Vitamin C absorption band at 265 nm when the solution contained O_2 and AuNPs (Fig. 5.3 A). We did not observe such disappearance in the presence of only AuNPs or only oxygen within the same time range. Thus, we conclude that AuNPs catalyzed Vitamin C oxidation by O_2.

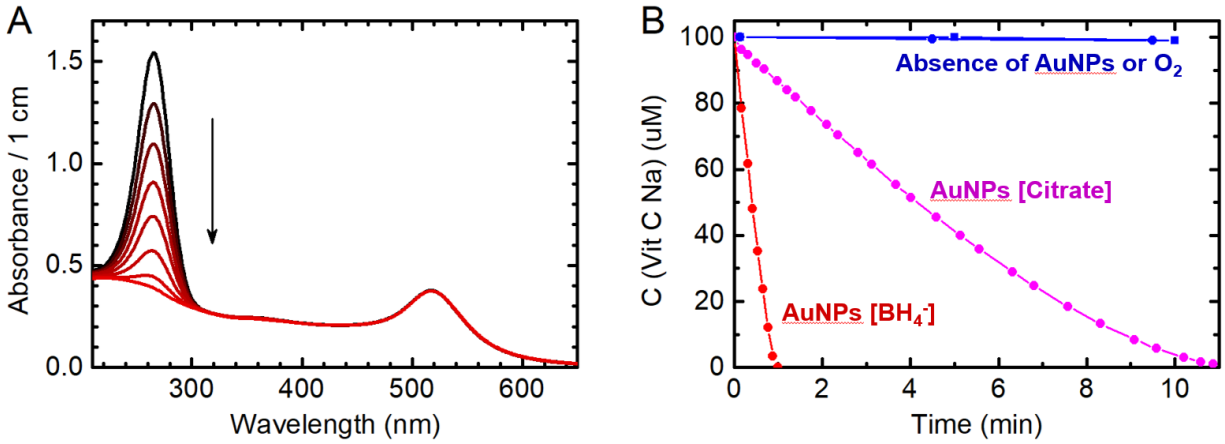

Figure 5.3. Oxidation of sodium ascorbate in the presence of AuNPs under air. **A** – absorption spectra of the solution contained 100 μM of sodium ascorbate (absoption band at 265 nm) and AuNPs (BH1) (red curve) with a gold concentration of 100 μM (0.002 wt.%); **B** – kinetics of sodium ascorbate in the absence of AuNPs or oxygen (blue) and in the presence of two types of AuNPs stabilized by citrate (pink, TM2 samples) and borohydride (red, BH1 samples).

Catalytic properties of nanomaterials are often neglected in biomedical applications because it is believed that when large molecules stabilize nanoparticles, the surface becomes inaccessible. Indeed, all catalytic reactions strongly depend on the surface of the catalyst. In our experiments, 20 nm AuNPs prepared by reduction with sodium borohydride catalyzed Vitamin C oxidation more efficient than 15 nm AuNPs prepared by the Turkevich method (Figure 5.3 B). The results can be explained by the fact the surface of AuNPs prepared by the borohydride reduction method is more accessible since

nanoparticles are stabilized by $B(OH)_4^-$ and BH_4^-,[48] on the contrary to a more massive stabilization by citrate and acetone dicarboxylic acid for particles prepared by the Turkevich method.[126] These results show that the stabilizers affect the catalytic activity of AuNP but do not turn it off. In addition, we have performed similar experiments utilizing commercial AuNPs AuroVist™, which were used in the seminal work of J. Hainfeld and many other works demonstrating the radiosensitizing effect of gold.[20] AuroVist™ nanoparticles are 1.9 nm in diameter and stabilized by large molecules of 50 kD. The results of experiment 3 are presented in Figure 5.4. The trend is the same for all types AuNPs used in our experiments. Catalytic activity is lower for AuNPs stabilized with large molecules. However, even AuroVist™ nanoparticles covered by molecules of 50 kD do accelerate vitamin C oxidation by oxygen.

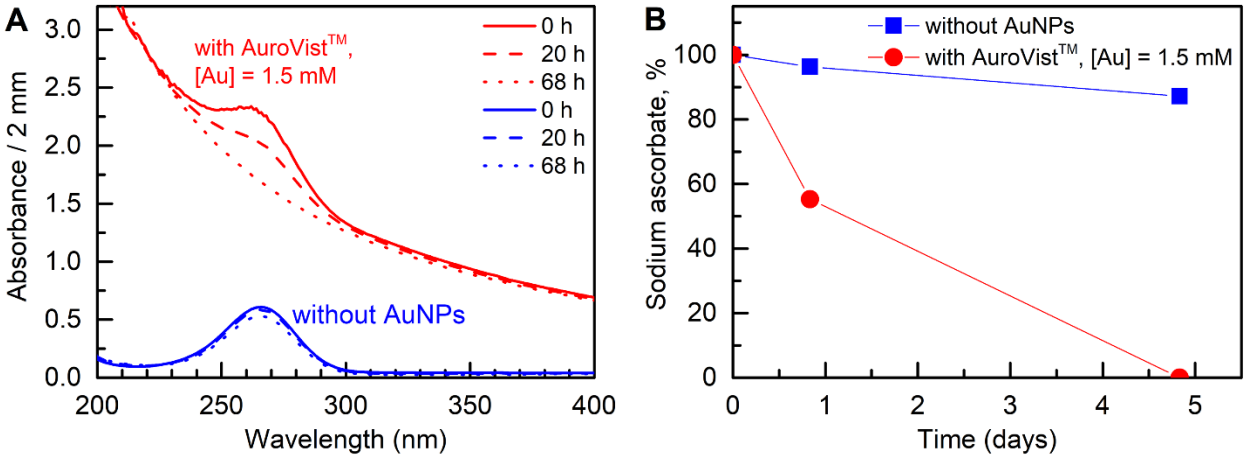

Figure 5.4. Results of Vitamin C oxidation by oxygen catalyzed by 1.9 nm AuroVist nanoparticles. **A** - absorption spectra (absorption band at 265 nm is attributed to sodium ascorbate), red – in the presence of AuNPs and blue – in the absence. **B** - kinetics of sodium ascorbate oxidation. [sodium ascorbate] = 200 μM, [Au] = 1.5 mM (0.03 wt.%). For more details see experiment 3 in the experimental section.

In order to observe the significant acceleration of ascorbate oxidation, the concentration of AuroVist™ nanoparticles was increased up to 1.5 mM (0.03 wt.%) of gold, compared to 100 μM (0.002 wt.%) for other types of AuNPs. It took one day to oxidize half of Vitamin C in the presence of 1.9 nm AuroVist™ nanoparticles. However, even such low catalytic activity of AuroVist™ nanoparticles is reasonable to consider for understanding their radiosensitizing effect, taking into account the time of nanoparticles presence in cells during in vivo experiments. For example, in the work of J. Hainfeld,[20] gold concentrations in the tumour peaked at 7.0 ± 1.6 min and fell to one-half of its peak value at 41.2 ± 19.5 min. The gold concentration was 7 mg Au per g of the tumour, which corresponds

approximately to 0.7 wt.%. Thus, a higher concentration of gold than used in our experiments can be accumulated in cells at least for one hour. Even if we take into account that Au NPs are additionally covered with proteins and peptides in cells, we still think that the catalytic properties of nanoparticles must be considered. This simple example of Vitamin C oxidation indicates that AuNPs could interact with other electron donor molecules and cannot be treated as an inert material to cellular biochemistry. For the radiosensitization study, these results mean that cells loaded with AuNPs have fewer means to protect themselves from the damaging radicals when ionising radiation is applied. Additionally, these results could explain observed gold toxicity for cells.[127–130]

To have more information about the mechanism of Vitamin C oxidation, we performed experiment 4 (see experimental section). When the concentration of sodium ascorbate was greater than the concentration of oxygen, the reaction stopped after the depletion of oxygen (Figure 5.5). We used that to find a material balance of the reaction by measuring the rest of Vitamin C after oxygen consumption.

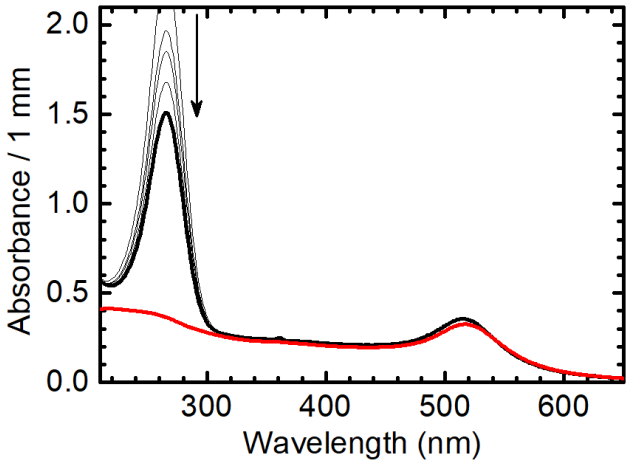

Figure 5.5. Oxidation of sodium ascorbate in the presence of oxygen and AuNPs (BH1). 3.07 mM of sodium ascorbate, [Au] = 1 mM, [O_2] = 1.2 mM. Absorption band at 265 nm is attributed to sodium ascorbate. The absorption at 265 nm decreases with time but stops after oxygen depletion (bold black curve). The red curve is absorption spectrum of AuNPs (BH1, [Au] = 1 mM).

We calculated that the consumed concentration of sodium ascorbate was 2.44 mM. Considering the O_2 concentration of 1.2 mM in oxygen saturated solution, we found that one molecule of oxygen oxidizes two molecules of Vitamin C (reaction 5.0). The first step of the process may include catalytic reduction of oxygen to superoxide radical via one-electron transfer from Vitamin C (H_2A) (reaction 5.1). The superoxide radical is a strong

oxidizing agent capable of oxidizing both the vitamin C radical ($HA^{\bullet}$) and Vitamin C itself,[131] being reduced to hydrogen peroxide. However, to explain the material balance found in experiment 4 (Figure 5.5), the second step must be Vitamin C radical ($HA^{\bullet}$) oxidation to dehydroascorbic acid (DHA) by $O_2^{\bullet-}$ (reaction 5.2). This reaction is not necessarily catalyzed by gold. The last step is hydrogen peroxide disproportionation into water and oxygen (reaction 5.3). Electrochemical studies support it, showing that H_2O_2 undergoes a disproportionation reaction on the metal surface, forming an oxygen layer, which can then be reduced to H_2O_2.[118] Then all steps are repeated until oxygen is consumed.

$$\mathbf{H_2A + ½O_2 + \rightarrow DHA + H_2O \ (R\ 5.0)}$$

$$H_2A + O_2 \xrightarrow{AuNP} HA^{\bullet} + O_2^{\bullet-} + H^+ \ (R.\ 5.1)$$

$$HA^{\bullet} + O_2^{\bullet-} + H^+ \rightarrow DHA + H_2O_2 \ (R.\ 5.2)$$

$$H_2O_2 \xrightarrow{AuNP} ½O_2 + H_2O \ (R.\ 5.3)$$

The proposed mechanism supports the idea of catalytic ROS formation in the presence of AuNPs proposed in the literature. However, since $O_2^{\bullet-}$ and H_2O_2 are formed on the AuNP's surface, they can be catalytically transformed to water without reacting with biomolecules in the cell. It is an exciting topic for further study for two reasons. First, the catalytic oxidation of biomolecules and their oxidation upon reaction with ROS do not lead to the formation of the same oxidation products, which can affect further biochemical and biological processes. Some oxidation products can work as signaling molecules that provoke apoptosis. Secondly, it is known that ROS themselves work as signalling molecules. Therefore, it is crucial to know whether nanoparticles can catalytically produce ROS or not.

To date, all experiments presented in the literature $O_2^{\bullet-}$ and H_2O_2 are measured by fluorescent dyes such as hydroethidine and 2,7-dichlorodihydrofluorescein, which are good electron donors. The dyes can be catalytically oxidized in the presence of AuNPs. Therefore, their oxidation does not mean ROS formation. As is the case with the detection of hydroxyl radicals, the use of fluorescent dyes for the detection of ROS in the presence of nanoparticles is not a suitable method due to their catalytic activity.

5.4. CONCLUSIONS

Our results demonstrate that AuNPs can catalyse the oxidation of antioxidants by molecular oxygen. These results agree with observed oxidation stress in living cells loaded with AuNPs even in the absence of ionizing radiation. Although the experiments presented are simple, it is important that they were discussed in the context of radiosensitization research. We do not reject the idea of catalytic $O_2^{\bullet -}$ and H_2O_2 formation in the presence of AuNPs without ionizing radiation, but it requires further investigation by appropriate methods, not by using fluorescent dyes. More attention should be paid to different RedOx reactions, which can be catalyzed by AuNPs in cells, affecting cell functioning and radiation protection systems.

CHAPTER 6. CONCLUSIONS AND PERSPECTIVES

This conclusive chapter will shortly underline all results presented in this work. The main findings are schematically illustrated in Figure 6.1. In the discussion below, we will try to incorporate them into the current understanding of AuNPs' radiosensitizing effect and suggest some perspectives for further research.

In a recent review,[12] the authors emphasized that the radiosensitizing effect of AuNPs begins after they are loaded into cells, even before radiation is applied. Our results on the Vitamin C oxidation by molecular oxygen catalyzed by different AuNPs without ionizing radiation support this idea. We suppose that AuNPs can catalyze various RedOx reactions in cells leading to the oxidation of electron donors and consequently causing oxidative stress. In addition, the influence of AuNPs on various proteins and genes in cells should be taken into account.[12] Thus, AuNPs can disrupt cell functioning and weaker its radiation protection systems before radiation. This fact must be considered in understanding of AuNPs' role in radiosensitization.

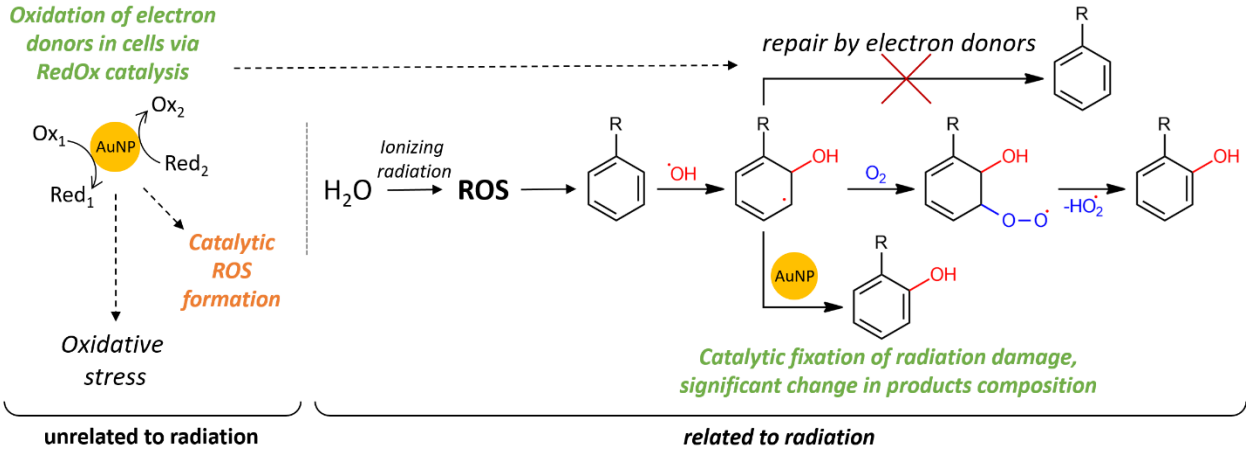

Figure 6.1. Schematic representation of the mechanism of AuNPs radiosensitizing effect based on main findings of the work.

When ionizing radiation is applied, it causes water radiolysis. At a gold concentration in the order of hundreds μg per ml, AuNPs do not cause the dose enhancement effect. The local dose enhancement by low-energy Auger electrons is not detectable in a homogenous solution and can be only estimated by simulations. Therefore, we consider these physical effects negligible at any radiation energy due to the low concentration of gold. The results of pulse and gamma radiolysis experiments showed that AuNPs at a concentration up to 600 μg ml^{-1} do not affect water radiolysis and primary water radicals formation. But we found a substantial AuNPs effect on the chemistry of organic radicals

formed in reaction with water radicals: they catalyze the oxidation of organic radicals. This effect is similar to the oxygen effect leading to the fixation of damage caused by radiation. Thus, even under hypoxic conditions, AuNPs will increase the damage caused by radiation.

Our results show that AuNPs simultaneously act as at least two types of radiosensitizers: inhibitors of radioprotective agents and oxygen mimics discussed in Chapter 1. Thus, the main characteristic of the material is not the Z number but its catalytic properties. It explains why the radiosensitizing effect has been observed even at low nanoparticle concentrations.

This new vision completely changes the strategy for developing and utilizing nanoparticle-based radiosensitizers. The strategy of using a high concentration of nanoparticles made of high-Z materials should be replaced by utilization of a lower concentration but catalytically active nanoparticles. For a better understanding of nanoparticles catalytic properties in solutions, we recommend works on RedOx electrocatalysis by nanoparticles in solution,[121,132–134] and mixpotential theory.[135]

Apart from two clearly demonstrated effects, catalysis of mild electron donors oxidation leading to lowering of cell radio-protection and catalysis of reactions involving organic radicals leading to damage fixation caused by radiation, two other effects require further study. The first effect is catalytic ROS formation discussed in Chapter 5. The proposed mechanism of Vitamin C oxidation includes $O_2^{\bullet-}$ and H_2O_2 formation as intermediates. However, from our experiments, we cannot say whether catalytically produced ROS can directly react with biomolecules or, eventually, are catalytically reduced to water. Thus, this question remains open. The second effect is that the catalysis of radical reactions changes the composition of final products, affecting later biochemical and biological processes. This opens a new and broad research area in radiation chemistry. As it was done for radical chemistry of biomolecules, the catalysis of radical reactions should be more investigated. To date, all we know is that conductive particles can catalyze reactions involving organic radicals. If the radicals are good electron donors, nanoparticles catalyze their oxidation. In such reactions, even water can work as an electron acceptor being reduced to hydrogen. If the radicals are poor electron donors, nanoparticles can catalyze their dimerization. This was shown for methyl and tyrosin radicals. [107,114] Despite that such catalysis is out of industrial interest, it has great importance in fundamental research. For example, the lack of knowledge in this area has led to the emergence and strengthening of the hypothesis on $^{\bullet}OH$ radical overproduction in the presence of nanoparticles under radiation.

REFERENCES

1 E. Rossenbalt and E. Zubizarreta, *Radiotherapy in cancer care: Facing the global challenge*, International Atomic Energy Agency, 2017.

2 A. Norlund, Costs of radiotherapy, *Acta Oncol. (Madr).*, 2003, **42**, 411–415.

3 J. W. T. Spinks and R. J. Woods, *An introduction to radiation chemistry*, John Wiley & Sons, Inc., New York, London, Sydney, 1964.

4 J. P. Pouget and S. J. Mather, General aspects of the cellular response to low- and high-LET radiation, *Eur. J. Nucl. Med.*, 2001, **28**, 541–561.

5 S. Le Caër, Water radiolysis: Influence of oxide surfaces on H_2 production under ionizing radiation, *Water*, 2011, **3**, 235–253.

6 Y. Galduel, S. Pommeret, A. Migus and A. Antonetti, Femtosecond Dynamics of Geminate Pair Recombination In Pure Liquid Water, *J. Phys. Chem.*, 1989, **93**, 3880–3882.

7 A. Mozumder, *Fundamentals of Radiation Chemistry*, Academic Press, 1999.

8 F. Wang, U. Schmidhammer, J. P. Larbre, Z. Zong, J. L. Marignier and M. Mostafavi, Time-dependent yield of the hydrated electron and the hydroxyl radical in D_2O: a Picosecond Pulse Radiolysis Study, *Phys. Chem. Chem. Phys.*, 2018, **20**, 15671–15679.

9 S. Rosa, C. Connolly, G. Schettino, K. T. Butterworth and K. M. Prise, Biological mechanisms of gold nanoparticle radiosensitization, *Cancer Nanotechnol.*, 2017, **8**, 1–25.

10 E. Rossenbalt and E. Zubizarreta, *Radiotherapy in cancer care: Facing the global challenge*, 2017.

11 H. R. Withers, *The Four R's of Radiotherapy*, Academic press, Ink., 1975, vol. 5.

12 S. Penninckx, A. C. Heuskin, C. Michiels and S. Lucas, Gold nanoparticles as a potent radiosensitizer: A transdisciplinary approach from physics to patient, *Cancers (Basel).*, 2020, **12**, 1–36.

13 M. Joiner and A. van der Kogel, *Basic Clinical Radiobiology*, 2009.

14 G. E. Adams, Chemical radiosensitization of hypoxic cells., *Br. Med. Bull.*, 1973, **29**, 48–53.

15 J. F. Fowler, G. E. Adams and J. Denekamp, Radiosensitizers of hypoxic cells in solid tumors., *Cancer Treat. Rev.*, 1976, **3**, 227–256.

16 P. Wardman, Chemical Radiosensitizers for Use in Radiotherapy, *Clin. Oncol.*, 2007, **19**, 397–417.

17 H. Wang, X. Mu, H. He and X. D. Zhang, Cancer Radiosensitizers, *Trends Pharmacol. Sci.*, 2018, **39**, 24–48.

18 C. von Sonntag, *Free-Radical-Induced DNA Damage and Its Repair*, Springer, 2006.

19 J. Cadet, T. Delatour, T. Douki, D. Gasparutto, J.-P. Pouget, J.-L. Ravanat and S. Sauvaigo, Hydroxyl radicals and DNA base damage, *Mutat. Res. Mol. Mech. Mutagen.*, 1999, **424**, 9–21.

20 J. F. Hainfeld, D. N. Slatkin and H. M. Smilowitz, The use of gold nanoparticles to enhance radiotherapy in mice, *Phys. Med. Biol.*, 2004, **49**, 309–315.

21 A. Subiel, R. Ashmore and G. Schettino, Standards and methodologies for characterizing radiobiological impact of high-Z nanoparticles, *Theranostics*, 2016, **6**, 1651–1671.

22 K. T. Butterworth, S. J. McMahon, F. J. Currell and K. M. Prise, Physical basis and biological mechanisms of gold nanoparticle radiosensitization, *Nanoscale*, 2012, **4**, 4830–4838.

23 S. Her, D. A. Jaffray and C. Allen, Gold nanoparticles for applications in cancer radiotherapy: Mechanisms and recent advancements, *Adv. Drug Deliv. Rev.*, 2017, **109**, 84–101.

24 D. Howard, S. Sebastian, Q. V. C. Le, B. Thierry and I. Kempson, Chemical mechanisms of nanoparticle radiosensitization and radioprotection: A review of structure-function relationships influencing reactive oxygen species, *Int. J. Mol. Sci.*, 2020, **21**, 1–23.

25 I. Kempson, Mechanisms of nanoparticle radiosensitization, *Wiley Interdiscip. Rev. Nanomedicine Nanobiotechnology*, 2021, **13**, 1–19.

26 T. Guo, Physical, chemical and biological enhancement in X-ray nanochemistry, *Phys. Chem. Chem. Phys.*, 2019, **21**, 15917–15931.

27 D. F. Regulla, L. B. Hiebert and M. Seidenbusch, Physical and Biological Interface Dose Effects in Tissue due to X-Ray- Induced Release of Secondary Radiation from Metallic Gold Surfaces, *Radiat. Res.*, 1998, **150**, 92–100.

28 D. M. Herold, I. J. Das, C. C. Stobbe, R. V. Iyer and J. D. Chapman, Gold microspheres: A selective technique for producing biologically effective dose enhancement, *Int. J. Radiat. Biol.*, 2000, **76**, 1357–1364.

29 R. A. Davidson and T. Guo, Average Physical Enhancement by Nanomaterials under X-ray, *J. Phys. Chem. C*, 2014, **118**, 30221–30228.

30 H. Lodish, A. Berk, C. A. Kaiser, A. Amon, H. Ploegh, A. Bretscher, M. Krieger and K. C. Martin, *Molecular Cell Biology*, Macmillan Learning: New York, NY, USA, 2016.

31 A. Nel, T. Xia, L. Mädler and N. Li, Toxic potential of materials at the nanolevel, *Science*, 2006, **311**, 622–627.

32 M. Misawa and J. Takahashi, Generation of reactive oxygen species induced by gold nanoparticles under x-ray and UV Irradiations, *Nanomedicine Nanotechnology, Biol. Med.*, 2011, **7**, 604–614.

33 M. Gilles, E. Brun and C. Sicard-Roselli, Quantification of hydroxyl radicals and solvated electrons produced by irradiated gold nanoparticles suggests a crucial role of interfacial water, *J. Colloid Interface Sci.*, 2018, **525**, 31–38.

34 C. Sicard-Roselli, E. Brun, M. Gilles, G. Baldacchino, C. Kelsey, H. McQuaid, C. Polin, N. Wardlow and F. Currell, A new mechanism for hydroxyl radical production in irradiated nanoparticle solutions, *Small*, 2014, **10**, 3338–3346.

35 Y. Zheng, P. Cloutier, D. J. Hunting and L. Sanche, Radiosensitization by gold nanoparticles: Comparison of DNA damage induced by low and high-energy electrons, *J. Biomed. Nanotechnol.*, 2008, **4**, 469–473.

36 X. Yao, C. Huang, X. Chen, Y. Zheng and L. Sanche, Chemical radiosensitivity of DNA induced by gold nanoparticles, *J. Biomed. Nanotechnol.*, 2015, **11**, 478–485.

37 T. Turnbull, M. Douglass, N. H. Williamson, D. Howard, R. Bhardwaj, M. Lawrence, D. J. Paterson, E. Bezak, B. Thierry and I. M. Kempson, Cross-Correlative Single-Cell Analysis Reveals Biological Mechanisms of Nanoparticle Radiosensitization, *ACS Nano*, 2019, **13**, 5077–5090.

38 J. Turkevich, P. C. Stevenson and J. Hillier, A study of the nucleation and growth processes in the synthesis of colloidal gold, *Discuss. Faraday Soc.*, 1951, **11**, 55–75.

39 W. Leng, P. Pati and P. J. Vikesland, Room temperature seed mediated growth of gold nanoparticles: mechanistic investigations and life cycle assesment, *Environ. Sci. Nano*, 2015, **2**, 440–453.

40 P. Zhao, N. Li and D. Astruc, State of the art in gold nanoparticle synthesis, *Coord. Chem. Rev.*, 2013, **257**, 638–665.

41 S. Al Gharib, J.-L. Marignier, A. K. El Omar, A. Naja, S. Le Caer, M. Mostafavi and J. Belloni, Key Role of the Oxidized Citrate-Free Radical in the Nucleation Mechanism of the Metal Nanoparticle Turkevich Synthesis, *J. Phys. Chem. C*, 2019, **123**, 22624–22633.

42 M. Treguer, C. de Cointet, H. Remita, J. Khatouri, M. Mostafavi, J. Amblard, J. Belloni and R. de Keyzer, Dose Rate Effects on Radiolytic Synthesis of Gold−Silver Bimetallic Clusters in Solution, *J. Phys. Chem. B*, 1998, **102**, 4310–4321.

43 J. H. Baxendale and A.-M. Koulkès-Pujo, Une étude par radiolyse pulsée sur l'espèce transitoire Au II, *J. Chim. Phys.*, 1970, **67**, 1602–1607.

44 A. S. Ghosh-Mazumdar and E. J. Hart, in *Radiation Chemistry*, 1968, pp. 193–209.

45 S. Wang, K. Qian, X. Bi and W. Huang, Influence of Speciation of Aqueous $HAuCl_4$ on the Synthesis, Structure, and Property of Au Colloids, *J. Phys. Chem. C*, 2009, **113**, 6505–6510.

46 G. Frens, Controlled Nucleation for the Regulation of the Particle Size in Monodisperse Gold Suspensions, *Nat. Phys. Sci.*, 1973, **241**, 20.

47 L. Shi, E. Buhler, F. Boué and F. Carn, How does the size of gold nanoparticles depend on citrate to gold ratio in Turkevich synthesis? Final answer to a debated question, *J. Colloid Interface Sci.*, 2017, **492**, 191–198.

48 C. Deraedt, L. Salmon, S. Gatard, R. Ciganda, R. Hernandez, M. Mayor and D. Astruc, Sodium borohydride stabilizes very active gold nanoparticle catalysts, *Chem. Commun.*, 2014, **50**, 14194–14196.

49 J. L. Marignier, J. Belloni, M. O. Delcourt and J. P. Chevalier, Microaggregates of non-noble metals and bimetallic alloys prepared by radiation-induced reduction, *Nature*, 1985, **317**, 344–345.

50 A. Henglein, Reactions of organic free radicals at colloidal silver in aqueous solution. Electron pool effect and water decomposition, *J. Phys. Chem.*, 1979, **83**, 2209–2216.

51 J. F. Hainfeld, D. N. Slatkin, T. M. Focella and H. M. Smilowitz, Gold nanoparticles: A new X-ray contrast agent, *Br. J. Radiol.*, 2006, **79**, 248–253.

52 H. Lusic and M. W. Grinstaff, X-ray-computed tomography contrast agents, *Chem. Rev.*, 2013, **113**, 1641–1666.

53 J. A. Coulter, S. Jain, K. T. Butterworth, L. E. Taggart, G. R. Dickson, S. J. McMahon, W. B. Hyland, M. F. Muir, C. Trainor, A. R. Hounsell, J. M. O'Sullivan, G. Schettino, F. J. Currell, D. G. Hirst and K. M. Prise, Cell type-dependent uptake, localization, and cytotoxicity of 1.9 nm gold nanoparticles, *Int. J. Nanomedicine*, 2012, **7**, 2673–2685.

54 J. F. Hainfeld, F. A. Dilmanian, Z. Zhong, D. N. Slatkin, J. A. Kalef-Ezra and H. M. Smilowitz, Gold nanoparticles enhance the radiation therapy of a murine squamous cell carcinoma, *Phys. Med. Biol.*, 2010, **55**, 3045–3059.

55 K. T. Butterworth, J. A. Coulter, S. Jain, J. Forker, S. J. McMahon, G. Schettino, K. M. Prise, F. J. Currell and D. G. Hirst, Evaluation of cytotoxicity and radiation enhancement using 1.9nm gold particles: Potential application for cancer therapy, *Nanotechnology*, 2010, **21**, 1–9.

56 F. Torche and J. L. Marignier, Direct Evaluation of the Molar Absorption Coefficient of Hydrated Electron by the Isosbestic Point Method, *J. Phys. Chem. B*, 2016, **120**,

7201–7206.

57 J. Ma, F. Wang, S. A. Denisov, A. Adhikary and M. Mostafavi, Reactivity of prehydrated electrons toward nucleobases and nucleotides in aqueous solution, *Sci. Adv.*, 2017, **3**, 1–8.

58 J. Ma, U. Schmidhammer, P. Pernot and M. Mostafavi, Reactivity of the strongest oxidizing species in aqueous solutions: The short-lived radical cation H_2O^+, *J. Phys. Chem. Lett.*, 2014, **5**, 258–261.

59 J. Ma, U. Schmidhammer and M. Mostafavi, Direct evidence for transient pair formation between a solvated electron and H_3O^+ observed by picosecond pulse radiolysis, *J. Phys. Chem. Lett.*, 2014, **5**, 2219–2223.

60 F. Wang, U. Schmidhammer, A. de La Lande, M. Mostafavi, T. P. Straatsma, H. J. J. Van Dam, D. Wang, J. Nieplocha, E. Apra, T. L. Windus, W. A. de Jong, H. Borie, T. Garvey, B. Jacquemard, B. Leblond, P. Lepercq, M. Omeich, M. Roch, J. Rodier and R. Roux, Ultra-fast charge migration competes with proton transfer in the early chemistry of $H_2O^{\cdot+}$, *Phys. Chem. Chem. Phys.*, 2017, **19**, 2894–2899.

61 R. Musat, S. A. Denisov, J.-L. Marignier and M. Mostafavi, Decoding the Three-Pronged Mechanism of $NO_3^{\bullet}$ Radical Formation in HNO_3 Solutions at 22 and 80 °C Using Picosecond Pulse Radiolysis, *J. Phys. Chem. B*, 2018, **122**, 2121–2129.

62 O. Roth, B. Dahlgren and J. A. Laverne, Radiolysis of water on ZrO_2 nanoparticles, *J. Phys. Chem. C*, 2012, **116**, 17619–17624.

63 E. Chelnokov, V. Cuba, D. Simeone, J.-M. Guigner, U. Schmidhammer, M. Mostafavi and S. Le Caer, Electron Transfer at Oxide/Water Interfaces Induced by Ionizing Radiation, *J. Phys. Chem. C*, 2014, **118**, 7865–7873.

64 R. M. Musat, A. R. Cook, J.-P. Renault and R. A. Crowell, Nanosecond Pulse Radiolysis of Nanoconfined Water, *J. Phys. Chem. C*, 2012, **116**, 13104–13110.

65 G. Buxton, in *Charge Particle and Photon Interactions with Matter*, New York, 2003, pp. 333–363.

66 K. Ghandi, F. Wang, C. Landry and M. Mostafavi, Naked Gold Nanoparticles and hot Electrons in Water, *Sci. Rep.*, 2018, **8**, 1–6.

67 K. Ghandi, A. D. Findlater, Z. Mahimwalla, C. S. MacNeil, E. Awoonor-Williams, F. Zahariev and M. S. Gordon, Ultra-fast electron capture by electrosterically-stabilized gold nanoparticles, *Nanoscale*, 2015, **7**, 11545–11551.

68 J. Belloni, H. Monard, F. Gobert, J. P. Larbre, A. Demarque, V. De Waele, I. Lampre, J. L. Marignier, M. Mostafavi, J. C. Bourdon, M. Bernard, H. Borie, T. Garvey, B. Jacquemard, B. Leblond, P. Lepercq, M. Omeich, M. Roch, J. Rodier and R. Roux, ELYSE - A picosecond electron accelerator for pulse radiolysis research, *Nucl.*

Instruments Methods Phys. Res. Sect. A Accel. Spectrometers, Detect. Assoc. Equip., 2005, **539**, 527–539.

69 V. Shcherbakov, S. A. Denisov and M. Mostafavi, On the Primary Water Radicals' Production in the Presence of Gold Nanoparticles: Electron Pulse Radiolysis Study, *Nanomaterials*, 2020, **10**, 2478.

70 G. V. Buxton, C. L. Greenstock, W. P. Helman and A. B. Ross, Critical Review of rate constants for reactions of hydrated electrons, hydrogen atoms and hydroxyl radicals ($^{\bullet}OH/^{\bullet}O^{-}$) in Aqueous Solution, *J. Phys. Chem. Ref. Data*, 1988, **17**, 513–886.

71 J. Hermannsdörfer, N. De Jonge and A. Verch, Electron beam induced chemistry of gold nanoparticles in saline solution, *Chem. Commun.*, 2015, **51**, 16393–16396.

72 A. M. Nowicka, U. Hasse, M. Hermes and F. Scholz, Hydroxyl radicals attack metallic gold, *Angew. Chemie - Int. Ed.*, 2010, **49**, 1061–1063.

73 F. A. Villamena, in *Reactive Species Detection in Biology*, 2017, pp. 163–202.

74 G. L. Newton and J. R. Milligan, Fluorescence detection of hydroxyl radicals, *Radiat. Phys. Chem.*, 2006, **75**, 473–478.

75 A. Gomes, E. Fernandes and J. L. F. C. Lima, Fluorescence probes used for detection of reactive oxygen species, *J. Biochem. Biophys. Methods*, 2005, **65**, 45–80.

76 G. Louit, S. Foley, J. Cabillic, H. Coffigny, F. Taran, A. Valleix, J. P. Renault and S. Pin, The reaction of coumarin with the OH radical revisited: Hydroxylation product analysis determined by fluorescence and chromatography, *Radiat. Phys. Chem.*, 2005, **72**, 119–124.

77 N. Getoff, Pulse radiolysis of aromatic amino acids - State of the art, *Amino Acids*, 1992, **2**, 195–214.

78 M. Dizdaroglu and P. Jaruga, Mechanisms of free radical-induced damage to DNA, *Free Radic. Res.*, 2012, **46**, 382–419.

79 C. L. Greenstock, J. W. Hunt and M. Ng, Pulse radiolysis studies of uracil and its derivatives. Primary species attack, *Trans. Faraday Soc.*, 1969, **65**, 3279–3287.

80 R. Kaczmarek, S. Ward, D. Debnath, T. Jacobs, A. D. Stark, D. Korczynski, A. Kumar, M. D. Sevilla, S. A. Denisov, V. Shcherbakov, P. Pernot, M. Mostafavi, R. Dembinski and A. Adhikary, One Way Traffic: Base-to-Backbone Hole Transfer in Nucleoside Phosphorodithioate, *Chem. Eur. J.*, 2020, **26**, 9495–9505.

81 S. A. Denisov, S. Ward, V. Shcherbakov, A. D. Stark, R. Kaczmarek, E. Radzikowska-Cieciura, D. Debnath, T. Jacobs, A. Kumar, M. D. Sevilla, P. Pernot, R. Dembinski, M. Mostafavi and A. Adhikary, Modulation of the Directionality of Hole Transfer

between the Base and the Sugar-Phosphate Backbone in DNA with the Number of Sulfur Atoms in the Phosphate Group, *J. Phys. Chem. B*, 2022, **126**, 430–442.

82 J. Ma, A. Kumar, Y. Muroya, S. Yamashita, T. Sakurai, S. A. Denisov, M. D. Sevilla, A. Adhikary, S. Seki and M. Mostafavi, Observation of dissociative quasi-free electron attachment to nucleoside via excited anion radical in solution, *Nat. Commun.*, 2019, **10**, 1–7.

83 X. M. Pan, M. N. Schuchmann and C. Von Sonntag, Oxidation of benzene by the OH radical. A product and pulse radiolysis study in oxygenated aqueous solution, *J. Chem. Soc. Perkin Trans. 2*, 1993, 289–297.

84 D. Wang, H. P. Schuchmann and C. Sonntag von, Phenylalanine: Its $^{\bullet}OH$ and $SO_4^{\bullet-}$-Induced Oxidation and Decarboxylation. A Pulse Radiolysis and Product Analysis Study, *Zeitschrift fur Naturforsch. - Sect. B J. Chem. Sci.*, 1993, **48**, 761–770.

85 N. N. Cheng, Z. Starkewolf, R. A. Davidson, A. Sharmah, C. Lee, J. Lien and T. Guo, Chemical enhancement by nanomaterials under X-ray irradiation, *J. Am. Chem. Soc.*, 2012, **134**, 1950–1953.

86 J. Lien, M. Su and T. Guo, Identification of Individual Reaction Steps in Complex Radical Reactions Involving Gold Nanoparticles, *ChemPhysChem*, 2018, **19**, 3328–3333.

87 G. C. Bond, The catalytic properties of gold, *Gold Bull.*, 1972, **5**, 11–13.

88 G. C. Bond and P. A. Sermon, Gold catalysts for olefin hydrogenation - Transmutation of catalytic properties, *Gold Bull.*, 1973, **6**, 102–105.

89 M. Haruta, T. Kobayashi, H. Sano and N. Yamada, Novel Gold Catalysts for the Oxidation of Carbon Monoxide at a Temperature far Below 0 °C, *Chem. Lett.*, 1987, **16**, 405–408.

90 A. Henglein, Catalysis of Hydrogen Formation from an Organic Radical in Aqueous Solutions by Colloidal Silver, *Angew. Chemie Int. Ed. English*, 1979, **18**, 418–418.

91 D. Meisel, Catalysis of Hydrogen Production in Irradiated Aqueous Solutions by Gold Sols, *J. Am. Chem. Soc.*, 1979, **101**, 6133–6135.

92 P. L. Freund and M. Spiro, Colloidal Catalysis: The Effect of Sol Size and Concentration, *J. Phys. Chem.*, 1985, **89**, 1074–1077.

93 A. Corma and H. Garcia, Supported gold nanoparticles as catalysts for organic reactions, *Chem. Soc. Rev.*, 2008, **37**, 2096–2126.

94 Y. Mikami, A. Dhakshinamoorthy, M. Alvaro and H. García, Catalytic activity of unsupported gold nanoparticles, *Catal. Sci. Technol.*, 2013, **3**, 58–69.

95 J. Kiwi, Hydrogen and Oxygen Production via Redox Catalysis in Colloidal Systems,

Isr. J. Chem., 1979, **18**, 369–374.

96 K. Kopple, D. Meyerstein and D. Meisel, Mechanism of the catalytic hydrogen production by gold sols. H/D isotope effect studies, *J. Phys. Chem.*, 1980, **84**, 870–875.

97 K. Kalyanasundaram, J. Kiwi and M. Grätzel, Hydrogen Evolution from Water by Visible Light, a Homogeneous Three Component Test System for Redox Catalysis, *Helv. Chim. Acta*, 1978, **61**, 2720–2730.

98 J. Kiwi, E. Borgarello, E. Pelizzetti, M. Visca and M. Grätzel, Cyclic water cleavage by visible light: drastic improvment of yield of H_2 and O_2 with bifunctional redox catalysts, *Angew. Chemie Int. Ed.*, 1980, **19**, 646–648.

99 J. Kiwi and M. Grätzel, Colloidal Redox Catalysts for Evolution of Oxygen and for Light-Induced Evolution of Hydrogen from Water, *Angew. Chemie Int. Ed. English*, 1979, **18**, 624–626.

100 J. Kiwi and M. Gratzel, Hydrogen evolution from water induced by visible light mediated by redox catalysis, *Nature*, 1979, **281**, 657–658.

101 D. Meisel, W. A. Mulac and M. S. Matheson, Catalysis of Methyl Viologen Radical Reactions by Polymer-Stabilized Gold Sols, *J. Phys. Chem.*, 1981, **85**, 179–187.

102 A. Henglein and J. Lilie, Storage of Electrons in Aqueous Solution: The Rates of Chemical Charging and Discharging the Colloidal Silver Microelectrode, *J. Am. Chem. Soc.*, 1981, **103**, 1059–1066.

103 A. Henglein, B. Lindig and J. Westerhausen, Photochemical electron storage on colloidal metals and hydrogen formation by free radicals, *J. Phys. Chem.*, 1981, **85**, 1627–1628.

104 Z. Zhang, A. Berg, H. Levanon, R. W. Fessenden and D. Meisel, On the interactions of free radicals with gold nanoparticles, *J. Am. Chem. Soc.*, 2003, **125**, 7959–7963.

105 P. Ionita, M. Conte, B. C. Gilbert and V. Chechik, Gold nanoparticle-initiated free radical oxidations and halogen abstractions, *Org. Biomol. Chem.*, 2007, **5**, 3504–3509.

106 P. Ionita, B. C. Gilbert and V. Chechik, Radical mechanism of a place-exchange reaction of Au nanoparticles, *Angew. Chemie - Int. Ed.*, 2005, **44**, 3720–3722.

107 T. Zidki, H. Cohen and D. Meyerstein, Reactions of alkyl-radicals with gold and silver nanoparticles in aqueous solutions, *Phys. Chem. Chem. Phys.*, 2006, **8**, 3552–3556.

108 I. Rusonik, H. Polat, H. Cohen and D. Meyerstein, Reaction of Methyl Radicals with Metal Powders Immersed in Aqueous Solutions, *Eur. J. Inorg. Chem.*, 2003, 4227–

4233.

109 R. Bar-Ziv, I. Zilbermann, T. Zidki, G. Yardeni, V. Shevchenko and D. Meyerstein, Coating Pt^0 nanoparticles with methyl groups: The reaction between methyl radicals and Pt^0-NPs suspended in aqueous solutions, *Chem. - A Eur. J.*, 2012, **18**, 6733–6736.

110 R. Bar-Ziv, I. Zilbermann, O. Oster-Golberg, T. Zidki, G. Yardeni, H. Cohen and D. Meyerstein, On the lifetime of the transients (NP)-(CH_3) n (NP=Ag^0, Au^0, TiO_2 nanoparticles) formed in the reactions between methyl radicals and nanoparticles suspended in aqueous solutions, *Chem. - A Eur. J.*, 2012, **18**, 4699–4705.

111 T. Zidki, A. Hänel and R. Bar-Ziv, Reactions of methyl radicals with silica supported silver nanoparticles in aqueous solutions, *Radiat. Phys. Chem.*, 2016, **124**, 41–45.

112 R. Bar-Ziv, T. Zidki, I. Zilbermann, G. Yardeni and D. Meyerstein, Effect of Hydrogen Pretreatment of Platinum Nanoparticles on their Catalytic Properties: Reactions with Alkyl Radicals – A Mechanistic Study, *ChemCatChem*, 2016, **8**, 2761–2764.

113 R. Bar-Ziv and T. Zidki, The effect of negatively charged metallic nanocatalysts on their reactions with alkyl radicals, *J. Coord. Chem.*, 2018, **71**, 1791–1798.

114 Y. M. Narode, B. G. Singh, S. Naumov, K. K. K. Sharma and G. K. Sharma, Gold Nanoparticle as a Lewis Catalyst for Water Elimination of Tyrosine-$^{\bullet}$OH Adducts: A Radiation and Quantum Chemical Study, *J. Phys. Chem. B*, 2020, **124**, 3591–3601.

115 V. Feigenbrugel, C. Loew, S. Le Calvé and P. Mirabel, Near-UV molar absorptivities of acetone, alachlor, metolachlor, diazinon and dichlorvos in aqueous solution, *J. Photochem. Photobiol. A Chem.*, 2005, **174**, 76–81.

116 K. D. Asmus, H. Mockel and A. Henglein, Pulse radiolytic study of the site of OH · radical attack on aliphatic alcohols in aqueous solution, *J. Phys. Chem.*, 1973, **77**, 1218–1221.

117 V. Shcherbakov, S. A. Denisov and M. Mostafavi, Selective Oxidation of Transient Organic Radicals in the Presence of Gold Nanoparticles, *Nanomaterials*, 2021, **11**, 727.

118 X. Cai, E. E. L. Tanner, C. Lin, K. Ngamchuea, J. S. Foord and R. G. Compton, The mechanism of electrochemical reduction of hydrogen peroxide on silver nanoparticles, *Phys. Chem. Chem. Phys.*, 2018, **20**, 1608–1614.

119 S. A. Denisov and M. Mostafavi, Presolvated electron reactivity towards CO2 and N2O in water, *Phys. Chem. Chem. Phys.*, 2021, **23**, 5804–5808.

120 V. Shcherbakov, S. A. Denisov and M. Mostafavi, The mechanism of organic radical oxidation catalysed by gold nanoparticles, *Phys. Chem. Chem. Phys.*, 2021, **23**, 26494–26500.

121 P. Peljo, M. D. Scanlon, A. J. Olaya, L. Rivier, E. Smirnov and H. H. Girault, Redox Electrocatalysis of Floating Nanoparticles: Determining Electrocatalytic Properties without the Influence of Solid Supports, *J. Phys. Chem. Lett.*, 2017, **8**, 3564–3575.

122 M. Comotti, C. Della Pina, R. Matarrese and M. Rossi, The catalytic activity of 'naked' gold particles, *Angew. Chemie - Int. Ed.*, 2004, **43**, 5812–5815.

123 P. Beltrame, M. Comotti, C. Della Pina and M. Rossi, Aerobic oxidation of glucose I. Enzymatic catalysis, *J. Catal.*, 2004, **228**, 282–287.

124 P. Beltrame, M. Comotti, C. Della Pina and M. Rossi, Aerobic oxidation of glucose: II. Catalysis by colloidal gold, *Appl. Catal. A Gen.*, 2006, **297**, 1–7.

125 I. B. Butler, M. A. A. Schoonen and D. T. Rickard, Removal of dissolved oxygen from water: A comparison of four common techniques, *Talanta*, 1994, **41**, 211–215.

126 M. Wuithschick, A. Birnbaum, S. Witte, M. Sztucki, U. Vainio, N. Pinna, K. Rademann, F. Emmerling, R. Kraehnert and J. Polte, Turkevich in New Robes: Key Questions Answered for the Most Common Gold Nanoparticle Synthesis, *ACS Nano*, 2015, **9**, 7052–7071.

127 Y. Pan, A. Leifert, D. Ruau, S. Neuss, J. Bornemann, G. Schmid, W. Brandau, U. Simon and W. Jahnen-Dechent, Gold nanoparticles of diameter 1.4 nm trigger necrosis by oxidative stress and mitochondrial damage, *Small*, 2009, **5**, 2067–2076.

128 A. Chompoosor, K. Saha, P. S. Ghosh, D. J. MacArthy, O. R. Miranda, Z. J. Zhu, K. F. Arcaro and V. M. Rotello, The role of surface functionality on acute cytotoxicity, ROS generation and DNA damage by cationic gold nanoparticles, *Small*, 2010, **6**, 2246–2249.

129 W. Gao, K. Xu, L. Ji and B. Tang, Effect of gold nanoparticles on glutathione depletion-induced hydrogen peroxide generation and apoptosis in HL7702 cells, *Toxicol. Lett.*, 2011, **205**, 86–95.

130 I. Fratoddi, I. Venditti, C. Cametti and M. V. Russo, How toxic are gold nanoparticles? The state-of-the-art, *Nano Res.*, 2015, **8**, 1771–1799.

131 Y. J. Tu, D. Njus and H. B. Schlegel, A theoretical study of ascorbic acid oxidation and $HOO^{\bullet}/O_2^{\bullet-}$ Radical scavenging, *Org. Biomol. Chem.*, 2017, **15**, 4417–4431.

132 M. Spiro, Heterogeneous Catalysis in Solution, *J. Chem. Soc., Faraday Trans.*, 1979, **75**, 1507–1512.

133 D. S. Miller, G. McLendon, J. Ferguson and A. J. Bard, Catalytic Water Reduction at Colloidal Metal "Microelectrodes". 2. Theory and Experiment, *J. Am. Chem. Soc.*, 1981, **103**, 5336–5341.

134 E. Smirnov, P. Peljo, M. D. Scanlon and H. H. Girault, Interfacial Redox Catalysis on

Gold Nanofilms at Soft Interfaces, *ACS Nano*, 2015, **9**, 6565–6575.

135 C. Wagner and W. Traud, On the interpretation of corrosion processes through the superposition of electrochemical partial processes and on the potential of mixed electrodes, *Corrosion*, 2006, **62**, 844–855.

Appendix 1. Pulse radiolysis measurements

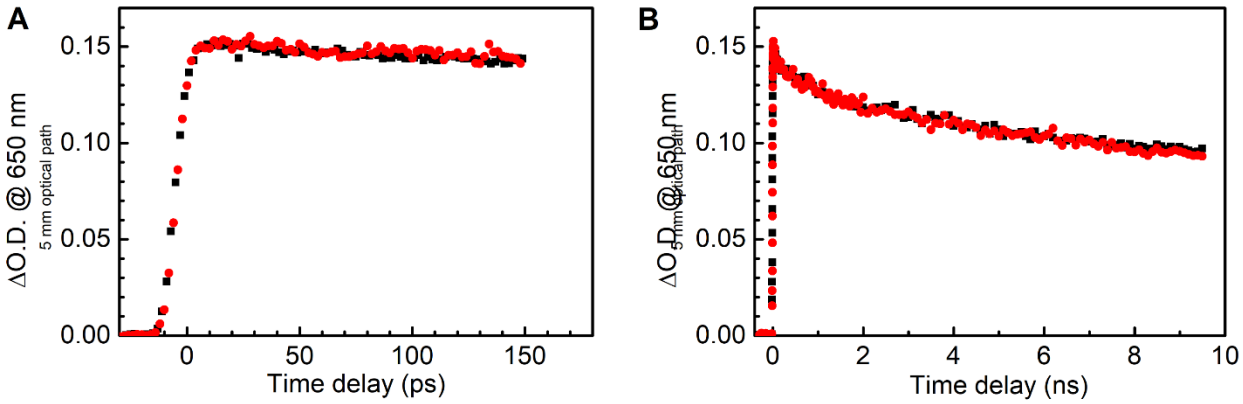

Figure S1. Kinetics of solvated electrons in water (black squares) and TM2 sample (red dots) - AuNPs prepared by the Turkevich method ([Au] = 2 mM, Au: citrate ratio is 1:4, λ_{max} = 519 nm, D_{TEM} = 15 ± 2 nm).

Appendix 2. Gamma radiolysis measurements

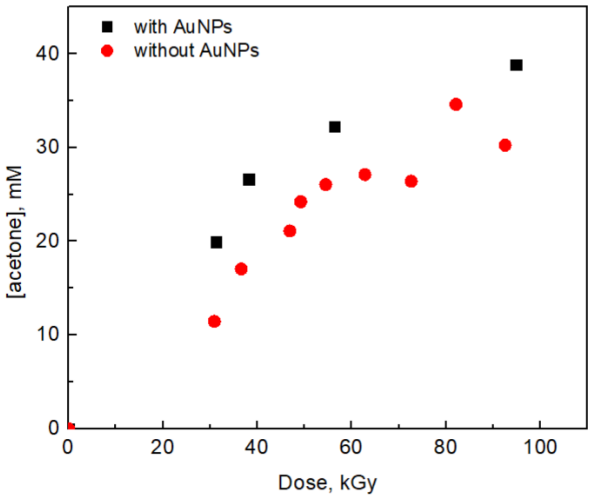

Figure S2. Acetone formation in AuNPs' suspension (BH1 sample, red dots) and its supernatant (black squares) under gamma radiation. Both solutions were oxygen saturated and contained 100 mM of 2-propanol and 20 mM of acetone.

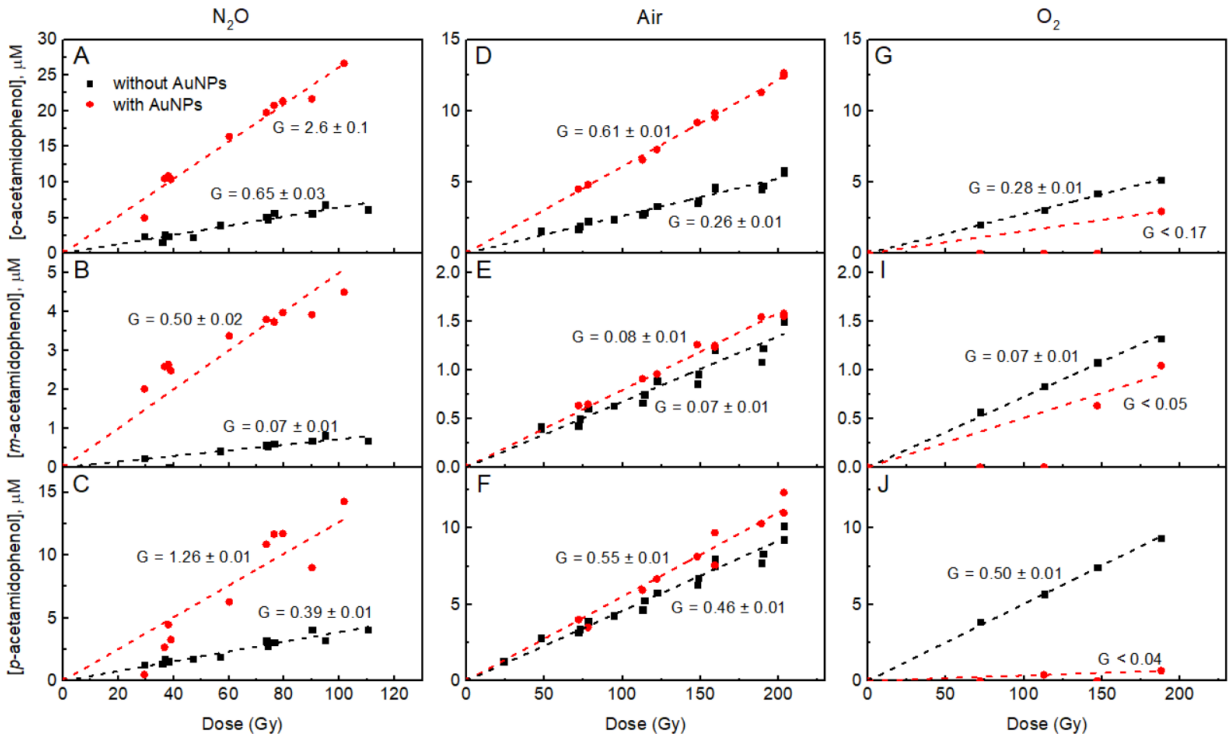

Figure S3. Formation of o-, m-, and p-hydroxyacetanilide in water radiolysis (^{60}Co) of 0.5 mM acetanilide aqueous solution (black squares) and in the presence of AuNPs (red dots) under three different atmospheres. AuNPs (BH1 sample diluted two times, [Au] = 1.5 mM). G is a radiolytic yield ($\times 10^{-7}$ mol J^{-1}).

List of chemicals

Table S1. List of used chemicals.

Reagent	Formula	Grade	Manufacturer	CAS
Potassium gold(III) chloride	$K[AuCl_4]$	98%	Sigma Aldrich	13682-61-6
Sodium citrate	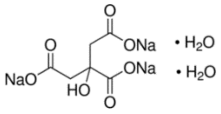	≥99.0%	Sigma Aldrich	6132-04-3
Sodium borohydride	$NaBH_4$	98%	Sigma Aldrich	16940-66-2
Poly(vinyl alcohol) (PVA), Mw = 85000-124000	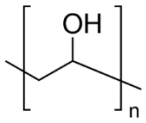	99+%	Sigma Aldrich	9002-89-5
2-propanol	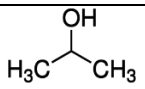	99.5%	Sigma Aldrich	67-63-0
Acetone	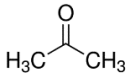	99.8%	Sigma Aldrich	67-64-1
Sodium hydroxide 30%	NaOH	-	VWR chemicals	1310-73-2
Sodium chloride	NaCl	99.9%	VWR chemicals	7647-14-5
Acetanilide	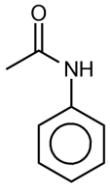	≤100%,	Jeulin	103-84-4
2-acetamidophenol	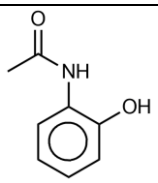	97%	Acros Organics	614-80-2
3- acetamidophenol	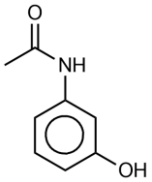	99+%	Acros Organics	621-42-1
4- acetamidophenol	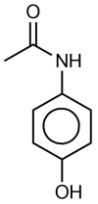	>99%	Sigma-Aldrich	103-90-2

L-ascorbic acid sodium salt	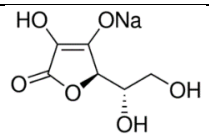	99%	Alfa Aesar	134-03-2
Argon	Ar	-	Alpha Gaz, Air Liquide	-
Nitrous oxide	N_2O	-	Alpha Gaz, Air Liquide	-
Oxygen	O_2	-	Alpha Gaz, Air Liquide	-

List of publications

Publication related to the PhD project

1. **Shcherbakov, V.**; Denisov, S. A.; Mostafavi, M. (2020). On the Primary Water Radicals' Production in the Presence of Gold Nanoparticles: Electron Pulse Radiolysis Study. *Nanomaterials*, *10*(12), 2478 doi.org/10.3390/nano10122478
2. **Shcherbakov, V.**; Denisov, S.A.; Mostafavi, M. (2021) Selective Oxidation of Transient Organic Radicals in the Presence of Gold Nanoparticles. *Nanomaterials*, *11*, 727. doi.org/10.3390/nano11030727
3. **Shcherbakov, V.**; Denisov, S. A.; Mostafavi, M. (2021). Mechanism of organic radicals' oxidation catalysed by gold nanoparticles. *Physical Chemistry Chemical Physics*. 2021, 23, 26494-26500 doi.org/10.1039/D1CP03875C

Collaboration Publications

4. Dembinski, R; Kaczmarek, R; Ward, S; Debnath, D; Jacobs, T; Stark, A; Korczyński, D; Kumar, A; Sevilla, M; Denisov, S; **Shcherbakov**, **V;** Pernot, P; Mostafavi, M; Adhikary, A. One Way Traffic: Base-to-backbone Hole Transfer in Nucleoside Phosphorodithioates. (2020) *Chemistry—A European Journal*, 26, 9495-9505 doi.org/10.1002/chem.202000247
5. Pignie, M. C.; **Shcherbakov, V.**; Charpentier, T.; Moskura, M.; Carteret, C.; Denisov, S.A.; Mostafavi M.; Thill A.; Le Caer, S. (2021). Confined water radiolysis in aluminosilicate nanotubes: the importance of charge separation effects. *Nanoscale*, *13*(5), 3092-3105. doi.org/10.1039/D0NR08948F
6. Puget, M.; **Shcherbakov, V.**; Denisov, S.; Moreau, P.; Dognon, J.P.; Mostafavi, M.; Le Caër, S. (2021). Reaction Mechanisms of the Degradation of Fluoroethylene Carbonate, an Additive of Lithium-Ion Batteries, Unraveled by Radiation Chemistry. *Chemistry–A European Journal,* 23(31), 8185-8194. doi.org/10.1002/chem.202100562
7. Denisov, S.A.; Ward, S.; **Shcherbakov, V.**; Stark, A.; Kaczmarek, R.; Radzikowska-Cieciura, E.; Debnath, D.; Jacobs, T.; Kumar, A.; Sevilla, M.; Pernot, P.; Dembinski, R.; Mostafavi, M.; Adhikary, A. (2022) Modulation of the Directionality of Hole Transfer Between the Base and the Sugar-phosphate Backbone in DNA with the Number of Sulfur atoms in the Phosphate Group. *The Journal of Physical Chemistry B*, 126, 2, 430–442 doi.org/10.1021/acs.jpcb.1c09068

List conferences

1. Miller Conference on Radiation Chemistry *(oral presentation)*, September 2019, Manchester, United Kingdom.
2. Workshop «l'Or en Occitanie» *(poster),* December 2019, Montpellier, France.
3. 45th Annual Meeting of the European Radiation Research Society *(oral presentation,* Young Investigator Award*),* September 2020, online.
4. EUGLOH Annual Student Research Conference *(oral presentation),* September 2020, online.
5. Radiation Research Society Annual Meeting *(poster),* October 2020, online.
6. iNanoTheRad conference "Advanced Strategies for Radiotherapy" *(oral presentation),* November 2021, Orsay, France.
7. 46th Annual Meeting of the European Radiation Research Society *(poster),* November 2021, Caen, France.

RÉSUMÉ

La radiothérapie (ou radiothérapie) est l'une des principales méthodes de lutte contre le cancer, avec la chirurgie et les thérapies systémiques (par exemple, chimio, ciblage, immunothérapie). Environ 50 % des patients reçoivent une radiothérapie seule ou en combinaison avec d'autres méthodes. En même temps, c'est le moyen le moins cher de soigner le cancer, puisqu'il ne représente que 5 % du coût total. Malgré son efficacité, le traitement par radiothérapie s'accompagne souvent de différents effets secondaires. Dans la plupart des cas, les patients souffrent de nausées, de vomissements et de fatigue après la radiothérapie, ce qui réduit considérablement leur qualité de vie. La radiothérapie provoque également des dommages visibles sur la peau et peut provoquer des cancers secondaires. En outre, l'utilisation des radiations est limitée par la dose autorisée pour les tissus sains et les organes vitaux proches de la tumeur. Dans certains cas, la dose autorisée n'est tout simplement pas suffisante pour tuer les cellules cancéreuses.

L'un des moyens d'accroître l'efficacité de la radiothérapie et de réduire les effets secondaires consiste à utiliser des radiosensibilisateurs, c'est-à-dire des agents qui augmentent la mort cellulaire provoquée par les rayonnements. Les nanoparticules sont des radiosensibilisateurs prometteurs, qui ont démontré leur capacité à augmenter la mort cellulaire et la destruction des tumeurs causées par les rayonnements dans de nombreuses recherches menées ces 17 dernières années. Pour la première fois, l'effet radiosensibilisant des nanoparticules a été démontré par les nanoparticules d'or (AuNPs). À ce jour, les AuNPs sont les plus étudiées. Cependant, elles ne sont pas encore utilisées en clinique.

L'utilisation de l'or a été motivée par l'effet dit d'augmentation de la dose. L'or ayant un numéro atomique élevé (Z=79), il absorbe plus d'énergie dans la gamme des keV que l'eau ou les tissus mous, ce qui augmente l'ionisation globale du volume irradié en raison de l'émission d'électrons secondaires et de photons. Par la suite, la divergence entre l'effet radiosensibilisant observé et les résultats prédits par l'hypothèse "physique" initiale a incité les scientifiques à rechercher d'autres mécanismes en biologie et en chimie.

Aujourd'hui, le mécanisme proposé pour la radiosensibilisation induite par les nanoparticules comprend différents effets physiques, chimiques et biologiques. Cependant, il n'y a pas de consensus sur le mécanisme exact du rôle des NPs.

La chimie de la radiosensibilisation reste le domaine le moins étudié. La raison principale est que les AuNPs ont longtemps été considérées comme chimiquement inertes. Dans la

recherche biomédicale, les nanoparticules sont encore souvent considérées comme des matériaux inertes. Une autre raison est que les chimistes, en particulier les chimistes spécialisés dans les rayonnements, ne sont pas suffisament impliqués dans l'étude de l'effet radiosensibilisant des AuNPs que les physiciens et les biologistes. Nous pensons que le mécanisme de l'effet radiosensibilisant des AuNps n'est toujours pas compris en raison de l'étude insuffisante du rôle chimique des AuNPs.

Les effets chimiques sont généralement associés à une formation accrue d'espèces réactives de l'oxygène (ROS), telles que les radicaux hydroxyles ($^{\bullet}OH$), les radicaux superoxydes ($O_2^{\bullet-}$) et le peroxyde d'hydrogène (H_2O_2), en présence de nanoparticules. La principale méthode de détection des ROS dans les études biologiques est l'utilisation de colorants fluorescents. Elle est basée sur l'oxydation d'une molécule non fluorescente en une molécule fluorescente lors de la réaction avec les ROS, en supposant que l'augmentation de l'intensité de la fluorescence est proportionnelle à l'augmentation de la concentration des ROS. Cependant, le processus d'oxydation d'un colorant est un processus à plusieurs étapes qui comprend la formation d'une variété de produits (pas seulement le produit fluorescent). Les AuNPs possèdent une activité catalytique, qui peut modifier les différents chemins reactionnels.

Dans le présent travail, nous avons tout d'abord examiné l'idée d'une production accrue de ROS en présence d'AuNPs avec et sans l'utilisation de rayonnements ionisants. Nous avons étudié l'effet des AuNPs sur la radiolyse de l'eau en mesurant directement l'évolution du rendement de l'électron solvaté en fonction du temps en utilisant la technique de radiolyse par impulsions picosecondes. Ces observations spectroscopiques directes ont montré qu'il n'y a pas d'augmentation de la production de radicaux primaires de l'eau en présence de AuNPs de différentes tailles et à une concentration allant jusqu'à 3 mM d'or (600 µM/m ou 0,06 % en poids) sous un faisceau d'électrons de 8 MeV.

Ensuite, nous avons étudié l'effet des AuNPs sur la chimie des radicaux organiques par des expériences stationnaire en utilisant la radiolyse gamma. Pour deux types de radicaux produits dans des réactions avec des radicaux $^{\bullet}OH$: le radical α-hydroxyisopropyle formé par l'abstraction de l'atome $^{\bullet}H$ du carbone α du 2-propanol, et les produits formes á partir de l'adduit OH sur de le cycle benzénique de l'acetanilide. Dans les deux cas, nous avons constaté que les AuNPs catalysaient l'oxydation des radicaux organiques transitoires. Ces résultats démontrent que la détection des ROS par des colorants fluorescents ne peut pas être utilisée en présence de nanoparticules catalytiquement actives comme l'or car, dans

cette méthode, les radicaux organiques transitoires sont toujours formés comme intermédiaires et les produits des réactions peuvent être modifiés.

En outre, les résultats préliminaires sur l'oxydation de la vitamine C par l'oxygène moléculaire catalysée par les AuNPs sans rayonnement ionisant sont présentés, démontrant la capacité des AuNPs à catalyser les réactions RedOx, ce qui doit être pris en compte lorsque l'on travaille avec des cellules vivantes en présence de ces NPs.

Tous nos résultats indiquent que la propriété cruciale des nanoparticules causant l'effet radiosensibilisant est leur activité catalytique. Dans cette optique, nous proposons un nouveau mécanisme de radiosensibilisation induit par les AuNPs. Nos résultats montrent que les AuNPs agissent simultanément au moins de deux manières : 1) elles catalysent l'oxydation des agents radio-protecteurs rendant les cellules moins radio-résistantes ; 2) elles provoquent la fixation des dommages causés par les radiations en catalysant l'oxydation des radicaux organiques. Ainsi, nous présentons une nouvelle vision sur le rôle des NPs métalliques dans le traitement du cancer.